FACULTY OF PURE AND APPLIED SCIENCES
DEPARTMENT OF BIOLOGICAL SCIENCES

DISSECTING THE ROLE OF HISTONE N-TERMINAL ACETYLTRANSFERASE NAA40 IN GENE REGULATION, METABOLISM AND CANCER

CHRISTINA DEMETRIADOU

A dissertation submitted to the University of Cyprus in partial fulfillment of the requirements for the Degree of Doctor of Philosophy

MAY 2021

Validation Page

Doctoral Candidate: Christina Demetriadou

Doctoral Thesis Title: Dissecting the role of histone N-terminal acetyltransferase NAA40 in gene regulation, metabolism and cancer

The present Doctoral Dissertation was submitted in partial fulfillment of the requirements for the degree of Doctor of Philosophy at the Department of Biological Sciences and was approved on the 28.05.2021 by the members of the examination committee.

Examination Committee:

Research Supervisor: Dr. Antonis Kirmizis, Associate Professor

Committee Member: Dr. Katerina Strati, Assistant Professor

Committee Member: Dr. Paris Skourides, Associate Professor

Committee Member: Dr. Marcus Buschbeck, Group Leader

Committee Member: Dr. Argyris Papantonis, Professor

Declaration of Doctoral Candidate

The present doctoral dissertation was submitted in partial fulfillment of the requirements for the degree of Doctor of Philosophy of the University of Cyprus. It is a product of original work of my own, unless otherwise mentioned through references, notes, or any other statements.

…… [Full Name of Doctoral Candidate]

…… [Signature]

Περίληψη

Η Ν-άλφα-ακετυλτρανσφεράση 40 (NAA40) καταλύει τη μεταφορά μιας ακετυλομάδας στο άλφα αμινοτελικό άκρο της σερίνης 1 (S1) στις ιστόνες Η4 και Η2Α. Παρόλο που προηγούμενες μελέτες έχουν συνδέσει την NAA40 με τον καρκίνο, η λειτουργία του επιγενετικού αυτού παράγοντα δεν έχει διερευνηθεί. Στην μελέτη αυτή δείχνουμε ότι το NAA40 ένζυμο βρίσκεται συχνά αυξημένο σε ασθενείς με καρκίνο του εντέρου ενώ μειωμένη έκφραση της NAA40 αναστέλλει την επιβίωση των καρκινικών κυττάρων του εντέρου και καθυστερεί την ανάπτυξη ανθρώπινων όγκων σε ποντίκια. Σε μοριακό επίπεδο ανακαλύψαμε ότι η NAA40 ενεργοποιεί την έκφραση της PRMT5 (Protein arginine methyltransferase 5) πρωτεΐνης η οποία στη συνέχεια καταλύει τη μεταφορά μεθυλομάδων στην πλευρική αλυσίδα της αργινίνης 3 (H4R3me2s) ελέγχοντας την έκφραση σημαντικών γονιδίων που σχετίζονται με την ανάπτυξη του καρκίνου του εντέρου. Επιπλέον, ανάλυση του μεταγραφήματος και μεταβολισμού των κυττάρων έδειξε ότι η NAA40 ελέγχει την έκφραση βασικών γονιδίων στον κύκλο του άνθρακα και την αφθονία των αντίστοιχων μεταβολιτών. Συγκεκριμένα, μέσω της δράσης της ως ακετυλτρανσφεράση, η NAA40 ρυθμίζει τον μεταβολικό κύκλο της μεθιονίνης επηρεάζοντας έτσι τα επίπεδα μεθυλίωσης των ιστονών και την επιβίωση των καρκινικών κυττάρων του εντέρου. Είναι επίσης σημαντικό να σημειωθεί ότι η αναδιαμόρφωση του μεταβολισμού που μεσολαβείτε από την NAA40 προάγει την αντίσταση των καρκινικών κυττάρων του εντέρου στη χημειοθεραπεία. Συγκεκριμένα, η NAA40 διεγείρει τη μεταγραφή του μεταβολικού γονιδίου TYMS (Thymidylate synthase) το προϊόν του οποίου στοχεύετε από το χημειοθεραπευτικό φάρμακο 5-FU (5-Fluorouracil). Κατά συνέπεια σε όγκους από ασθενείς με καρκίνο του εντέρου η έκφραση της NAA40 σχετίζεται με τα επίπεδα του TYMS και μειωμένη ανταπόκριση στο 5-FU. Μηχανιστικά, η NAA40

ενεργοποιεί το TYMS εμποδίζοντας την τοποθέτηση της κατασταλτικής τροποποίησης H2A/H4S1ph στην περιφέρεια του πυρήνα των κυττάρων. Συνολικά, τα ευρήματα της μελέτης αυτής καθορίζουν τον ρυθμιστικό ρόλο της NAA40 στον καρκίνο του εντέρου και σημειώνουν την δυνατότητά της να χρησιμοποιηθεί ως ένας νέος προγνωστικός παράγοντας και θεραπευτικός στόχος.

Abstract

N-alpha-acetyltransferase 40 (NAA40) catalyzes the transfer of an acetyl moiety to the alpha-amino group of serine 1 (S1) on histones H4 and H2A. Although previous studies have linked NAA40 to cancer, the functional role of this epigenetic modifier in colorectal cancer (CRC) development was not investigated. Here, we show that NAA40 is commonly increased in CRC patient tissues while depletion of NAA40 inhibits CRC cell survival and delays the growth of human CRC xenograft tumors. Molecularly, we reveal that NAA40 activates the expression of protein arginine methyltransferase 5 (PRMT5), which then mediates the deposition of H4R3me2s in order to control the expression of essential cancer-associated genes and sustain CRC cell growth. Furthermore, using transcriptomic and metabolomic analysis we demonstrate that NAA40 controls key one-carbon metabolic genes and the abundance of corresponding metabolites. In particular, through its acetyltransferase activity NAA40 regulates the methionine cycle thereby affecting global histone methylation and CRC cell survival. Importantly, NAA40-mediated metabolic rewiring promotes resistance of CRC cells to chemotherapy *in vitro* and *in vivo*. Specifically, NAA40 stimulates transcription of the one-carbon metabolic gene thymidylate synthase (TYMS), whose product is targeted by 5-fluorouracil (5-FU) and accordingly in primary tumours NAA40 expression associates with TYMS levels and poorer 5-FU response. Mechanistically, NAA40 activates TYMS by preventing enrichment of repressive H2A/H4S1ph at the nuclear periphery. Overall, these findings define a regulatory role for NAA40 in CRC and signify its potential as a novel predictive factor and therapeutic target.

Acknowledgments

First of all, I would like to thank my supervisor Dr. Antonis Kirmizis, for giving me the opportunity to work in his lab and for his continuous support and guidance throughout my studies. I am deeply thankful for everything he taught me and for sharing the same motivation and enthusiasm for science.

I would also like to thank all the members in the A.K lab for all the constructive discussions and their constant help and support. Especially, I would like to express my gratitude to my special lab mates/friends Maria Kouma, Ariel Klavaris, Andria Drousioti and Dr. Costas Koufaris for always being there for me and for all the incredible moments that we shared together. I feel very lucky that I had the chance to work with you in the lab. I would also like to thank my friends Dr. Panayiota Louka, Dr. Andri Christodoulou and Dr. Stela Michael for their support, invaluable advice, and helpful discussions.

Moreover, I would like to thank all my friends for their limitless patience and understanding. I also want to thank Andreas Nicolas Ioannides for his love and encouragement. Lastly, I would like to express my deepest gratitude to my parents, Pantelis and Rena for their love and everything they have done for me.

This Ph.D. thesis is dedicated to my parents

Table of Contents

List of Figures

List of Tables

List of Abbreviations

1C-metabolism	One-carbon metabolism
5mC	5-methylcytosine
5-FU	5-Fluorouracil
Ac-CoA	Acetyl-Coenzyme A
α-KG	Alpha-ketoglutarate
ACLY	ATP-citrate lyase
ACSS	acyl-CoA synthetase short-chain
CDKN1	Cyclin Dependent Kinase Inhibitor 1A
ChIP	Chromatin Immunoprecipitation
CGIs	CpG islands
CRC	Colorectal cancer
CTCF	CCCTC-Binding Factor
CTH	Cystathionine gamma-lyase
CTMs	Co-translational modifications
DNMT	DNA methyltransferase
dUMP	Deoxyuridine monophosphate
dTMP	Deoxythymidine monophosphate
EIF4E	Eukaryotic Translation Initiation Factor 4E
FGFR3	Fibroblast Growth Factor Receptor 3
GNAT	Gcn5-related N-acetyltransferase
H2A/H4S1ph	Histone H2A/H4 Serine 1 phosphorylation
H3K4me3	Histone H3 Lysine 4 trimethylation
H3K36me3	Histone H3 Lysine 36 trimethylation
H3K9me3	Histone H3 Lysine 9 trimethylation
H3K27me3	Histone H3 Lysine 27 trimethylation

H3K79me3	Histone H3 Lysine 79 trimethylation
H3K79me2	Histone H3 Lysine 79 dimethylation
H4R3me2a	Histone H4 Arginine 3 asymmetric dimethylation
H4R3me2s	Histone H4 Arginine 3 symmetric dimethylation
HAT	Histone acetyltransferase
HDAC	Histone deacetylase
hCYS	Homocysteine
IDH	Isocitrate dehydrogenase
In-ac	Internal acetylation
In-me	Internal methylation
JMJDs	Jumonji C domain containing KDMs
KDM	Lysine demethylase
KMT	Lysine methyltransferase
LADs	Lamina-associated domains
MAT1A	Methionine adenyltransferase 1A
me-THF	5,10-methylene-tetrahydrofolate
MMAA	Metabolism of cobalamin associated A
m-THF	5-methyl-tetrahydrofolate
MTHFR	Methylenetetrahydrofolate reductase
NAA40	N-alpha-acetyltransferase 40
N-acH4/H2A	N-terminal acetylation of histone H4/H2A
NATs	N- terminal acetyltransferases
Nt-ac	N-terminal acetylation
Nt-me	N-terminal methylation
PRMTs	Protein arginine methyltransferases
PTMs	Post-translational modifications
RBL2	Rb Transcriptional Corepressor Like 2
RNA-seq	RNA sequencing
SAM	S-adenosylmethionine

SAH	S-adenosyl-homocysteine
SCR	Scramble
shRNA	short hairpin RNA
siRNA	small interfering RNA
SIRT	Sirtuins
TADs	Topologically associated domains
TET	Ten-eleven translocase
TYMS	Thymidylate synthase
UMP	Uridine monophosphate
WT	Wild type

CHAPTER 1

INTRODUCTION

1.1 'On top' of genetics

The diverse types of cells that shape an organism harbor vastly identical genetic material which is however differentially processed to guide the development of functional tissues. The field of epigenetics was originally introduced by Conrad Waddington in 1942 and has evolved as the study of potentially heritable traits that occur in the absence of any alteration in the genomic DNA sequence itself (Goldberg et al. 2007). The major epigenetic mechanisms that orchestrate gene expression encompass DNA and histone modifications.

1.2 Chromatin structure

Within the nucleus of eukaryotic cells, DNA is packaged by orders-of-magnitude into a tightly organized chromatin structure which serves as a physical barrier to regulate the accessibility of DNA binding proteins such as chromatin remodeling enzymes and transcription factors. At the lowest scale, the building blocks of chromatin, known as nucleosomes, each comprises of 147 base pairs of DNA wrapped around an octameric protein complex consisting of two copies of each of the four histone proteins, H3, H4, H2A and H2B (Luger et al. 1997). Chromatin emerges in two distinct states: a more loosely packed, gene-rich and permissive for transcription form known as euchromatin and a highly compacted, gene-poor and transcriptionally silenced configuration called heterochromatin. At a higher scale, chromatin fibers are further folded into the tightly packed chromosome structure (Figure 1.1A).

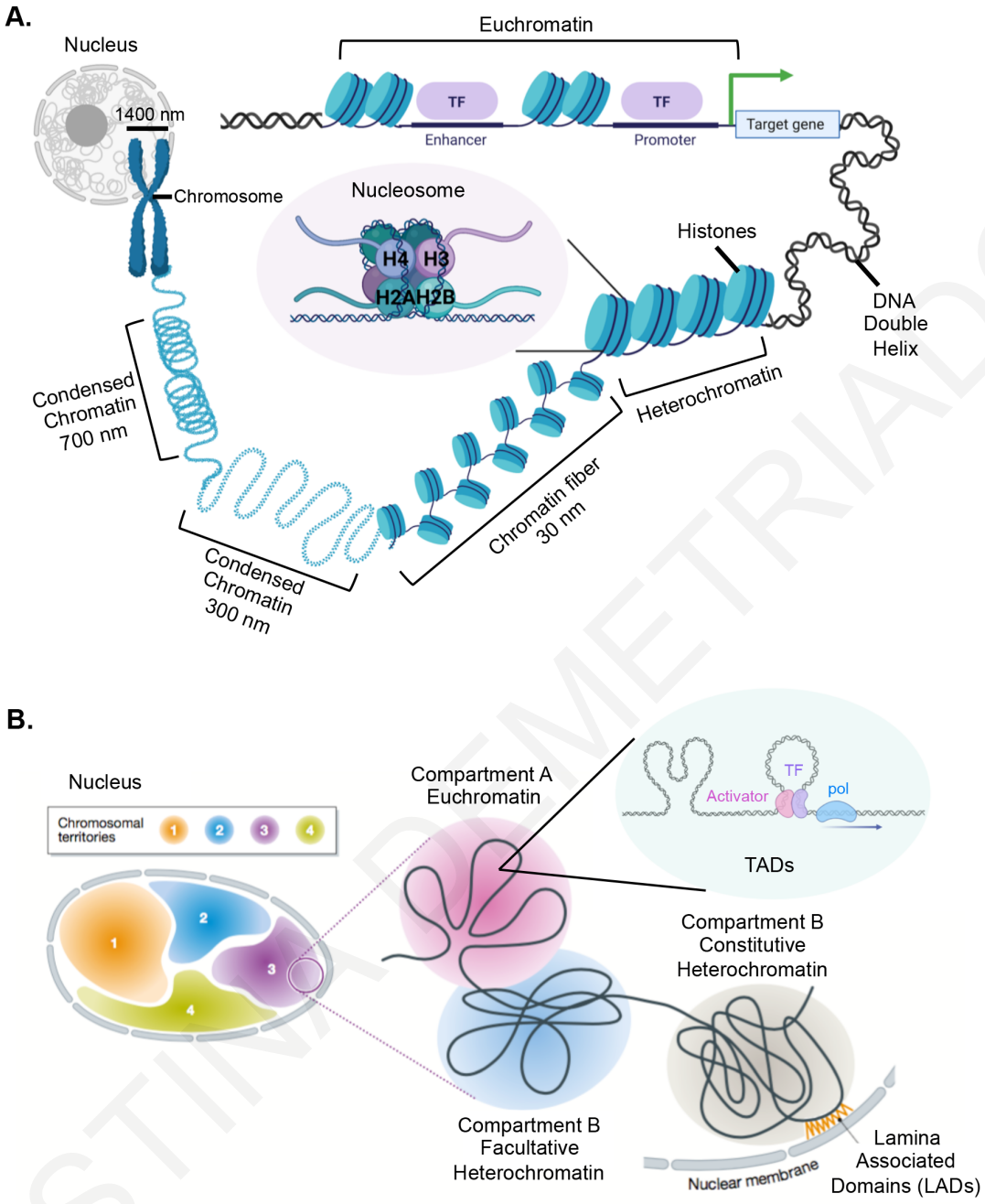

Figure 1.1. Chromatin organization. (A) Eukaryotic cells package their genomes in a highly regulated structure within their nucleus known as chromatin. Two copies of each of the four core histone proteins, H2A, H2B, H3, and H4, form an octamer around which 147 base pairs of DNA are wrapped, constructing the nucleosome, which is the fundamental repeating unit of chromatin. Nucleosomes are packed into higher order structures including the 30 nm chromatin fiber (solenoid) and the highly condensed interphase chromosome structure. Chromatin is mainly found in two distinct states: Euchromatin which is associated with an open, active for transcription configuration and heterochromatin which is associated with a closed and repressive for transcription conformation. TF, transcription factor. **(B)** Chromosomes are elegantly packed into distinct territories within the nucleus. Further compartmentalization of each territory reveals transcriptionally permissive euchromatin regions that are more centrally positioned

and less dynamic transcriptionally inactive heterochromatin domains which can be found at the nuclear periphery (LADs). Each compartment is in turn partitioned into topologically associated domains (TADs) which mediate enhancer-promoter interactions enabling gene expression. Adapted from Rada-Iglesias et al. 2018.

Chromosomes are not randomly distributed within the three-dimensional nuclear space but they are spatially arranged into discrete territories based on their chromatin conformation and activity (Figure 1.1B). This chromosome compartmentalization is defined by two distinct domains at the megabase-resolution. Compartment A represents a euchromatic active region that is more centrally positioned within the nucleus. Compartment B refers to tightly packed heterochromatic regions that are predominately located at the nuclear periphery broadly known as lamina-associated domains (LADs) (Figure 1.1B) (Buchwalter et al. 2018; Danieli and Papantonis 2020; Karoutas and Akhtar 2021; Rada‐Iglesias et al. 2018) or the nucleolar periphery forming the nucleolus-associated domains (NADs) (Girelli et al. 2020). At the next level of organization, each of these compartments is further sub-divided into topologically associated domains (TADs) which are formed by several chromatin loops mainly arranged through the function of CTCF and cohesin complexes facilitating the establishment of enhancer-promoter spatial interactions (Figure 1.1B) (Mizi et al. 2020).

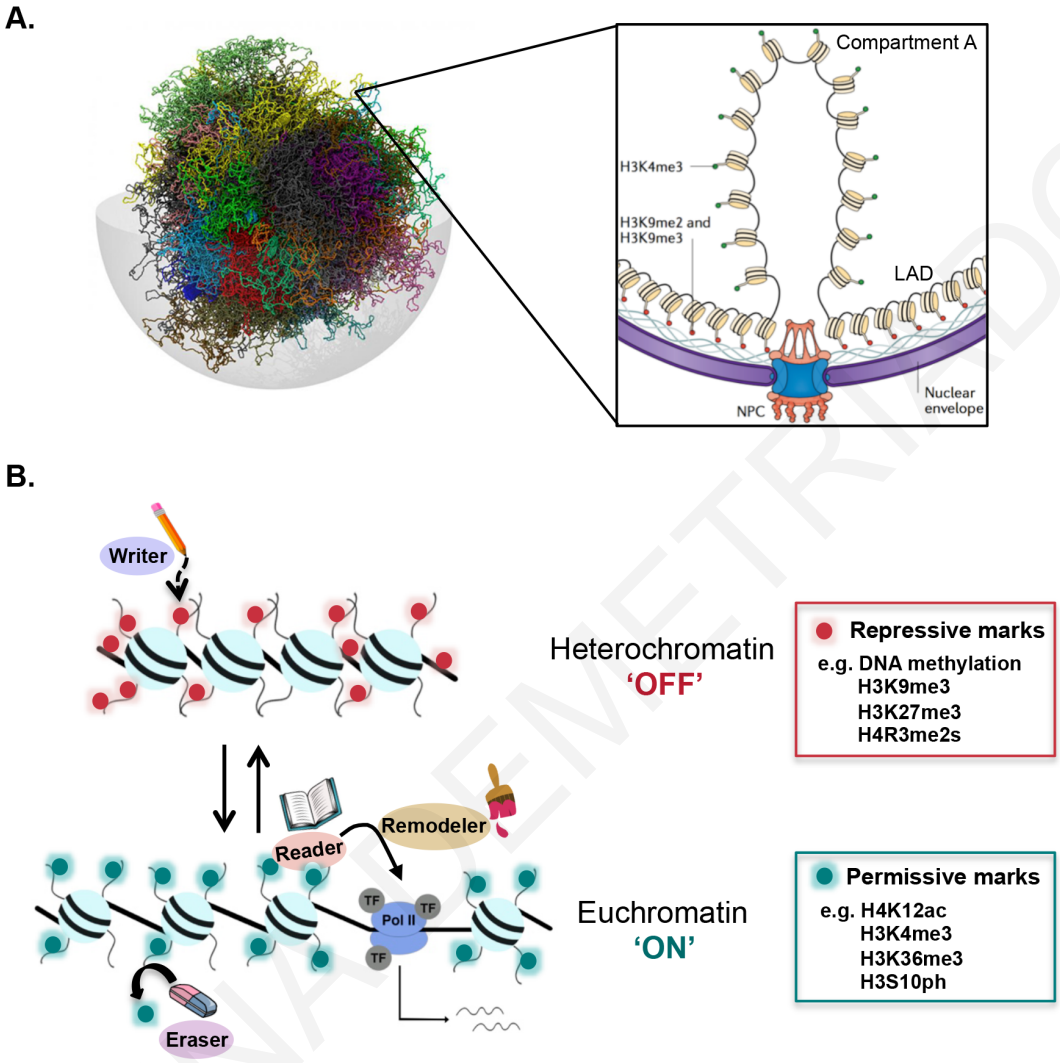

Figure 1.2. Regulation of chromatin structure and transcription. (A) The 3D organization of chromatin within the nucleus is tightly regulated by epigenetic modifications. The euchromatic environment of Compartment A is enriched with active histone marks such as H3K4me3. Conversely, heterochromatin located at the nuclear lamina is composed of repressive marks such as H3K9me2/me3. Adapted from Buchwalter et al. 2019. **(B)** Epigenetic modifications occurring on DNA and histone proteins shape chromatin states and are dynamically regulated by three distinct group of proteins: i) the "writers" that deposit modifications, ii) the "erasers" that remove those modifications and iii) the "readers" that recognize specific modifications or combinations of different marks recruiting or occluding chromatin remodelers and the transcriptional machinery. Repressive epigenetic marks, including methylation on DNA and histones establish heterochromatin and prevent gene transcription. Conversely, activating marks, including acetylation, methylation and phosphorylation of specific histone residues are enriched in relaxed euchromatic regions that are accessible for transcription. Adapted from Demetriadou et al. 2017.

1.3 Epigenetic modifications

The establishment of 3D genome organization to enable faithful gene activation or gene repression is mediated through an expanding repertoire of chromatin modifications (Figure 1.2A) (Bannister and Kouzarides 2011). Among them, histone modifications and DNA methylation are considered the most well characterized. Modifications occurring on histone proteins include the deposition of numerous chemical groups, such as acetylation, methylation, phosphorylation, ubiquitinylation, succinylation and propionylation on the structured globular domain of histones or their unstructured tails protruding outwards from the nucleosome core, whereas DNA methylation includes the covalent addition of methyl marks on cytosine bases of the genome (Bergman and Cedar 2013; Kebede et al. 2015; Kouzarides 2007; Xie et al. 2012). Epigenetic modifications sequentially or in combination influence chromatin states to allow or prevent the recruitment of protein complexes modulating all DNA-based processes, including DNA replication, transcription and DNA damage response and repair (Figure 1.2B). Generally, chromatin modifications are dynamically regulated by the function of three different group of specialized proteins: the “writers” which catalyze the addition of specific modifications, the “erasers” which are responsible for the removal of those modifications and the “readers” which recognize and interpret modifications to translate them into a specific functional outcome (Figure 1.2B).

1.3.1 DNA methylation

The DNA molecule can be methylated by DNA methyltransferase (DNMT) enzymes which transfer a methyl group from S-adenosyl methionine (SAM) to the fifth carbon of cytosine bases (5-methylcytosine or 5mC) in CpG dinucleotides

(Bergman and Cedar 2013). In healthy cells, CpG sites across the entire genome are heavily methylated, while CpG-rich promoter regions, known as CpG islands (CGIs), remain mostly unmethylated (Greenberg and Bourc'his 2019). In mammals, DNMT3A and DNMT3B enzymes catalyze *de novo* DNA methylation, whereas DNMT1 is responsible to sustain 5mC upon cell division (Lyko 2017). Methylated CpG regions facilitate heterochromatin formation near the nuclear lamina and mediate transcriptional silencing of the target genes (Bergman and Cedar 2013). Although DNA demethylase enzymes have not been discovered yet, DNA demethylation is conveyed by the Ten-eleven translocase (TET) family of dioxygenases through hydroxylation of 5-methylcytosine to hydroxymethylcytosine (5hmC), formylcytosine (5fC) and eventually carboxylcytosine (5caC) (Greenberg 2021; Wu and Zhang 2017). TET-mediated oxidized 5mC is reduced at actively transcribed genes but is enriched at bivalent promoters indicating a possible role in the transcriptional regulation of poised genes during differentiation. Higher levels of 5hmC were also seen in gene bodies as opposed to transcription start sites suggesting the contribution of 5mC oxidation in transcriptional elongation (Wu and Zhang 2017).

1.3.2 Histone modifications

Despite the variety of histone covalent modifications discovered thus far, acetylation and methylation added either during (CTMs) or after (PTMs) translation are the most well documented and typically exist in two distinct types. Internal (In) modifications occur on the side chain of internal amino acid residues (i.e., lysines, arginines, glutamines) on histone proteins, whereas N-alpha terminal (Nt) marks are located at the N-terminal end of histone tails (Figure 1.3A). Importantly, the

deposition of In and Nt histone modifications occurs through distinct sets of enzymes specialised for these tasks (Figure 1.3B-E).

The In-acetylation (In-ac) comprises the covalent attachment of an acetyl group from acetyl-coenzyme A (Ac-CoA) to the epsilon-amino group (N^{ε}) of an internal lysine residue, a process regulated by the opposing catalytic roles of histone acetyltransferases (HATs) and histone deacetylases (HDACs) (Figure 1.3B). HATs are classified into three major families based on their structure and sequence homology: MYST (MOZ, Ybf2/Sas3, Sas2 and TIP60) containing Tip60, HBO1, MOF, MOZ and MORF enzymes; GNAT (Gcn5-related N-acetyltransferase) consisted of HAT1, PCAF and GCN5 enzymes; and p300/CBP (p300 and CREB-binding protein) comprised of p300 and CBP acetyltransferases (Demetriadou and Kirmizis 2017). On the other hand, HDACs fall into four different categories: Class I (HDAC1-3), Class II (HDAC 4-10), Class III (SIRT1-7) and Class IV (HDAC11) (Li et al. 2020). In-lysine acetylation on histone proteins is generally associated with transcriptional activation either directly or indirectly.

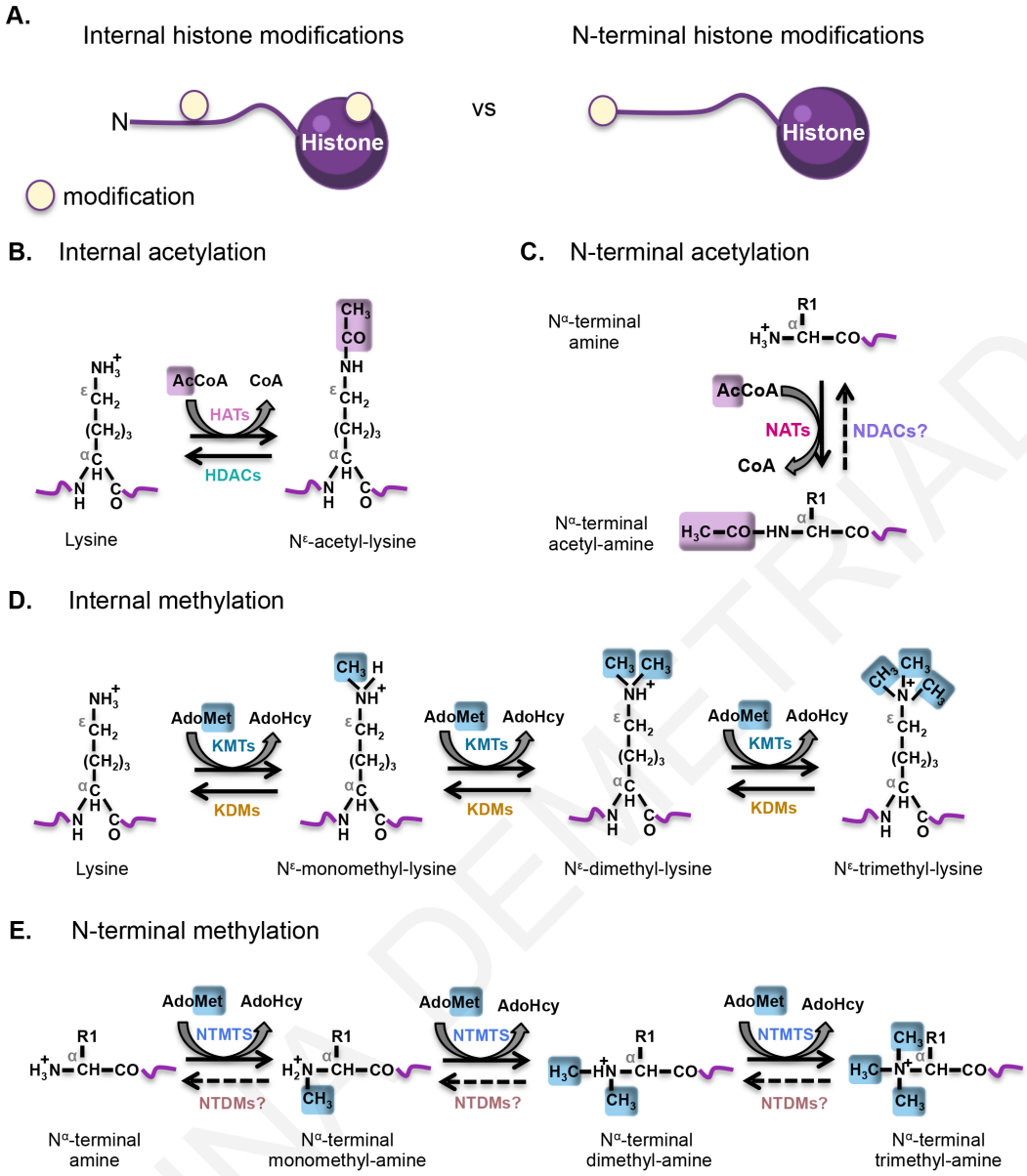

Figure 1.3. Comparison of Internal vs N-terminal histone modifications. (A) Internal (In) modifications are deposited on the amine group located on the side chain of internal amino acids on the octameric core domain or the N-terminal tails of histone proteins. Conversely, N-alpha terminal (Nt) marks are located at the N-terminal end of histone tails. **(B)** A HAT catalyzes the transfer of an acetyl group from Ac-CoA to the ε-amino group of an internal lysine residue. Nε-lysine acetylation is reversed by HDACs. **(C)** NATs transfer an acetyl group from Ac-CoA to the α-amino group of the first amino acid residue at the N-terminal tip of histone proteins. N-alpha terminal acetylation is believed to be static as no NDACs have been identified yet. **(D)** A variety of In-me are currently known to occur on different residues including lysine, arginine, and glutamine. As an example the mono-, di- or trimethylation of internal lysine ε-amino groups catalyzed by KMTs using SAM as the methyl donor. The lysine demethylase reaction is driven by KDMs (LSD1 and JmjC domain-containing proteins). **(E)** The mono-, di- and trimethylation of the α-amino group on the first amino acid residue of histones is catalyzed by NTMTs

using SAM as the methyl donor . N-alpha terminal methylation is described as a constitutive PTM as NTDMs remain to be discovered (Demetriadou et al. 2020).

The addition of an acetyl group on lysine side chains neutralizes the positive charge of histone proteins and thereby weakens the association with the negatively charged phosphate backbone of DNA unlocking chromatin for transcription. Alternatively, acetyl lysine marks can function as docking sites for bromodomain-containing proteins which act as 'readers' of these acetyl tags in order to recruit additional effector proteins, such as chromatin remodelers, to alter chromatin architecture ultimately enabling access to the transcriptional machinery (Demetriadou and Kirmizis 2017).

The In-methylation (In-me) is commonly deposited on lysine or arginine residues by histone methyltransferases. Within this group of enzymes, protein lysine methyltransferases (KMTs), transfer methyl groups from S-adenosylmethionine (SAM) to the epsilon (N^{ε}) amino group of internal lysine residues (Figure 1.3D). Each individual lysine residue can be mono- (N^{ε}-monomethyllysine), di- (N^{ε}-dimethyllysine), or trimethylated (N^{ε}-trimethyllysine) (Figure 1.3D). KMT family includes a wide variety of histone methyltransferase enzymes with different specificities towards histone residues such as SET1, MLL1-4, SUV39H1/2, G9α, Ezh1/2, NSD1 and DOT1L (Hyun et al. 2017). On the other hand, the guanidino (N^{G}) amino group of internal arginine residues is monomethylated (ω-N^{G}-monomethyl-L-arginine) or asymmetrically (ω-N^{G}, N^{G}-dimethyl-L-arginine)/symmetrically (ω-N^{G}, N^{G}-dimethyl-L-arginine) dimethylated by arginine methyltransferases (PRMTs). PRMTs are divided into three major classes: type I (PRMT1, PRMT2, PRMT3, PRMT4, PRMT6, PRMT8) which catalyze asymmetric dimethylarginine, type II (PRMT5 and PRMT9) that deposit symmetric dimethylation and type III (PRMT7) that mediates the formation of

monomethylarginine (Blanc and Richard 2017). Generally, the function of histone In-methylation is more complex than In-acetylation since it associates with both active and repressed chromatin states depending on the histone amino acid residue bearing the modification as well as, the degree of methylation. Typically, H3K4me3, H3K36me3, H3K79me2, H4R3me2a, and H3R2me2s are associated with transcriptionally active euchromatin at Compartment A within the nucleus while H3K9me3, H3K27me3, H4K20me2, H4R3me2s and H3R2me2a are linked to transcriptionally silenced heterochromatin at Compartment B (Figure 1.2) (Black et al. 2012; Blanc and Richard 2017). Histone In-me exerts its effects on gene expression by recruiting effector proteins containing certain motifs such as chromo-, tudor- or PHD-domains that can read the methylation site and remodel nucleosomes rather than by altering the local chemical environment (Hyun et al. 2017). In-methylation on lysine residues can be reversed by demethylases (KDMs) which are categorized into two enzymatic groups: the FAD-dependent containing KDMs (eg. LSD1/KDM1A and LSD2/KDM1B) and the Jumonji C (JMJC) domain containing KDMs (eg. JHDM2, JARID1 and NO66) (Black et al. 2012; Shi et al. 2004; Tsukada et al. 2005). Although arginine demethylases remain to be identified, there is supporting evidence that arginine demethylation can be catalyzed by the JMJC enzymes (Blanc and Richard 2017).

For many decades research on histone modifications has been focused almost solely on the biological role of modifications occurring at the side-chain of internal amino acid residues. In contrast, modifications on the terminal N-alpha amino group of histones—despite being highly abundant and evolutionarily conserved—have been largely overlooked. In contrast to In-modifications, Nt-marks occur on the alpha-amino group of the first amino acid residue of the histone proteins mainly upon the removal of the initiator N-terminal methionine

(iNt-Met) by Met-aminopeptidases (MetAPs). These Nt-modifications occur through the action of histone N-terminal-transferases (NTTs) which can establish the acetylation and methylation of the α-amino group (Demetriadou et al. 2020). N-alpha terminal acetylation (Nt-ac) of histones involves the transfer of an acetyl moiety from Ac-CoA to the free α-amino group of the first amino acid residue on nascent polypeptides through the action of N-terminal acetyltransferases (NATs); whereas, N-alpha terminal methylation (Nt-me) involves the addition of 1–3 methyl groups from SAM to the α-amino group on the very N-terminal tip of histones, and is specifically catalyzed by N-terminal methyltransferases (NTMTs) (Figure 1.3E). Unlike the highly dynamic In-modifications, Nt-marks are so far believed to be static and removed passively through cell division or histone exchange since neither N-terminal deacetylases (NDACS) nor N-terminal demethylases (NTDMs) have to our knowledge been discovered yet.

1.3.3 Crosstalk amongst epigenetic modifications

Epigenetic modifications often cross-regulate each other in order to generate a highly dynamic interplay amongst chromatin marks, which is essential in defining gene expression patterns (Suganuma and Workman 2008). Such synergistic or antagonistic cross-talks can occur either on the same histone (*cis*), or between different histone tails within the same nucleosome or on neighboring nucleosomes (*trans*), thus creating a highly complex histone language originally described as the 'histone code' (Lee et al. 2010; Molina-Serrano et al. 2013). Deregulation of epigenetic enzymes disrupts the highly dynamic interplay between chromatin modifications leading to aberrant expression of oncogenes and tumour suppressor genes and thus carcinogenesis (Dawson and Kouzarides 2012).

For instance, deacetylation of H3K27 residue by the NURD complex triggers polycomb repressive complex 2 (PRC2) recruitment and the deposition of H3K27me3 by Ezh2 leading to gene silencing (Figure 1.4) (Reynolds et al. 2012). Additionally, H3S10ph reinforces GCN5 histone acetyltransferase to catalyze H3K14ac, which is associated with transcriptionally active chromatin (Figure 1.4) (Lo et al. 2000). Interestingly, H3S10ph also promotes the recruitment of MOF acetyltransferase within the FOSL1 enhancer to catalyze H4K16ac and promote transcription in a trans-tail regulation interplay (Figure 1.4) (Zippo et al. 2009). Another trans-histone cross-talk was recently unveiled where the combination of H4K16ac and H2BK123Ub marks directly stimulates the catalytic activity of Dot1 methyltransferase towards H3K79me2/me3

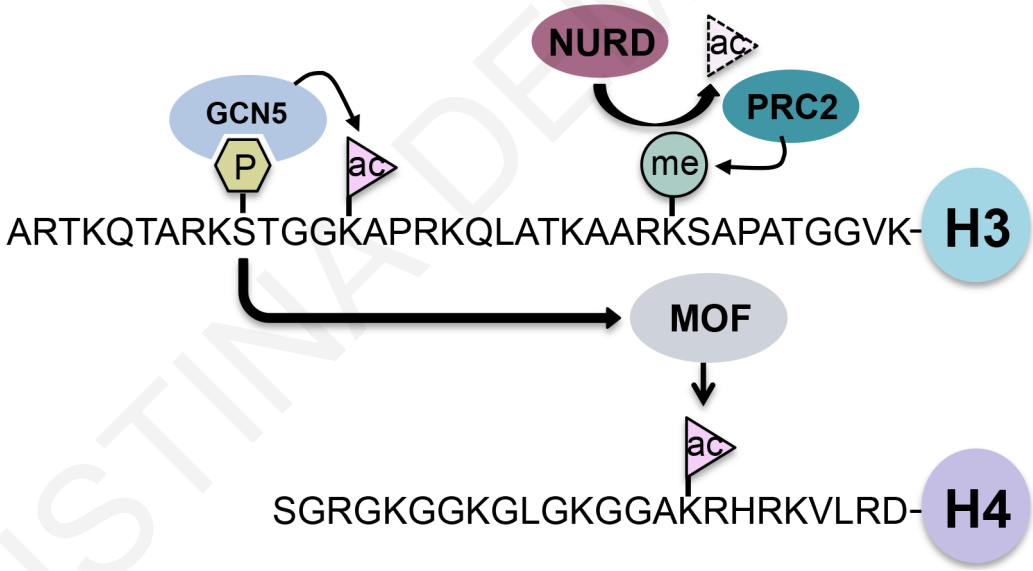

Figure 1.4. Interplay among histone marks. The wide variety of different histone modifications interplay with each other forming a complex web known as the "histone code". For instance, H3S10ph recruits GCN5 acetyltransferase to catalyze the adjacent H3K14ac. Additionally, removal of K27 acetylation by the NURD complex enables the recruitment of PRC2 complex to catalyze trimethylation on the same lysine residue. Cross-talk among histone modifications can also occur *in trans*. For example, H3S10ph can be also recognized by MOF acetyltransferase promoting acetylation of K16 on histone H4.

(Valencia-Sánchez et al. 2021). Additionally, it was recently reported that JARID2 and AEBP2 recognize and bind nucleosomes that are marked with H2AK119ub1, H3K4me3 and H3K36me3 to recruit PRC2 complex and mediate H3K27me3 (Kasinath et al. 2021). Of note, histone marks do not interplay only with each other but also with DNA methylation. For example, the ADD domain of DNMT3A and DNMT3B is occluded by the presence of H3K4me3 on the promoters of actively transcribed genes, while PRC2-mediated H3K27me3 can be repelled by DNMT3A-associated DNA methylation from the CGIs of neural genes during neurogenesis (Wu et al. 2010; Zhang et al. 2010). Additionally, DNMT3A recognizes and binds PRMT5-mediated H4R3me2s repressive mark to stimulate DNA methylation and support gene silencing (Zhao et al. 2009).

1.4 Linking metabolism with the epigenome

Epigenetic regulation of gene expression is in tune with cell metabolism dynamically influencing one another to maintain homeostasis (Figure 1.5). In fact, chromatin-modifying enzymes and their associated post-translational modifications (PTMs) alter the metabolome by modulating the transcription of genes encoding essential enzymes involved in metabolic pathways such as glycolysis, fatty acid synthesis and one-carbon metabolism (Dai et al. 2020; Li et al. 2018). Reciprocally, metabolic cell function controls the abundance of crucial intermediary metabolites which serve as substrates or co-factors of chromatin modifiers inevitably affecting epigenetic modifications (Figure 1.5) (Kinnaird et al. 2016; Schvartzman et al. 2018). Aberrant rewiring of these strongly interconnected pathways has been linked to a multitude of diseases, including diabetes, obesity, aging and cancer (Kinnaird et al. 2016; Campbell and Wellen 2018).

1.4.1 Metabolic control of the epigenome

The catalytic activity of writer and eraser enzymes towards chromatin covalent modifications is controlled by different metabolites. As the key regulators of transcription, histone acetylation and methylation of histones or DNA are reciprocally among the most responsive chromatin modifications to metabolic fluxes. More recently, metabolic regulation of additional histone marks, such as crotonylation and succinylation has been described (Figure 1.6) (Li et al. 2018).

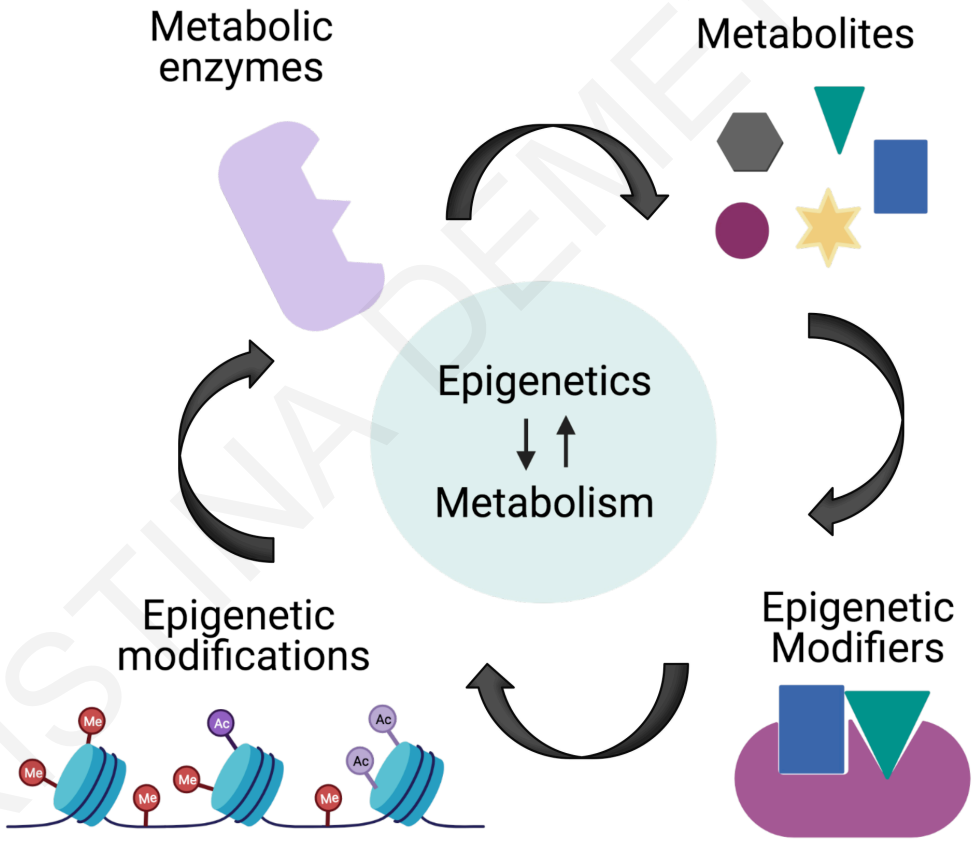

Figure 1.5. Epigenetics and metabolism cross-talk. Epigenetics and metabolism interact with each other. Epigenetic enzymes through chromatin modifications regulate the expression of genes encoding metabolic enzymes. Reciprocally, metabolic enzymes control the synthesis of intermediary metabolites which are utilized as substrates or cofactors of epigenetic enzymes to catalyze chromatin modifications such acetylation (ac) and methylation (me) on histones and/or DNA.

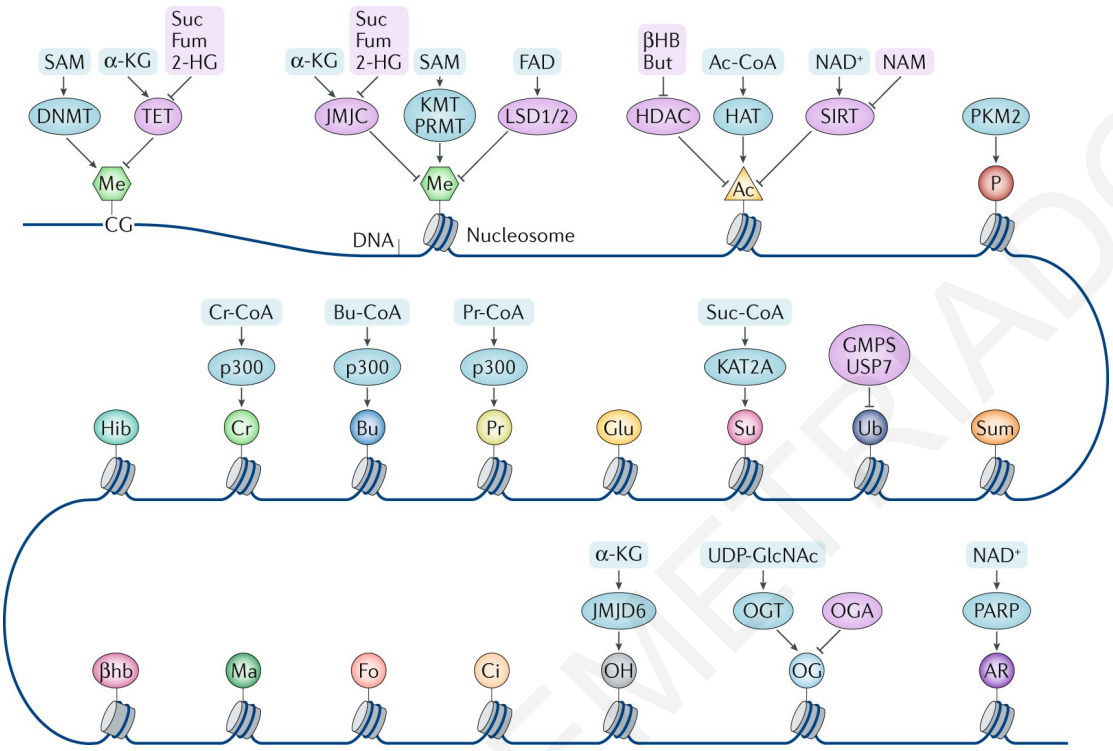

Figure 1.6. Epigenetic regulation by intermediary metabolites. The different covalent modifications on DNA and histone proteins are mediated or inhibited by metabolites that regulate the activity of epigenetic enzymes. Histone residues can be also modified directly by metabolic enzymes, such as PKM2. α-KG, α-ketoglutarate; βHB, β-hydroxybutyrate; βhb, β-hydroxybutyrylation; 2-HG, 2-hydroxyglutarate; Ac, acetylation; Ac-CoA, acetyl-CoA; AR, ADP ribosylation; Bu, butyrylation; Bu-CoA, butyryl-CoA; But, butyrate; Ci, citrullination; Cr, crotonylation; Cr-CoA, crotonyl-CoA; DNMT, DNA methyltransferase; Fo, formylation; Fum, fumarate; Glu, glutarylation; GMPS, GMP synthase; HAT, histone acetyltransferase; HDAC, histone deacetylase; Hib, 2-hydroxyisobutyrylation; JMJC, Jumonji C domain-containing demethylase; JMJD6, Jumonji domain-containing 6; KMT, lysine methyltransferase; LSD, lysine-specific histone demethylase; Ma, malonylation; Me, methylation; NAM, nicotinamide; OG, O-GlcNAcylation; OGA, O-GlcNAcase; OGT, O-GlcNAc transferase; OH, hydroxylation; P, phosphorylation; PARP, poly(ADP) ribose polymerase; PKM2, pyruvate kinase M2 isoform; Pr, propionylation; Pr-CoA, propionyl-CoA; PRMT, peptidyl-arginine methyltransferase; SAM, S-adenosylmethionine; SIRT, sirtuin; Su, succinylation; Suc, succinate; Suc-CoA, succinyl-CoA; Sum, sumoylation; TET, ten-eleven translocation (DNA demethylase); Ub, ubiquitylation; UDP-GlcNAc, uridine diphosphate N-acetylglucosamine; USP7, ubiquitin-specific processing protease 7 (Li et al. 2018).

1.4.1.1 Metabolic regulation of histone acetylation

HAT enzymes rely on acetyl-coA (Ac-CoA) intermediary metabolite as the sole acetyl donor for catalyzing either internal or N-terminal acetylation. Acetyl-CoA is produced by different enzymes during anabolic and catabolic pathways. It is primarily synthesized in the mitochondria from glucose-derived pyruvate through glycolysis by pyruvate dehydrogenase complex (PDC). Once it enters the tricarboxylic acid (TCA) cycle in the mitochondria, acetyl-CoA is combined with oxaloacetate to generate citrate. Citrate can then be exported in the cytoplasm and/or nucleus where it is used by ATP-citrate lyase (ACLY) enzyme to synthesize Ac-CoA within those compartments. Additionally, Ac-CoA can be generated from free acetate under stress conditions either through the function of acyl-CoA synthetase short-chain family members 1 and 3 (ACSS1/ACSS3) in the mitochondria or by the ACSS2 enzyme found within the cytosol or the nucleus (Figure 1.7) (Campbell and Wellen 2018; Haws et al. 2020; Schvartzman et al. 2018).

Fluctuations in the abundance of acetyl-CoA as a function of nutrient availability or disruption of the metabolic enzymes that produce it impact histone acetylation and gene expression (Sivanand et al. 2018; Kinnaird et al. 2016). For instance, high glucose concentrations induce ACLY-dependent histone hyperacetylation, while ACLY depletion reduces global histone acetylation which is accompanied by transcriptional repression of various glycolytic genes in a possible positive feedback loop mechanism (Wellen et al. 2009). Additionally, high acetyl-CoA availability produced by glucose or galactose in *Sacharomyces cerevisiae* enhances GCN5- mediated histone acetylation specifically at cell cycle progression genes to promote cell proliferation (Cai et al. 2011).

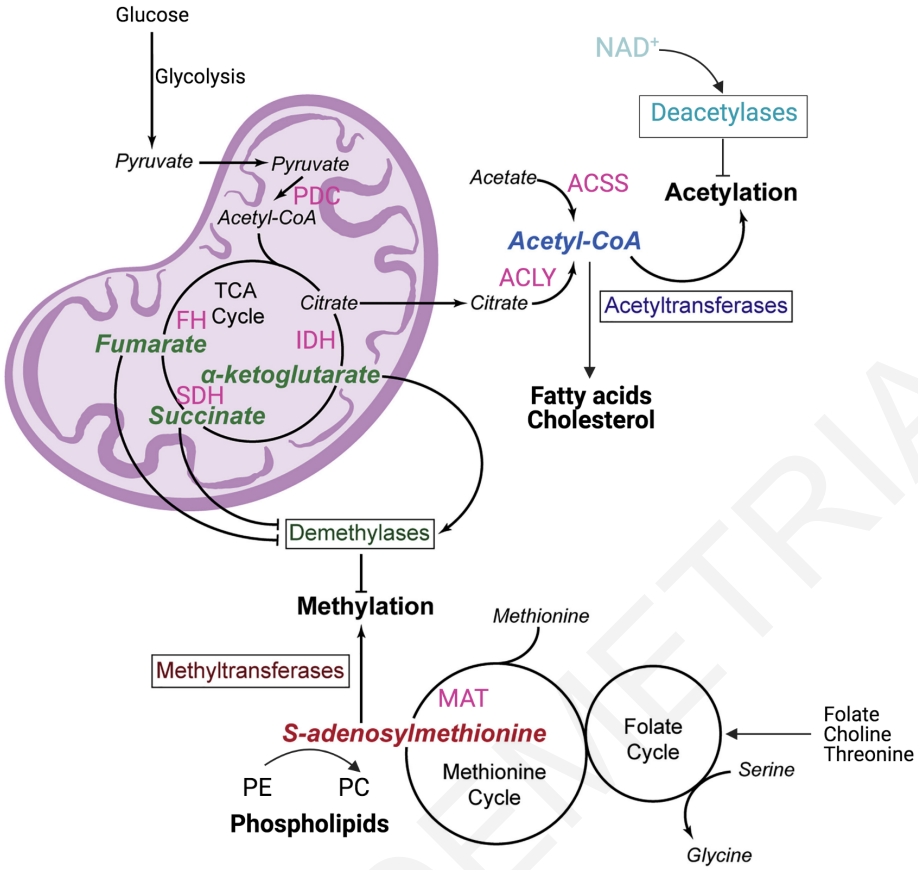

Figure 1.7. Metabolic regulation of acetylation and methylation. Metabolites derived from several biosynthetic pathways including the TCA cycle and one-carbon metabolism control acetylation and methylation reactions. Acetyl-CoA, produced from pyruvate, citrate or acetate by PDC, ACLY or ACSS enzymes, respectively supplies acetyl-groups for histone acetylation or alternatively for fatty acid and/or cholesterol synthesis. Histone acetylation is competed by sirtuins that use NAD^+ for the removal of acetyl groups. S-adenosylmethionine (SAM), synthesized by MAT enzyme in the methionine cycle donates carbon units for histone methylation while it can be also used for phospholipid production. Methylation turnover is mediated by demethylase enzymes whose activity is regulated by fumarate, succinate and α-ketoglutarate. ACLY, ATP-citrate lyase; ACSS, acyl-CoA synthetase short-chain; FH, fumarate hydratase; IDH, isocitrate dehydrogenase; MAT, methionine adenosyltransferase; PC, phosphatidylcholine; PDC, pyruvate dehydrogenase complex; PE, phosphatidylethanolamine; SDH, succinate dehydrogenase. Adapted from Campbell and Wellen 2018.

Histone acetylation in response to alterations in acetyl-CoA levels is competed by de novo fatty acid and cholesterol biosynthesis that also require acetyl-CoA (Figure 1.7). In addition to canonical acetyl-CoA-mediated histone acetylation, several histone acylation marks, including crotonylation, butyrylation, succinylation and propionylation require acyl-CoA groups such as crotonyl-CoA and propionyl-CoA (Figure 1.6). However, the metabolic enzymes involved and the effects of acyl-CoA fluctuations on histone acylation and gene expression await further study (Diehl and Muir 2020; Haws et al. 2020).

Histone deacetylation is also sensitive to changes in metabolite availability. The activity of Class I and Class II HDACs is inhibited by intermediary metabolites synthesized through fatty acid hydrolysis such as butyrate and β-hydroxybutyrate. Moreover, sirtuins require oxidized NAD (NAD^+) as a cofactor to deacetylate histones (Figure 1.7) (Chalkiadaki and Guarente 2012).

1.4.1.2 Metabolic control of chromatin methylation

Similarly to HATs, all histone and DNA methyltransferases utilize SAM intermediary metabolite as the primary methyl donor for both DNA and Internal/N-terminal histone methylation. SAM is synthesized in the methionine cycle from the adenylation of the essential amino acid methionine by the ATP-dependent methionine adenosyltransferase (MAT) (Figure 1.7) (Dai et al. 2020; Mentch and Locasale 2016). The methionine cycle is at the core of one-carbon metabolism that circulates carbon units derived from glucose, betaine or various amino acids (e.g. serine, glycine, threonine, methionine) used as “inputs” to produce several “outputs”, such as nucleotides, phospholipids, SAM and glutathionine supporting vital cellular

processes including DNA synthesis, lipogenesis, redox balance and epigenetic states (Figure 1.8). Within one-carbon metabolic network, methionine cycle is coupled to both the folate cycle and trans-sulfuration pathway which cooperate to sustain cellular homeostasis by governing the faithful dispersion of methyl units between the different outputs (Ducker and Rabinowitz 2017; Shuvalov et al. 2017).

By donating one methyl group to methyltransferases for the methylation of cytosine and histone residues or phospholipids, SAM is demethylated to form S-adenosyl-homocysteine (SAH), a competitive inhibitor of HMT and DNMT enzymes (Locasale 2013; Serefidou et al. 2019; Ye et al. 2017). Subsequently, SAH is hydrolyzed to homocysteine (hCYS) that enters the trans-sulfuration pathway to generate cysteine which is tightly linked to glutathionine synthesis and thus the maintenance of the redox state (Figure 1.8) (Locasale 2013). Importantly, in liver cells or under methionine-deprived conditions SAM intracellular pools are also supported by serine-derived methyl groups donated from the folate cycle for the recycling of hCYS back to methionine. The key enzyme that links the folate cycle with homocysteine remethylation and SAM synthesis is called Methylenetetrahydrofolatereductase (MTHFR) and catalyzes the transfer of a methyl group from 5,10-methyleneTHF (me-THF) to 5-methylTHF (m-THF).

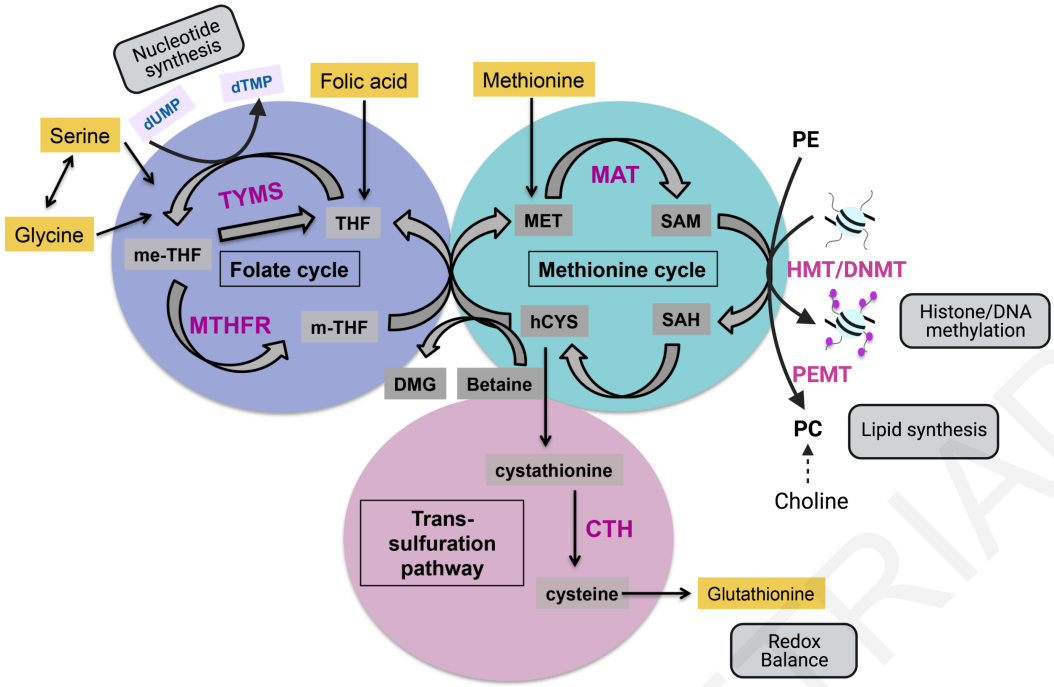

Figure 1.8. One-carbon metabolic network. One-carbon (1C) metabolism mainly consists of the three interconnected folate, methionine and transulfuration pathways which distribute carbon units among different acceptor molecules. Folate cycle is activated by methyl groups mainly derived from serine and glycine. me-THF is used by TYMS for the methylation of dUMP to dTMP serving nucleotide production and DNA synthesis. Alternatively, me-THF is reduced by MTHFR to m-THF which in turn donates one carbon unit for the remethylation of hCys resulting in the formation of methionine thus introducing methionine cycle. Methionine, which can also be obtained through diet, is used by MAT to form SAM which in turn donates a methyl group to HMTs/DNMTs or PEMT for chromatin methylation and lipidogenesis, respectively. hCys can be also recycled back to methionine through the conversion of betaine to DMG. After demethylation, SAM is converted to SAH which is then reduced back to hCys. The fraction of hCys that is not used for methionine remethylation enters the trans-sulfuration pathway for the synthesis of cysteine which is in turn used for glutathionine production supporting the cellular redox balance. CTH, cystathionine gamma-lyase; DMG, dimethylglycine; DNMT, DNA methyltransferase; hCYS, homocysteine; HMT, histone methyltransferase; MAT, methionine adenosyltransferase; me-THF, 5,10-methylenetetrahydrofolate; m-THF, 5-methyltetrahydrofolate; MTHFR, methylenetetrahydrofolatereductase; PC, phosphatidylcholine; PE, phosphatidylethanolamine; PEMT, PE methyltransferase; SAM, S-adenosylmethionine; TYMS, thymidylate synthase.

The latter supplies hCYS with the carbon unit needed for methionine formation. However, thymidylate synthase (TYMS), another key player of the folate cycle, converts deoxyuridine monophosphate (dUMP) to deoxythymidine monophosphate (dTMP) by competing with the MTHFR enzyme for the one-carbon unit me-THF therefore promoting DNA synthesis, at the cost of chromatin methylation (Figure 1.8) (Locasale 2013; Shuvalov et al. 2017). Moreover, SAM production can also be mediated through hCYS remethylation in a folate-independent manner via the utilization of choline-derived betaine as the carbon source resulting in methionine and dimethylglycine (DMG) (Serefidou et al. 2019).

Likewise to the effect of acetyl-CoA on histone acetylation levels, fluctuating levels of SAM based on nutrient availability or metabolic enzyme activity interfere with histone and/or DNA methylation (Schvartzman et al. 2018). Accumulating evidence shows that methionine deprivation in cultured cells rapidly lowers SAM abundance leading to global reduction of histone and/or DNA methylation levels (Mentch et al. 2015; Roy et al. 2020; Shiraki et al. 2014). In mouse embryonic stem cells (ESCs) reduction of SAM intracellular concentration via threonine restriction decreases histone methylation and in particular H3K4me2/me3, impeding pluripotency and stimulating differentiation (Shyh-Chang et al. 2012). Surprisingly, it was also shown that under methionine starvation conditions, serine contributes to intracellular SAM pools and DNA methylation by supporting *de novo* ATP synthesis independently of homocysteine remethylation (Maddocks et al. 2016). A supporting study depicted that lipopolysaccharide-induced inflammation of macrophages induces the methionine cycle and SAM accumulation through ATP synthesis leading to increased H3K36me3 occupancy in inflammatory genes (Yu et al. 2019). Beyond dietary interventions, chromatin methylation can be influenced by the activity of metabolic enzymes implicated in

SAM generation and catabolism. For instance, excess Nicotinamide N-methyltransferase (NNMT), which consumes a methyl group from SAM to form nicotinamide, reduces SAM abundance resulting in decreased levels of total histone methylation at various lysine residues such as H3K4, H3K9, H3K27 and H4K20 (Ulanovskaya et al. 2013). Accordingly, NNMT-mediated SAM buffering lowers H3K27me3 on key developmental and metabolic genes preventing naïve-to-primed transition of human ESCs (Sperber et al. 2015). Furthermore, elevated glycine N-methyltransferase (GNMT) expression, the enzyme responsible for the methylation of glycine to sarcosine using SAM as the methyl donor, dampens homocysteine remethylation flux and lowers SAM concentration which reduces global 5mC levels (Wang et al. 2011). An additional study showed that loss of LAT1-mediated uptake of methionine reduces intracellular SAM levels and therefore decreases the bulk levels of several histone methylation marks including H3K27me2/me3, H3K4me3 and H4K20me2 (Dann et al. 2015).

Despite the fact that serine-derived carbon units entering the folate cycle encompass a major source for SAM synthesis through homocysteine remethylation, studies showing how carbon flux between methionine and folate cycles affects epigenetic states are limited. As mentioned above, the utilization of folate cofactors and in particular methyleneTHF is competed by nucleotide and SAM synthesis through the opposing functions of TYMS and MTHFR, influencing genome stability and transcription. This metabolic competition is tightly regulated by various metabolic enzymes such as C1 tetrahydrofolate synthase (MTHFD1) and serine hydroxymethyltransferase (SHMT) (Herbig et al. 2002; MacFarlane et al. 2009). MTHFD1 deficiency in mice diminishes homocysteine remethylation and thus SAM levels which is accompanied by reduction of trans-sulfuration pathway activity with concomitant induction of thymidylate synthesis (MacFarlane et al.

2009). However, the impact of those changes on histone or DNA methylation is unclear.

Chromatin methylation turnover also requires the presence of metabolites that are primarily generated as intermediates of the TCA cycle. For example, TET and JMJD enzymes use isocitrate dehydrogenase (IDH)-mediated alpha ketoglutarate (α-KG) as a co-substrate for the removal of methyl groups from DNA and histone proteins respectively (Figure 1.7) (Dai et al. 2020). Conversely, metabolites such as succinate dehydrogenase (SDH)-dependent succinate and fumarate hydratase (FH)-dependent fumarate are structurally similar to α-KG and hence function as competitive antagonists blocking the demethylase activity of TETs and JMJDs (Figure 1.7) (Campbell and Wellen 2018; Li et al. 2018). Impairment of SDH and FH enzymes leads to substantial accumulation of succinate and fumarate potentiating global histone and DNA methylation by poisoning the activity of TETs, KDM2A and KDM4A (Xiao et al. 2012). In addition to JMJDs, the activity of LSD histone demethylases is dependent on the flavin adenine dinucleotide (FAD) cofactor that is synthesized by riboflavin (Etchegaray and Mostoslavsky 2016). Depletion of riboflavin kinase (RFK), mutation on the FAD binding site of LSD1 or treatment of adipogenic cells with a riboflavin antagonist lead to reactivation of LSD1-target genes (Hino et al. 2012). Together, these studies suggest that epigenetic reprogramming in response to metabolic rewiring changes the expression of certain genes controlling cell growth, proliferation and differentiation. Nevertheless, future research will be needed to unveil whether specific alterations in transcription are indeed reflective of global changes in histone modifications.

1.4.2 Epigenetic regulation of metabolism

Although several lines of evidence support the impact of cellular metabolic activity on chromatin modifications, the influence of epigenetic modifiers in the regulation of metabolism at the gene expression level is underexplored. Intriguingly, it was previously reported that SIRT6 acts as a crucial regulator of glucose metabolism through Hif1α-mediated recruitment at the promoters of important glycolytic genes encoding glucose transporter (GLUT), lactate dehydrogenase (LDH), pyruvated dehydrogenase (PDH) and phosphofructokinase-1 (Pfk-1) to mediate their transcriptional repression via H3K9 deacetylation (Zhong et al. 2010). Additionally, *de novo* serine synthesis is directly regulated by the function of G9A (EHMT2) histone methyltransferase towards H3K9me1 at the transcriptional start site of associated metabolic genes including phosphoglycerate dehydrogenase (PHGDC) and hydroxymethyltransferase 2 (SHMT2) activating their expression (Ding et al. 2013). The serine biosynthetic pathway, as well as the biosyntheis of other amino acids including alanine, arginine and cysteine were also found to be regulated by KDM4C demethylase at the gene expression level. Particularly, it was shown that KDM4C (JMJD2C) catalyzes the removal of H3K9me3 at the promoter of several amino acid biosynthesis genes, such as PHDGC, phosphoserine aminotransferase 1 (PSAT1), argininosuccinate synthase 1 (ASS1) and cystathionine gamma-lyase (CTH) accelerating their expression (Zhao et al. 2016). Moreover, LSD1 histone demethylase drives energy metabolism through demethylation of H3K4me2/me3 and epigenetic silencing of various energy-expenditure genes, such as PPARγ coactivator-1α (PGC-1α) and pyruvate dehydrogenase kinase 4 (PDK4) (Hino et al. 2012).

Beyond the more conventional gene regulatory mechanisms employed by histone modifications and their associated epigenetic modifiers, another intriguing possibility is that changes in the global levels of very abundant histone marks can also directly influence cellular metabolic homeostasis. A compelling hypothesis put forward lately is that due to the abundance of histone proteins, the consumption of intermediate metabolites, such as Ac-CoA and SAM, during the deposition of PTMs/CTMs can alter the metabolite pools and influence cell metabolism (Martinez-Pastor et al. 2013; Ye and Tu 2018). Another interesting example of chromatin-associated metabolic regulation that is independent of transcription lies in the histone variant macroH2A1.1. It was recently shown that during myogenic differentiation macroH2A1.1 directly binds PARP-1 and compromises nuclear NAD^+ consumption by the latter leading to increased levels of the NAD^+ precursor, NMN. High levels of NMN enable mitochondrial NAD^+ synthesis and respiration thus fine-tuning energy metabolism (Posavec Marjanović et al. 2017).

1.4.3 Rewiring of the epigenetic-metabolism axis in cancer

In order for tumour cells to acquire and maintain unabated cell proliferation they need to remodel their intertwined epigenetic and metabolic programs favoring macromolecule biosynthesis, energy production, activation of oncogenes and inactivation of tumour suppressor genes (DeBerardinis and Chandel 2016; Flavahan et al. 2017). Oncogenic mutations or aberrant expression of histones, chromatin modifiers and metabolic enzymes can drive tumour initiation and progression. Hence, expanding our knowledge on the molecular mechanisms through which this bidirectional link between the epigenome and metabolome

shapes cancer-associated phenotypes is highly challenging and could open new avenues in cancer therapy.

One of the most well-known examples of the metabolic and epigenetic interplay in cancer stems from the discovery of oncogenic mutations in the isocitrate dehydrogenase (IDH1 and IDH2) enzymes that catalyze the reduction of isocitrate (ICT) to α-KG. As a result, mutated IDH1/2 in acute myelogenous leukemias and low-grade gliomas catalyze the conversion of α-KG to the structurally similar D-2-hydroxyglutarate (2-HG) oncometabolite which acts as a competitive inhibitor blocking the activity of TET and several JMJD enzymes and increasing global DNA and histone methylation (Xu et al. 2011). In a subsequent study it was reported that IDH point-mutant gliomas display CpG hypermethylation at cohesin and CTCF-binding sites attenuating the recruitment of CTCF at a topologically associated domain (TAD) boundary which is crucial for obstructing the enhancer-receptor tyrosine kinase (PDGFRA) gene interaction and PDGFR silencing (Flavahan et al. 2015). In the absence of oncogenic mutations, IDH1 and IDH3 aberrant activity in glioblastoma interferes with histone and DNA methylation through deregulation of α-KG and SAM generation, respectively (Calvert et al. 2017; May et al. 2019). Moreover, loss of SIRT6 tumour suppressor function was found to induce oncogene-independent malignant transformation and tumour formation in mice through activation of genes involved in glycolysis and ribosome metabolism (Sebastián et al. 2012). In hepatocellular carcinoma, increased acetate consumption by ACSS1/2 enzymes under hypoxic stress conditions rapidly induces H3K9ac, H3K27ac and H3K56ac on the promoters of lipogenic genes including FASN and ACACA stimulating their expression and promoting *de novo* fatty acid synthesis and carcinogenesis (Gao et al. 2016).

Malfunctions in one-carbon metabolism and particularly in the interplay between nucleotide biosynthesis and SAM-dependent histone methylation pathways are also linked to cancer progression. For instance, NNMT is frequently upregulated in various tumour types such as lung, liver and colon cancers and contributes to oncogenesis by diminishing SAM pools and maintaining low global histone methylation levels (Ulanovskaya et al. 2013; Wong et al. 2017). Moreover, TYMS also harbors oncogenic potential accelerating malignant transformation and the growth of xenograft tumours through high dTMP synthesis (Rahman et al. 2004). Therefore, elevated serine-glycine biosynthetic pathway facilitates cancer progression by providing an unlimited carbon source for nucleotide production and DNA synthesis or repair supporting the high demands of rapid cancer cell proliferation (Gao et al. 2019). Nevertheless, how the oncogenic induction of nucleotide metabolism by TYMS impacts SAM synthesis advocating cancer-related phenotypes is still elusive.

The crosstalk between epigenetics and metabolism in cancer biology has translational implications that should be taken into consideration in drug discovery and application. In particular, drugs known to target metabolic pathways could also target the epigenetic landscape. For example, caloric-restriction mimetics, such as the ACLY inhibitor SB-204990 and hydroxycitrate deplete acetyl-CoA pools and reduce histone acetylation (Hatzivassiliou et al. 2005; Madeo et al. 2014). Additionally, AGI-5198 specific inhibitor of mutant IDH1 lowers 2-HG levels and reduces methylation on H3K9 and H3K27 residues suppressing glioma cell survival (Rohle et al. 2013). Moreover, inhibition of mutant IDH2 by AG-221 inhibitor decreases 2-HG accumulation and DNA hypermethylation promoting differentiation of leuckemic cells (Yen et al. 2017). On the other hand, small-molecule inhibitors targeting chromatin modifiers, such as the HDAC inhibitors

could suppress tumour growth and metastasis by influencing the metabolome (Wong et al. 2017). Currently the efficacy of such epigenetic inhibitors remains poor mainly because of their low substrate specificity modifying numerous histone and non-histone proteins.

Targeting one-carbon metabolism by antimetabolite therapy is amongst the most commonly used chemotherapeutic regimens for a wide range of cancers. In particular, antifolates such as methotrexate and pemetrexed act as competitive inhibitors of natural folates, whereas 5-Fluorouracil and gemcitibine function as nucleoside analogs directly targeting nucleotide biosynthesis (Shuvalov et al. 2017). However, cancer cells often develop resistant mechanisms to escape antimetabolite chemotherapy. Interestingly, a recent study showed that methionine restriction reduces SAM pools and histone methylation on various cell growth-related genes while it synergizes with 5-FU that targets TYMS impeding the expansion of patient derived xenograft tumours in mice (Dai et al. 2018; Gao et al. 2019; Mentch et al. 2015).

1.5 Protein N-alpha terminal acetylation

N-alpha terminal acetylation (Nt-acetylation) decorating both histone and non-histone proteins occurs on 50-70% of soluble yeast proteins and 80-90% of all cytosolic human proteins therefore considered as one of the most widespread modifications in eukaryotes (Aksnes et al. 2016; Starheim et al. 2012). The addition of the acetyl moiety neutralizes the positively charged free α-amino group, thus inhibiting ionization and other modifications to occur at the N-terminus, constructing a larger more hydrophobic N-alpha terminal residue and altering the electrostatic features of proteins (Ree et al. 2018).

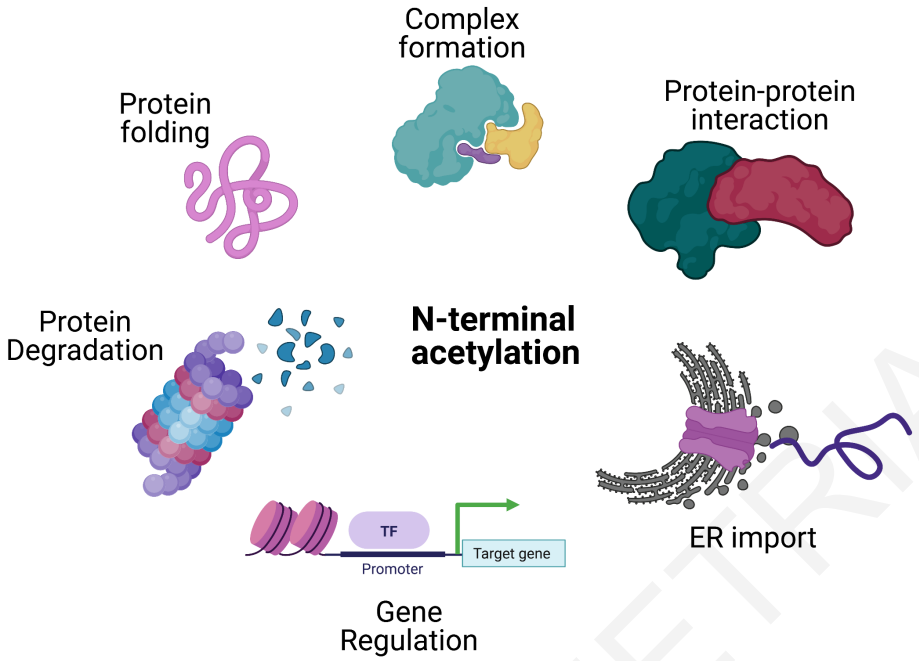

Figure 1.9. The different functions of protein N-terminal acetylation. N-terminally acetylated proteins can be targeted to proteasomal degradation through the Ac/N-end rule pathway. Alternatively, N-terminal acetylation can be involved in protein folding, protein-protein interactions, complex formation, ER import and regulation of gene expression. ER, endoplasmic reticulum; TF, transcription factor.

Traditionally, Nt-acetylation was considered a regulator of protein stability but over the years this role became highly controversial. Specifically, Nt-acetylation was shown to protect proteins from degradation by increasing their half-life and stability, whereas proteins with free α-amino groups were susceptible to ubiquitin-dependent proteasome-mediated protein degradation (Hershko 1984). However, more than two decades later, controversial evidence supports that acetylation of N-termini starting with Met, Ala, Val, Ser, Thr or Cys can act as a specific proteasomal degradation signal, termed Ac/N-degron, which is recognized by Doa10 and Not4 E3-ubiquitin ligases (Ac/N-recognins) (Hwang et al. 2010; Shemorry et al. 2013; Park et al. 2015). As a result, misfolded proteins or

abnormal assembly of protein complex subunits harboring N-terminal degrons are targeted for degradation through the Ac/N-end rule pathway, a new branch of the traditional N-end rule pathway (Shemorry et al. 2013; Lee et al. 2016). Recent work revealed new functional roles of Nt-ac beyond protein stability which involve protein-protein interactions, ER import and transcriptional control (Figure 1.9) (Aksnes et al. 2019; Ree et al. 2018).

1.5.1 Writing N-alpha terminal acetylation

N-alpha acetyltransferases (NATs) are the enzymes responsible for catalyzing Nt-acetylation. NATs are evolutionarily conserved enzymes and members of the GCN5-related N-acetyltransferase (GNAT) superfamily, all sharing the conserved Arg/Gln-X-X-Gly-X-Gly/Ala Ac-CoA binding motif (Deng and Marmorstein 2021; Varland et al. 2015). In total, eight NATs have been characterized thus far, designated NatA-NatH, differing in respect to their subunit composition and substrate specificity (Figure 1.10). In the lower eukaryote *Saccharomyces cerevisiae* five types (NatA-NatE) are present that are conserved in multicellular eukaryotes, which furthermore include NatF (Aksnes et al. 2019). The less conserved NatH is only found in the animal kingdom, while the plant specific NatG post-translationally modifies the N-alpha terminus of proteins in the chloroplast lumen of *Arabidopsis Thaliana* (Aksnes et al. 2019).

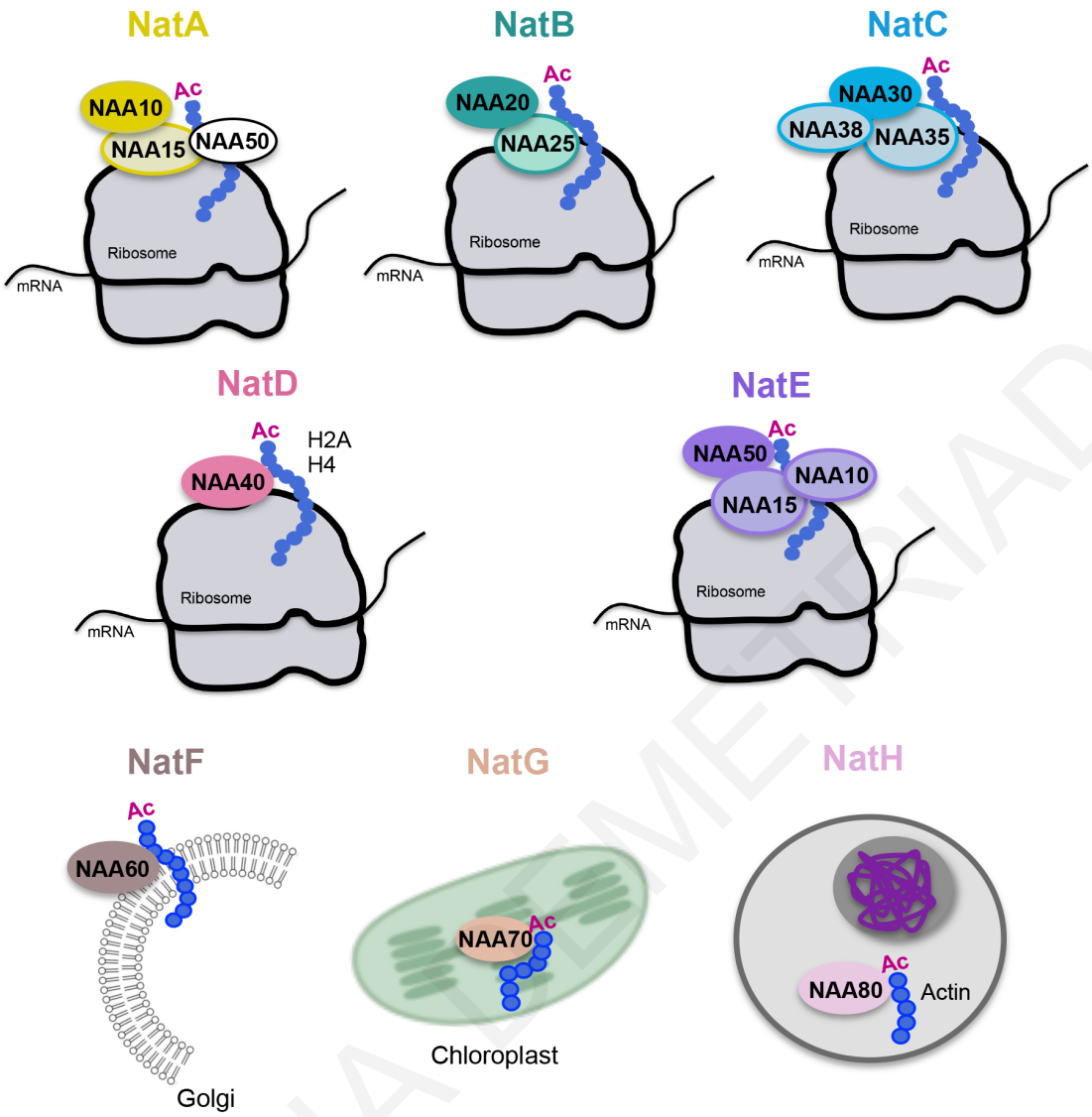

Figure 1.10. The writers of protein N-terminal acetylation. Eight N-alpha acetyltransferase (NAT) complexes namely NatA-NatH are composed of one catalytic subunit (NAA10, NAA20, NAA30, NAA40, NAA50, NAA60, NAA70 and NAA80) and up to two auxiliary subunits (NAA15, NAA25, NAA35 and NAA38). NatA-NatE are mainly bound to ribosomes within the cytosol. However, certain NATs are found in non-ribosomal forms. Specifically, NatF is localized to the Golgi membrane, NatG is found in the chloroplast lumen and NatH exist freely in the cytoplasm. Although most NAT complexes have broad substrate specificity, NatD and NatH are highly selective acetylating histone proteins and actin, respectively. Adapted from Aksnes et al., 2016.

The NAT complex is generally formed by a unique catalytic subunit and up to two auxiliary subunits that contribute to various functions including stability of the catalytic domain and ribosome anchoring (Figure 1.10). NATs are mainly

localized in the cytosol and are bound to ribosomes catalyzing Nt-acetylation in a co-translational manner when the first 25-50 amino acid residues of the emerging polypeptide chain protrude from the ribosomal exit tunnel (Gautschi et al. 2003). However, evidence indicates that distinct NAT subunits can also be localized in non-ribosomal forms within the nucleus or other organelles, suggesting that NATs may catalyze Nt-ac post-translationally, as well (Figure 1.10) (Drazic et al. 2018; Hole et al. 2011; Dinh et al. 2015; Van Damme et al. 2011).

Nt-acetylation can occur either on the alpha amino-group of initiator Nt-methionine (iNt-Met) or the first protein residue following excision of iNt-Met by MetAPs. The substrate specificity of NATs is usually resolved by the first two amino acid residues (Drazic et al. 2016). Classically, NATs were considered to be highly promiscuous in the number of proteins they modify. For instance, NatA and NatB target an estimated 38% and 21% of the human proteome respectively (Aksnes et al. 2019). More recently, examples have emerged of NATs which are more specific in their targeting by expanding their selectivity beyond the first two amino acid residues of their target proteins. An interesting case is NAA80 that acts selectively on Actin (Figure 1.10) (Drazic et al. 2018). Similarly, NAA40 is believed to specifically act on histones H4 and H2A (Figure 1.10) (Hole et al. 2011).

1.5.2 NAA40 in a NATshell

NAA40 was originally identified in the yeast *S.cerevisiae* (Song et al. 2003) and after almost a decade the conserved human NAA40 ortholog has been also characterized (Hole et al. 2011). As discussed above, in contrast to the other members of the family which have broad substrate selectivity, NAA40 catalytic activity is restricted towards histones H4 and H2A hence acting as an epigenetic modifier.

1.5.2.1 Nt-acetylation of histones H4 and H2A via NAA40

Nt-acetylation of histones H4 (N-acH4) and H2A (N-acH2A) is an evolutionarily conserved modification from yeast to humans (Hole et al. 2011). Proteomic investigations of PTMs/CTMs on histones H4 and H2A through MS-based methods have consistently revealed these modifications to be perhaps the most abundant marks of histone proteins. Examining mouse brains using an electron transfer dissociation MS method it was estimated that Nt-acetylation of H2A is at 87% and of H4 at 93%. In the same samples Nt-acetylation was also detected in 58% of canonical H1, but not for H2B or H3 peptides (Tweedie-Cullen et al. 2012). Independently, the group of Nicolas Young has found very high levels of N-acH4 in human cancer cells, specifically 97-98% in SUM159 and MCF7 breast cancer cell lines (Wang et al. 2018b; Wang et al. 2018a).

The common factor underlying Nt-acetylation on histones H4 and H2A is the specific catalysis of this modification by the NAT family member NAA40 that shares the conserved GNAT motif (Magin et al. 2015a). This specificity of NAA40 for these two histone proteins possibly arises from its exclusive recognition of the N-terminal sequence Ser(1)-Gly(2)-Arg(3)-Gly(4) (SGRG), found at the beginning of H4 and H2A (Magin et al. 2015b). Besides H4 and H2A, this recognition motif is also present at the N-terminal tail of the histone variant H2A.X that potentially could be subjected to Nt-ac by NAA40, but this has not been experimentally tested yet. Due to its structural divergence compared to other NATs, NAA40 does not require an accessory protein in order to function (Figure 1.10). Instead, the unique N-terminal segment of NAA40 is necessary to stabilize the catalytic core domain, whereas its target specificity is achieved through direct interactions with serine 1

(S1), arginine 3 (R3) and the flanking glycine (G2 and G4) residues on the histone proteins (Magin et al. 2015a).

While most of the HAT enzymes modify histone proteins post-translationally, NAA40 is predominately localized in the cytosol where it binds to ribosomes and thought to catalyze N-acH4/H2A in a co-translational manner (Figure 1.10) (Poledova et al. 1999). However, immunofluorescence and biochemical fractionation experiments indicate that NAA40 can be also found in non-ribosomal forms within the nucleus (Hole et al. 2011; Jonckheere and Van Damme 2021), implying that it may catalyze histone Nt-ac post-translationally as well.

1.5.2.2 The dynamic nature and biological functions of H4 Nt-acetylation

Over the past few years work originating from our group and others has revealed that Nt-ac of histone H4 (N-acH4) is a dynamic modification, which influences

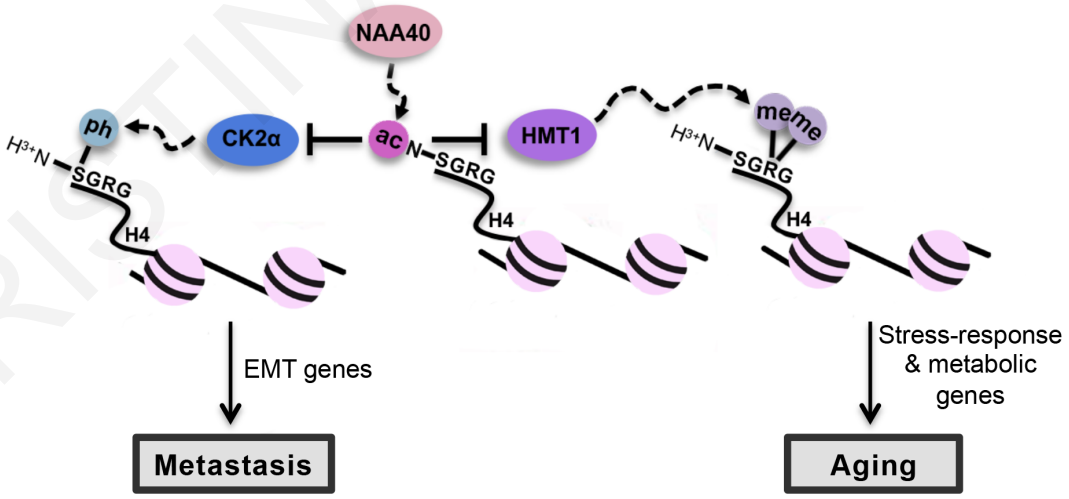

Figure 1.11. Interplay between N-terminal and Internal marks to control gene expression. N-terminal acetylation on histone H4 (N-acH4) blocks CK2α-mediated serine 1 (S1) phosphorylation controlling the expression of epithelial-mesenchymal transition (EMT) genes and promoting lung cancer metastasis.

Moreover, NAA40-mediated N-acH4 inhibits the activity of HMT1 towards H4R3me2a regulating metabolic and stress-response genes accelerating cellular aging. Adapted from Demetriadou et al., 2020.

important biological conditions such as cancer and longevity. Our group first postulated a role of N-acH4 in the control of ribosomal RNA expression and response to caloric restriction (Molina-Serrano et al. 2016; Schiza et al. 2013). Deletion of the yeast homolog of NAA40 (Nat4) and reduced deposition of N-acH4 induces Hmt1 methyltransferase to asymmetrically dimethylate histone H4 arginine 3 residue (H4R3me2a) leading to increased silencing of ribosomal DNA genes (Figure 1.11) (Schiza et al. 2013). In a subsequent study we reported that caloric restriction (CR) in yeast suppresses Nat4 expression and the associated loss of N-acH4 is an essential step in promoting the longevity effects of CR. In fact, constitutive overexpression of Nat4 was sufficient to reduce the lifespan extension associated with glucose starvation, and deletion of the enzyme mimicked caloric restriction at the transcriptomic level (Molina-Serrano et al. 2016). Functionally, it was shown that Nat4 and its corresponding N-acH4 control the CR-mediated longevity pathway by negatively regulating the expression of key metabolic and stress-response genes through crosstalk with methylation at the adjacent H4R3 residue. Of note, another study in mouse models has linked NAA40 to hepatic lipid metabolism and aging (Liu et al. 2012). In particular, NAA40 liver-specific knockout male mice exhibit reduced fat mass, aberrant lipid metabolism and are protected from age-associated hepatic steatosis (Liu et al. 2012).

Evidence for the involvement of NAA40 in cancer has also been presented in recently published studies. In lung cancer cells knockdown of NAA40 was shown to reduce invasion and metastasis *in vitro* and *in vivo*. The proposed mechanism

was that Nt-acetylation on serine 1 of histone H4 (N-acH4) antagonizes the CK2α-mediated phosphorylation on the side chain of the same serine residue (H4S1ph) to regulate Slug expression and metastasis (Figure 1.11) (Ju et al. 2017a). Recently, our group has reported that NAA40 can also affect the survival of colorectal cancer (CRC) cells. Loss of NAA40 in CRC cells triggered apoptosis through a p53-independent pathway (Pavlou and Kirmizis 2016). An additional article reported that NAA40 is downregulated in hepatocellular carcinoma tissues compared to its highly expressed levels in normal liver specimens supporting a potential context-specific tumour suppressive property of NAA40 (Liu et al. 2009b).

It is important to mention that the mechanisms through which Nt-ac of histones H4 and H2A influences gene expression are still incompletely understood. Although histone In-acetylation is a mark of active transcription (Kouzarides 2007), global reduction in H4/H2A Nt-acetylation was shown to cause both enhanced and reduced expression of specific genes depending on the molecular or cellular context (Molina-Serrano et al. 2016; Schiza et al. 2013). As mentioned before, direct cross-talk of Nt-acetylation with internal modifications has been implicated in the regulation of gene expression and cell phenotypes (Ju et al. 2017a; Schiza et al. 2013). This raises the possibility that the effects of N-acH4/H2A are propagated through the action of specialized “reader” and “eraser” proteins. Until now, there are no known deacetylases or readers acting on the acetylated histone N-terminal tip. However, further research is required to illuminate the biological and physiological relevance of N-acH4 and that of the less characterized NAA40-mediated N-acH2A.

1.6 Rationale and Scientific Hypothesis

Colorectal cancer (CRC) is driven by multiple genetic and epigenetic alterations and is considered the third most prevalent malignant neoplasm, with an incidence of over one million new cases diagnosed every year (Benson et al. 2018; Schmoll et al. 2012). Inhibition of nucleotide biosynthesis by antimetabolites, such as 5-FU is the frontline regimen for patients with colorectal cancer. Although considerable progress has been made in the diagnosis and treatment of this malignancy, CRC remains a major cause of cancer related mortality in both genders mainly as a result of an acquired resistance to 5-FU-based chemotherapy leading to disease recurrence (Benson et al. 2018; Schmoll et al. 2012). Thus, there is an urgent need to identify novel biomarkers that would predict poor drug response and eliminate treatment failure. Additionally, insights for new combinatorial therapies are needed in order to improve the efficacy of current conventional chemotherapies and overcome the poor clinical outcome of CRC patients.

Several lines of evidence have implicated NAA40 in tumorigenesis. A recent multi-omic analysis revealed that NAA40 is upregulated in a diverse range of cancers and correlates with poor overall survival of cancer patients (Koufaris and Kirmizis 2020). Our group has also previously unveiled a pro-survival role for NAA40 in CRC cells suggesting that it may stimulate cancer cell growth (Pavlou and Kirmizis 2016). Furthermore, it was shown that NAA40 and its associated N-acH4 directly regulate the expression of certain genes to control aging and cancer metastasis through crosstalk with H4R3me2a and H4S1ph marks, respectively (Figure 1.11) (Ju et al. 2017a; Schiza et al. 2013).

Based on the above evidence, we hypothesized that NAA40 and its corresponding histone N-terminal acetylation would have a regulatory role in

sustaining colorectal carcinogenesis by monitoring transcription through cross-talk with adjacent histone marks.

1.7 Specific objectives of the project

The overarching objective of the current project is to decipher the role of NAA40 in CRC and unravel the molecular mechanism through which NAA40 promotes the malignant properties of colorectal cancer cells. In order to accomplish this objective we divided our project into two specific aims:

Aim 1: Elucidate the role of human NAA40 in gene expression and colon cancer development

During this aim we explored NAA40 deregulation in colorectal cancer patient samples and deciphered the effects of NAA40 depletion in CRC cell lines and xenograft tumours. Additionally, we examined the crosstalk of NAA40 with histone arginine methylation in CRC cells.

Aim 2: Evaluate NAA40 function at the intersection of metabolism and epigenetics to control chemoresistance

During the second aim of the project we investigated the regulatory link between NAA40 and cancer cell metabolism, and explored how this link contributes towards the development of CRC drug resistance.

CHAPTER 2

METHODOLOGY

2.1 Cell culture

The HCT116 cell line was kindly provided by Dr. Pantelis Hatzis (Biomedical Sciences Research Center 'Alexander Fleming') and the HT-29 (catalogue no. HTB-38), SW480 (catalogue no. CCL-228) and SW620 (catalogue no. CCL-227) cell lines were purchased from ATCC. All CRC cell lines were cultured in McCoy's 5a medium (Gibco, Invitrogen) supplemented with 10% fetal bovine serum (Gibco, Invitrogen) and 1% penicillin/streptomycin (Gibco, Invitrogen). The human embryonic kidney HEK-293 T (catalogue no. CRL-3216) cell line was purchased from ATCC and was cultured in DMEM medium (Gibco, Invitrogen) supplemented with 10% fetal bovine serum and 1% antibiotic (penicillin/streptomycin). Cells were grown in a humidified atmosphere at 37^{o}C containing 5% CO_2 and were routinely tested for mycoplasma contamination. All cell lines were used to construct dox-inducible shRNA-knockdown lines for NAA40 or Scramble (SCR) control as previously described (Demetriadou et al). For CK2α inhibition cells were treated with 7 μM or 5 μM of CX-4945/Silmitasertib (HY-50855, MCE) for 24 h and 48 h, respectively.

Table 1: List of shRNA oligos

Name	Forward	Reverse
SCR	CCGGTTCTCCGAACGTGTCA CGTTTCTCGAGAAA CGTGAC ACGTTCGGAGAATTTTTG	AATTCAAAAATTCTCCGAACG TGTCACGTTTCTCGAGAAACG TGACACGTTCGGAGAA
NAA40-KD1	CCGGGGAAGTTCCTCATACA GATCCCTCGAGGGATCTGTA TGAGGAACTTCCTTTTTG	AATTCAAAAAGGAAGTTCCTC ATACAGATCCCTCGAGGGAT CTGTATGAGGAACTTCC
NAA40-KD2	CCGGGAAGGTTATGTTAACA GTATTCTCGAGAATACTGTTA ACATAACCTTCTTTTTG	AATTCAAAAAGAAGGTTATGT TAACAGTATTCTCGAGAATAC TGTTAACATAACCTTC

2.2 Plasmid construction, lentivirus production and infection

The annealed shSCR and shNAA40 sequences were introduced between *AgeI* and *EcoRI* restriction sites in the lentiviral Tet-pLKO-puro vector (Addgene plasmid # 21915). The short hairpin RNA oligonucleotides used for plasmid construction were purchased from Integrated DNA Technologies (IDT) (Table 1). The pLenti/p53-V5_wt plasmid (Addgene,

#22945) containing a C-terminal V5 tag was used in which p53 was replaced with the full-length human NAA40 cDNA subcloned from pOTB7 vector between BamHI and XhoI restriction sites constructing the pLenti/NAA40-V5_wt plasmid (Sensitive NAA40(WT)-V5). As a control, pLenti/V5-empty vector (Empty vector) was used that is not encoding for anything between the two restriction sites. To generate the shRNA-resistant constructs, six silent mutations were introduced by site-directed mutagenesis using the Pfu Turbo DNA polymerase (Agilent Technologies) in the region of NAA40 cDNA that is targeted by NAA40-KD2 shRNA (5'-GAAAGTGATGCTGACGGTGTT-3' where substituted nucleotides are underlined) hence constructing the shRNA-resistant wild-type pLenti/NAA40-V5rescue plasmid (Resistant NAA40(WT)-V5). The synonymous mutations have been introduced sequentially using three different sets of primers (Table 2). Catalytically dead Resistant NAA40(E139Q)-V5 plasmid was generated by site-directed mutagenesis of the pLenti/NAA40-V5rescue vector. The primers used for the site-directed mutagenesis were purchased from Integrated DNA Technologies (IDT) (Table 2). The generated constructs were verified by DNA sequencing. For lentiviral packaging, each of the recombinant vectors was

Table 2: Primers for the generation of overexpression constructs

Subcloning of NAA40 cDNA from the pOTB7 vector	**Forward**	**Reverse**
Subcloning primer set	TGCGGATCCAATGGGGAGAAAGTCAAGC	TTGCTCGAGCCGTGGCAGCAGCCACCACA
Generation of the Empty vector plasmid	**Forward**	**Reverse**
Empty vector primer set	CGACTGGATCCACGACGCAAGGAATTTCGGACTCTCGAGGACTC	GAGTCCTCGAGAGTCCGAAATTCCTTGCGTCGTGGATCCAGTCG
Generation of the shRNA Resistant plasmid	**Forward**	**Reverse**
Rescue primer set A	GCACACAGATGAAGAAAGTGATGTTAACAGTA	TACTGTTAACATCACTTTCTTCATCTGTGTGC
Rescue primer set B	GAAGAAAGTGATGCTGACAGTATTTA AACAC	GTGTTTAAATACTGTCAGCATCACTTTCTTC
Rescue primer set C	GAAAGTGATGCTGACGGTGTTTAAACACAATCATGG	CCATGATTGTGTTTAAACACCGTCAGCATCACTTTC
Generation of the catalytic mutant shRNA Resistant plasmid	**Forward**	**Reverse**
Catalytic mutant primer set	GTCCTGTACTGCTATCAAGTGCAGTTGGAAAGC	GCTTTCCAACTGCACTTGATAGCAGTACAGGAC

co-transfected with the psPAX2 lentivirus packaging vector and the PMD2G lentivirus envelope plasmid in HEK-293T cells by using X-tremeGENE 9 DNA transfection reagent (Roche) according to manufacturer's instructions. Upon 48 h of transfection the virus containing supernatant was collected and used to stably

infect CRC cells in the presence of 10μg/ml polybrene. The pool of efficiently transduced cells was selected in complete McCoy's 5a medium containing 2 μg/ml puromycin (Sigma-Aldrich) for 96 h and/or 20μg/ml BlasticidinS-HCL (A1113903, Thermo Fisher Scientific) for 4 d. For the shRNA induction, cells were treated with doxycycline hyclate (Sigma-Aldrich) at an assay dependent concentration and time period.

2.3 Transient RNA interference

Non-targeted scramble siRNA (SCR) and two NAA40-specific siRNAs (NAA40-KD1 and NAA40-KD2) were purchased from GenePharma (Shanghai, China) (Table 3). The NAA40 siRNA1 and NAA40 siRNA2 sequences were taken from Liu *et al*. (Liu et al. 2009a). The HCT116 cells were seeded in antibiotic-free medium and grown to 30%-40% confluence at the time of transfection. Subsequently, the cells were transiently transfected with 7.5 nM of siNAA40, 20nM of siMTHFR (4392420, s9036, Ambion), 10nM of siTYMS (4392420, s14538, Ambion) or the negative control for 72 h using Lipofectamin RNAiMAX (Invitrogen) according to manufacturer's instructions. Parental HCT116 cells treated with siNAA40 for 24 h were transfected with 1 μg of pcDNA-myc-empty or pcDNA-myc-PRMT5 expression vectors kindly provided by Prof. Naoya Fujita (Cancer Chemotherapy Centre of JFCR) using X-tremeGene9 reagent (Sigma-Aldrich), for 48 h. MTHFR knockdown was preformed in HCT116/SCR and HCT116/NAA40-KD stable cells in the presence or absence of 1μg/ml doxycycline. For TYMS silencing experiments, the transiently transfected HCT116 Empty vector or o/e NAA40(WT)-V5 stable cells were also treated with 5 μM of 5-FU (F 6627, Sigma) or DMSO control (Gibco, Invitrogen).

Table 3: List of siRNA oligos for transient transfection

Name	Forward	Reverse
SCR	UUCUCCGAACGUGUCACGUTT	ACGUGACACGUUCGGAGAATT
NAA40-KD1	CUUUCCCAGUGUUCAAGAATT	UUCUUGAACACUGGGAAAGTT
NAA40-KD2	GAAGGUUAUGUUAACAGUATT	UACUGUUAACAUAACCUUCTT

2.4 Immunofluorescence analysis in patient-derived tissues

The patient tissue microarrays were purchased from Abcam (ab178122, ab178131 and ab178132). The slides were heated at 60^{o}C for 30 min and then permeabilised at RT in 4% paraformaldehyde for 10 min. After blocking in PBG (0.2% cold water fish gelatin, 0.5% BSA in 1X PBS) for 45 min, the tissues were incubated with the NAA40 antibody (1:100; ab106408, Abcam) overnight at 4^{o}C. Slides were stained with anti-rabbit FITC-conjugated secondary antibody (1:500; 711-095-152, Jackson ImmunoResearch) for 1 h at RT. Nuclei were visualized with DAPI (Dako). Immunofluorescence images were acquired using a ZeissAxio Observer.A1 microscope.

2.5 Meta-analysis of CRC datasets

Colorectal cancer data were extracted from The Cancer Genome Atlas (TCGA) datasets TCGA-COAD (colon adenocarcinoma, n=480) and TCGA-READ (rectum adenocarcinoma, n=167) and represent only untreated primary tumors. Normal solid colorectal tissue data were also extracted from the same datasets (colon normal, n=41 and rectum normal, n=10). Patients who received neo-adjuvant therapy were excluded from the study. In specific, we extracted “level 3” mRNA-seq expression data of the genes of interest (NAA40, PRMT5, PRMT7), along with

the corresponding patient clinical information from the Genomic Data Commons (GDC) Data Portal of TCGA program (https://portal.gdc.cancer.gov/). Total raw read counts per gene were divided by the gene's maximum transcript length to represent a coverage depth estimate. Coverage estimates were then scaled to sum to a total depth of 1e6 per sample and interpreted as Transcripts Per Million (TPM) after adding a 0.01 offset to remove the zero counts from calculations. RNA-seq expression data for NAA40 and TYMS mRNA levels in colorectal cell lines were obtained from Depmap portal (https://depmap.org/portal/) (Ghandi et al. 2019) where the cancer genome atlas (TCGA) data where obtained using the UCSC Xena tool (Goldman et al. 2019). Pearson's correlation was then calculated. NAA40 microarray data were extracted from GEO omnibus for two studies of colorectal cancer patients receiving FOLFOX chemotherapy regiment and for which patients were classified into "responders" and "non-responders" (GSE69657 and GSE28702). For both these studies transcriptomics were performed using the same platform (GPL570 [HG‐U133_Plus_2] Affymetrix Human Genome U133 Plus 2.0 Array). The values for the two NAA40 probes in this platform (222369_at and 218734_at) were extracted and averaged without any further normalisation. P values were calculated using Fisher method.

2.6 MTT assay

To assess cell viability, CRC cells were seeded in a 96-well plate at a concentration of $2{,}5x10^4$ cells/ml. At the end of each treatment, 1 mg/ml MTT dye (Invitrogen) was added to each well and then cells were placed at 37^{o}C for 3 h. The formazan product was solubilized in DMSO and the plate was shaken for 20

min in dark. The absorbance was read at 570 nm by using a Perkin Elmer Wallac Victor 1420-002 Multilabel Counter.

2.7 Cell cycle analysis

Cells were harvested by trypsinization, washed in 1X PBS and fixed in 70% ice-cold ethanol overnight at 4^{o}C. Fixed cells were pelleted by centrifugation at 2000 rpm for 5 min and resuspended in 1X PBS with 0.2 mg/ml RNase A (12091-021, Invitrogen) and 0.01 mg/ml PI (40017, BIOTIUM). After incubation at 37^{o}C for 30 min, samples were analyzed using Guava EasyCyte^{TM} flow cytometer and the GuavaSoft analysis software (Millipore, Watford, UK).

2.8 Tumor xenografts in nude mice

The xenograft studies were performed at the animal facility of the Cyprus Institute of Neurology and Genetics under animal project license (CY/EXP/PR.L10/2018) issued and approved by the Cyprus Veterinary Services which is the Cyprus national authority for monitoring animal research for all academic institutions according to the regulations contained in the Cyprus Law N.55 (I)/2013 and the EU Directive 2010/63/EU. Regarding the knockdown experiments, a total of 2.5 x 10^6 NAA40-KD2 or SCR control HCT116 and 2.5 x 10^6 NAA40-KD2 or SCR control HT-29 cells were suspended in 40 μl serum-free McCoy's 5a medium and inoculated subcutaneously in the flank of 6-week old male CD1 nude immunodeficient mice. Once the tumors reached an average size of about 100 mm^3 (HCT116) or 50 mm^3 (HT-29), all groups were size-matched (n=7) and mice received daily 0.2 ml dox (100 mg/kg) or PBS (-dox/control) through oral gavage. For the overexpression experiments, 2.5x10^6 HCT116 cells stably transfected with

Empty vector or o/e NAA40(WT)-V5 plasmid were suspended in 40 μl of serum-free McCoy's 5a medium and inoculated subcutaneously in the left flank of 6 week-old male CD1 nude immunodeficient mice. Once the tumors reached an average size of about 50 mm^3 (day 10) groups were size-matched (n=8) and mice were treated with 5-FU (50 mg/kg every 72 hours) or saline vehicle control through intraperitoneal injection. Throughout the experiment, mice were monitored for their overall health condition. Tumor volume was measured using a digital caliper and calculated using the volume of an ellipsoid and assuming that the third dimension, *z*, is equal to $\sqrt{x\,y}$. Therefore, the volume was given by the equation: $V = \frac{4\pi}{3}\frac{(xyz)}{8}$. At the end of each study mice were euthanized and tumors were excised, weighted and subjected to histological analysis.

2.9 Histological analysis of xenograft tumors

Primary tumors isolated from mice inoculated with either HCT116 or HT-29 colorectal cancer cells (NAA40-KD2 or SCR control, as described above), were fixed in 4% parafolmaldehyde and embedded in paraffin. Tissue sections (10μm-thick) were performed using an SRM200 microtome (Sakura), followed by staining with hematoxylin and eosin (H&E) using standard protocols, as previously described(Papageorgis et al. 2015). Immunohistochemical detection of mitotic cells and PRMT5 protein levels was performed by staining sections with anti-Ki67 (1:50; ab15580, Abcam) and rabbit anti-PRMT5 (1:100; cat. 07-405, Millipore) antibodies, respectively, followed by FITC-conjugated secondary antibodies (1:400; 711-095-152, Jackson ImmunoResearch). All nuclei were stained with DAPI (Dako). Immunofluorescence microscopy images were obtained using a BX53 (Olympus) fluorescence microscope.

Table 4: List of qRT-PCR primer sequences

Gene name	Forward	Reverse
NAA40	ATGTAAGCGAGTGTCTGGACT	TGGTTTGCATATTCGTTTTGGTC
β-actin	AGAGCTACGAGCTGCCTGAC	AGCACTGTGTTGGCGTACAG
PRMT5	TTGCCGGCTACTTTGAGACT	ACAGATGGTTTGGCCTTCAC
PRMT7	AGTGTGTGTACTTCCTGCCA	TAGTCATCGTGGTGGGCTAC
EIF4E	GGTGCCTGACATCGTGTTTT	AACACAGAGCCCCAACAGTA
FGFR3	CTGTACGTGCTGGTGGAGTA	GCAGGTGTCGAAGGAGTAGT
CDKN1A	TGTCTTGTACCCTTGTGCCT	CTGAGAGTCTCCAGGTCCAC
RBL2	TTGTTGGGTGCTTTTTATATATGC	TTTCCATAAACTAAGTCCAAAGCA
CDH1	TTGCACCGGTCGACAAAGGAC	TGGAGTCCCAGGCGTAGACCAA
THOC1	TGTGGACGGATTCAGCTCTT	GGGTGCTTTCCTGCTCATTT
C-MYC	CAGCTGCTTAGACGCTGGATTT	ACCGAGTCGTAGTCGAGGTCAT
MYB	GTCCGAAACGTTGGTCTGTT	GCCACCTCTCCCTACATTGT
POLA1	ATGTGTGCAAAGCTCCTCAC	CTTTGGCATGTTGGATCGCT
TYMS	GGGACTTGGGCCCAGTTTAT	CTTCTGTCGTCAGGGTTGGT
MTHFR	AGCCGATTTCATCATCACGC	CATGCCTTCACAAAGCGGAA
MAT1A	TGCTGCTGTGTGGTGAGAT	GATGTGCTTGATGGTGTCCC
CTH	CCACCCAGAAGGTGATTGA	CACGACCAAAATAATGTCTCC
MMAA	TGCATACATCAGGCCATCTC	GCTTCATTTGTGGTCCTTGTC
IFIT1	TTCTCCTTGCCCTGAAGCTT	TCTGTGAGGACATGTTGGCT

2.10 RNA extraction and quantitative Real Time PCR

Total RNA was extracted using the RNeasy Mini kit (Qiagen) according to the manufacturer's instructions and was then treated with DNAse using the TURBO

DNAse kit (Ambion). An amount of 0.5 μg total RNA was then reverse transcribed to complementary DNA using the PrimeScript RT reagent kit (Takara) with random primers. qRT-PCR was carried out using KAPA SYBR Green (SYBR Green Fast qPCR Master Mix) and the Biorad CFX96 Real-Time System. Expression data were normalized to the mRNA levels of the β-actin housekeeping gene and calculated using the $2^{-\Delta\Delta Ct}$ method. Primer sequences were obtained from IDT (Table 4).

2.11 RNA-sequencing and bioinformatics analysis

Total RNA was isolated from the HCT116/SCR and HCT116/NAA40-KD engineered cells in the presence or absence of 1μg/ml dox for 96 h using the RNeasy mini kit (Qiagen) according to manufacturer's instructions. Four independent RNA samples were prepared from each of the four conditions: SCR (-dox), SCR (+dox), NAA40-KD (-dox) and NAA40-KD (+dox). Efficient NAA40 knockdown was evaluated through qRT-PCR using specific primers against NAA40 and β-actin (Supplementary Table 2). Total RNA was isolated from the HCT116/SCR and HCT116/NAA40-KD engineered cells in the presence or absence of 1μg/ml dox for 96 h using the RNeasy mini kit (Qiagen) according to manufacturer's instructions. Four independent RNA samples were prepared from each of the four conditions: SCR (-dox), SCR (+dox), NAA40-KD (-dox) and NAA40-KD (+dox). Efficient NAA40 knockdown was evaluated through qRT-PCR using specific primers against NAA40 and β-actin (Supplementary Table 2). Sequencing libraries were prepared using the NEBNext stranded RNA library prep kit according to the manufacturer's protocol. Sequenced reads were aligned to the mm10 genome via STAR (v 2.4.1b) (Dobin et al. 2013). Gene counts were

calculated using featureCounts of the Rsubread package (R/Bioconductor). Only reads with counts per million > 1 were kept for subsequent analysis. Counts were normalized using the internal TMM normalisation in edgeR (Robinson and Oshlack 2010) and differential expression was performed using the limma package (Ritchie et al. 2015). Significant genes with an absolute logFC > 1 and adjusted *P*-value < 0.05 were considered differentially expressed.

2.12 Protein extraction

Protein extracts were isolated using Lysis Buffer (50 mM Tris-HCL pH 8, 3 mM EDTA, 100 mM NaCL, 1% Triton-X-100, 10% glycerol, 0.5 mM PMSF and 1X protease inhibitor cocktail) and total protein concentration was quantified by Bradford assay (BioRad). For efficient NAA40 detection, whole cell extracts were resuspended in a tenfold volume of Laemmli sample buffer (50 mM Tris-HCL pH 6.8, 2% SDS, 10% glycerol, 1% β-mercaptoethanol, 12.5 mM EDTA and 0.02% bromophenol blue) and alternatively boiled and chilled three times to disrupt cell membranes. For histone acid extraction, cells were lysed in hypotonic lysis buffer (10 mM Tris-HCL pH 8, 1 mM KCL, 1,5 mM $MgCl_2$, 0,1% Triton X-100 and 1X protease inhibitor cocktail) and incubated for 30 min with constant agitation at 4^{o}C. Isolated nuclei were then washed once in hypotonic lysis buffer and after centrifugation at 6,500g for 10 min, were resuspended in 0,2 M HCL (4X10^{7} nuclei per ml) and incubated overnight with constant rotation at 4^{o}C. Histones were isolated by centrifugation at 6,500 g for 10 min and the pH was neutralized with 2M NaOH at 1/10 of the volume of the supernatant.

Table 5. List of antibodies

Antibody name	Host species	Dilution	Catalog #	Vendor
PRMT5	Rabbit	1:5000	07-405	Millipore
PRMT7	Rabbit	1:2000	07-639	Millipore
H4	Rabbit	1:1000	05-805	Millipore
H4R3me1	Rabbit	1:1000	ab17339	Abcam
H4R3me2a	Rabbit	1:1000	ab8284	Abcam
H4R3me2s	Rabbit	1:1000	ab5823	Abcam
c-myc	Rabbit	1:2000	sc-763	Santa Cruz
H4/H2AS1ph	Rabbit	1:1000	ab177309	Abcam
H3K4me3	Rabbit	1:2000	ab8580	Abcam
H3K36me3	Rabbit	1:2000	ab9050	Abcam
H3K9me3	Rabbit	1:1000	ab8898	Abcam
H3K27me3	Rabbit	1:1000	39156	Active motif
H3K79me3	Rabbit	1:1000	ab2621	Abcam
H3K79me2	Rabbit	1:1000	ab3594	Abcam
H3	Rabbit	1:4000	ab1791	Abcam
H2A	Rabbit	1:1000	Ab18255	Abcam
β-actin	Rabbit	1:1000	sc-1616-R	Santa Cruz
V5	Rabbit	1:10,000	AB3792	Millipore
GAPDH	Rabbit	1:2000	ab9485	Abcam
Lamin A/C	Mouse	1:1000	ab238303	Abcam
NAA40	Rabbit	1:1000	ab106408	Abcam

2.13 Immunoblotting

Twenty-five micrograms of protein extract, six micrograms of histone extracts or 10% of the laemmli-extracted samples were separated on SDS-PAGE and then transferred to a nitrocellulose membrane (GE Healthcare). After blocking with 5% TBS-T/BSA for 1 h at RT, the membranes were incubated with the primary antibodies overnight at 4^{o}C. The primary antibodies that were used in this study are listed in Table 5. The rabbit polyclonal N-acH4 antibody was raised against the ac-NH-SGRGKGGKGLGKC antigen as previously described(Pavlou and Kirmizis 2016). For secondary antibody a Horseradish peroxide (HRP)-conjugated goat anti-rabbit IgG (Thermo Scientific) was used at a dilution of 1:30000 and an HRP-conjugated goat-anti mouse IgG (P0447, Dako) was used at a dilution of 1:1000.

The intensity values were normalized against β-actin and are expressed relative to the SCR control.

2.14 Metabolite extractions

HCT116 SCR and NAA40-KD cells were seeded at a density of $1.5x10^5$ cells/ml and treated with 4µg/ml doxycycline for 24 h. Metabolites were extracted from cells using a modified method of Folch and colleagues (Folch et al. 1957). Briefly, $5x10^6$ cells were homogenized in chloroform/methanol (2:1, v/v, 750 µL). Samples were sonicated for 15 min and deionized water was added (300 µL). The organic and aqueous phases were separated following centrifugation (13,000 x g for 20 min). The resulting organic and aqueous phases were dried under a stream of nitrogen gas and a vacuum centrifuge, respectively.

2.15 Metabolomic analysis

Aqueous extracts were reconstituted in acetonitrile 10 mM ammonium carbonate (7:3, v/v, 50 µL) containing an internal standard mix (AMP 13C10, 15N5; ATP 13C10, 15N5; Glutamate U13C, U15N; Leucine-d10, Phenylalanine-d5, Proline U13C, U15N; and Valine-d8). Samples were injected onto a Vanquish UHPLC attached to a TSQ Quantiva triple quadrupole mass spectrometer (Thermo Scientific) with a heated ESI source.

For the normal phase analysis, metabolites were separated with a BEH-amide (150 x 2.1 mm 1.7 µm) column at 30 °C. The mobile phase consisted of: (A) 0.1% of ammonium carbonate and (B) acetonitrile and was pumped at a flow rate of 0.6 mL/min. The gradient was programmed as follows: 80% of B for 1.50 min followed

by a linear decrease from 80% to 40% of B for 3.5 min and finally returned to initial conditions.

For reverse phase analysis, samples were dried and reconstituted in 10 mM ammonium acetate solution and analyzed with an ACE C18 PFP (150 x 2.1 mm 5 µm) column at 30 °C. The mobile phase consisted of: (A) 0.1% formic acid in water and (B) 0.1% formic acid in acetonitrile, pumped at 0.5 mL/min. The gradient was programmed as follows: 0% of B for 1.60 min followed by a linear increase from 0% to 30% of B for 4 min and to 90% by 4.5 min, held for 1 min and then returned back to initial conditions.

The mass spectrometer was operated in SRM mode in both positive and negative ion mode; collision energies and RF lens voltages were generated for each species using the TSQ Quantiva optimisation function. Xcalibur Software (Thermo Scientific) was used to identify peaks, process mass spectra and normalize data to the closest-eluting internal standard. All variables were log transformed and subjected to Pathway analysis and metabolite set enrichment analysis of significant metabolites in Metaboanalyst 4.0 (www.metaboanalyst.ca).

2.16 Sub-cellular fractionation

Ten million cells were harvested in 1X PBS and lysed in Buffer A (10 mM HEPES, 10 mM KCL, 1.5 mM $MgCl_2$, 0.34 mM sucrose, 10% glycerol, 0.1% Triton X-100 and 1X protease inhibitor cocktail) on ice for 10 min. Following centrifugation at 1300g for 5 min at 4^{o}C, the supernatant S1 was centrifuged at maximum speed for 10 min and the supernatant S2 was taken as the cytoplasmic fraction. Pellet P1 was washed in Buffer A (without 0.1% Triton X-100), lysed in Buffer B (3 mM EDTA, 0.2 mM EGTA, 10 mM HEPES and 1X protease inhibitor cocktail) for 30

min on ice and pelleted at 6000g for 10 min to obtain supernatant S3 that represents the nucleoplasmic fraction. The insoluble chromatin pellet P3 was then washed twice in Buffer B and resuspended in 1X Laemmli sample buffer. For whole cell extract control ten million cells were resuspended in 1X Laemmli sample buffer and alternatively boiled and chilled three times.

Table 6. List of ChIP-qPCR primer sequences

Gene name	Forward	Reverse
PRMT5	ATAGCTGACACACTAGGGGC	CTAGTCTGCCCTTCTCCGTC
TYMS	TCTCTGTGGCTCGACACTTC	TGTGAAGACAACACCAAGCA
JUN	ACTCTGAGCCCTTATCCAGC	AAAGAAGGGCCCGACTGTAG

2.17 Chromatin Immunoprecipitation (ChIP) assay

Doxycycline treated SCR and NAA40-KD HCT116 cells were first fixed in 1% PFA for 10 min and quenched with 125 mM of glycine for 10 min. After the cells were lysed in SDS lysis buffer (1% SDS, 10 mM EDTA, 50 mM Tris-HCL pH 8 and protease inhibitor cocktail), the DNA was sheared by sonication (40sec ON/40sec OFF for 6 cycles) in a Bioruptor (Diagenode) to obtain chromatin fragments between 300-800 bp. The chromatin was diluted 1:10 in IP buffer (1% Triton X-100, 2 mM EDTA, 50 mM Tris-HCL pH 8, 150 mM NaCl and protease inhibitor cocktail) followed by 1 h pre-clearing in a 1:1 A/G Sepharose beads mix (#17-5280-01 and #17-0618-01, GE Healthcare) at RT. Thirty micrograms of chromatin were incubated with H4/H2AS1ph (ab177309, Abcam; 3 µg), Lamin A/C (sc-7292X, Santa Cruz; 5 µg), H3 (ab1791, Abcam; 2 µg) or IgG (Biogenesis 5180-2104) antibodies for 1 h at 4^{o}C and subsequently 50% slurry protein A or G beads

(blocked in salmon sperm DNA and BSA) were added and incubated overnight at 4ºC. Following washing steps, the immunoprecipitated chromatin was eluted in freshly prepared elution buffer (1% SDS and 0.1 M NaHCO3) and reverse cross-linked using 200 mM NaCl containing 0.5 μg/μl RNase (Roche) at 65ºC for 5 h. The samples were purified using the QIAquick PCR purification kit (QIAGEN) and analyzed with qRT-PCR. The sequence of the primers used in this analysis are listed in Table 6.

2.18 ChIP-seq library preparation, sequencing, and peak calling

Twenty nanograms of ChIP DNA was used for ChIP-seq library construction that was performed using the KAPA library preparation kit (Roche, 07962355001). Briefly, for end repair and A-tailing ChIP DNA was mixed with End Repair & A-tailing buffer and enzyme mix and incubated for 30 min at 20ºC followed by 30 min at 65ºC. Next, for adapter ligation the end repair & A-tailing reaction product was mixed with adapter stock, ligation buffer and the DNA ligase and incubated at 20ºC for 15 min. Next, library amplification was performed using KAPA Hifi HotStart ready mix and KAPA Library amplification primer mix. The following cycling protocol was used: 98ºC for 45 seconds, then 10 cycles of 98ºC for 15 seconds, 60ºC for 30 seconds and 72ºC for 30 seconds, finishing with 72ºC for 1 minute. Size selection (300-700 bp) was performed using the MagSI-NGS Dynabeads (#MD61021; MagnaMedics) according to the manufacturer's instructions. The size and purity of the adapter-ligated ChIP DNA was confirmed on a high-sensitivity DNA chip on a 2200 TapeStation (Agilent). The ChIP libraries were single-end deep sequenced and reads were aligned to the mm10 genome using Bowtie2 (v 2.2.6) (Langmead and Salzberg 2012). Peak calling and peak

annotation was performed via the ChIP-Enrich R package as previously described (Mylonas and Tessarz 2018).

2.19 EPIC DNA methylation arrays

Five hundred nanograms of genomic DNA was extracted from HCT116 SCR and NAA40-KD cells treated with doxycycline for 96h using the DNeasy kit for genomic DNA extraction according to the manufacturer's instructions. The Illumina EPIC BeadArrays were performed at the USC Molecular Genomics Core (Moran et al. 2016; Easwaran et al. 2012) and the raw signal intensities were extracted using the 'noob' function in the minfi software programe in R computing language. The beta values indicating the methylation level at CpG sites were calculated as the ratio of the methylated (M) signal intensity for each specific probe divided by the sum of methylated (M) and unmethylated (U) probe intensities (M/(M+U)). Only probes with fluorescent intensity of P-value < 0.05 were considered statistically significant.

2.20 Co-Immunoprecipitation

Ten million cells were harvested in 1X PBS and lysed in 1 ml ice-cold IP buffer (20 mM Tris-HCL p^H8, 137 mM NaCl, 1% Triton X-100, 2 mM EDTA and 1X protease inhibitor cocktail) for 30 min with constant mixing at 4^{o}C. Following centrifugation at 12,000 rpm for 20 min at 4^{o}C, the soluble supernatant fraction was pre-cleared with Protein A sepharose beads for 1 h at 4^{o}C. Five percent of the lysate was kept as "Input" to serve as a positive control. Lysates were then mixed with 60 µl of Protein A sepharose beads that were pre-incubated with 4 µg of H4/H2AS1ph (ab177309, Abcam) or IgG (Biogenesis 5180-2104) antibodies for 4 hours and blocked in salmon sperm DNA for 40 min. Following overnight incubation with

constant agitation at 4°C, the antibody-beads-protein complexes were centrifuged and washed three times with low salt buffer (10 mM Tris-HCL p^H7.4, 1 mM EDTA, 1mM EGTA, 150mM NaCl, 1% Triton X-100 and 1X protease inhibitor cocktail) and IP samples were eluted in 2X Laemmli buffer at 95°C for 10 min.

2.21 Immunofluorescence imaging

Cells were fixed in 100% ice-cold methanol at -20°C for 10 min, washed three times with 1X PBS and further permeabilized in 0.3% Triton X-100 for 10 min. Following blocking in 10% normal goat serum (MP Biomedicals), cells were incubated with the primary antibody in blocking buffer at 4°C overnight. The following antibodies were used for immunofluorescence: H4/H2AS1ph (ab177309, Abcam; 1:2000), Lamin A/C (ab238303, Abcam; 1:1000), H3K4me3 (ab8580, Abcam; 1µg/ml) and H3K36me3 (ab9050, Abcam; 1 µg/ml). Next, cells were washed three times with 1X PBS and following incubation with Alexa Fluor 568 goat anti-rabbit (A11011, Thermo Fisher Scientific; 1:1000) and Alexa Fluor 488 goat anti-mouse (A11001, Thermo Fisher Scientific; 1:1000) secondary antibodies for 1 h at room temperature, nuclei were stained with DAPI (Dako) or Hoechst 33342 (Invitrogen). Samples were imaged on a ZeissAxio Observer.A1 microscope. For confocal and super resolution microscopy imaging was carried out on a ZEISS LSM 900 with Airyscan 2 using Zen blue for acquisition and processing. Airyscan2 images were processed using the default deconvolution settings and histogram stretching, applied when required, was identical between control and treated samples for each channel.

2.22 Statistical analysis

All presented data are the mean ± s.d. of at least three independent experiments. Statistical analysis was carried out using GraphPad Prism (v.6.01, La Jolla, CA). Comparisons between groups were performed using Unpaired Student's t-test unless otherwise stated in the figure legend. Differences with $^{*}p<0.05$ were considered to be statistically significant.

CHAPTER 3

RESULTS OF AIM 1

3.1 NAA40 is highly expressed in CRC patients

We have previously reported that NAA40 activity controls the survival of colon cancer cells (Pavlou and Kirmizis 2016). To explore the clinical relevance of NAA40 expression in patients with colorectal cancer, we initially examined NAA40 protein levels on tissue microarrays harboring colon cancer tissues and adjacent normal specimens. Immunofluorescence analysis showed that NAA40 is increased in colon adenocarcinomas compared to benign lesions and normal colon specimens (Figure 3.1A). In particular, the positive rates of NAA40 staining were 11%, 44% and 64% for normal colon samples, benign tumors (polyps and adenomas) and adenocarcinomas, respectively (Figure 3.1B). Consistently, meta-analysis of transcriptome data extracted from The Cancer Genome Atlas (TCGA) GDC Portal showed that NAA40 mRNA levels in CRC patient tissues were significantly higher than those in normal colon tissues (Figure 3.1C). However, we observed no significant correlation between the different tumor stages of colon adenocarcinoma and NAA40 expression at both the mRNA and protein levels based on the tumour, node and metastasis (TNM) classification obtained from the commercially available tissue microarrays and the TCGA network (Figure 3.2). This may suggest that NAA40 upregulation occurs from the initial stages of malignant progression and is sustained along the different tumor stages. Overall, these results demonstrate that elevated NAA40 expression is a frequent event in colorectal carcinogenesis.

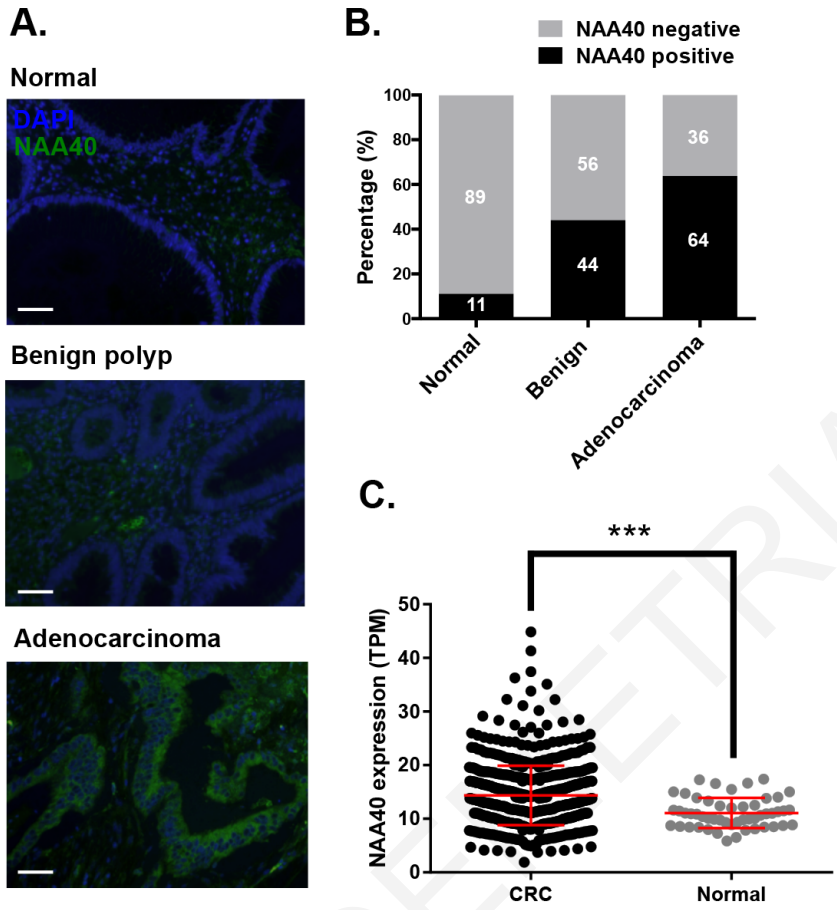

Figure 3.1. NAA40 is upregulated in CRC patient samples. (A) Representative images of immunofluorescence detection of NAA40 (green) on tissue microarrays containing a total of 318 normal and cancer colon tissues. Cell nuclei were visualized using DAPI staining (blue). Scale bar, 50 μm. **(B)** Graph showing the percentage of NAA40 positive and negative staining in normal adjacent tissue (n=56), benign lesions (n=30) and adenocarcinomas (n=232). **(C)** Meta-analysis of NAA40 mRNA expression levels extracted from the TCGA data portal in 647 colorectal cancer (CRC; COAD, n=480 and READ, n=167) and 51 normal patient samples (colon normal, n=41 and rectum normal, n=10). The Mann Whitney test was used for the statistical analysis (***p<0.001).

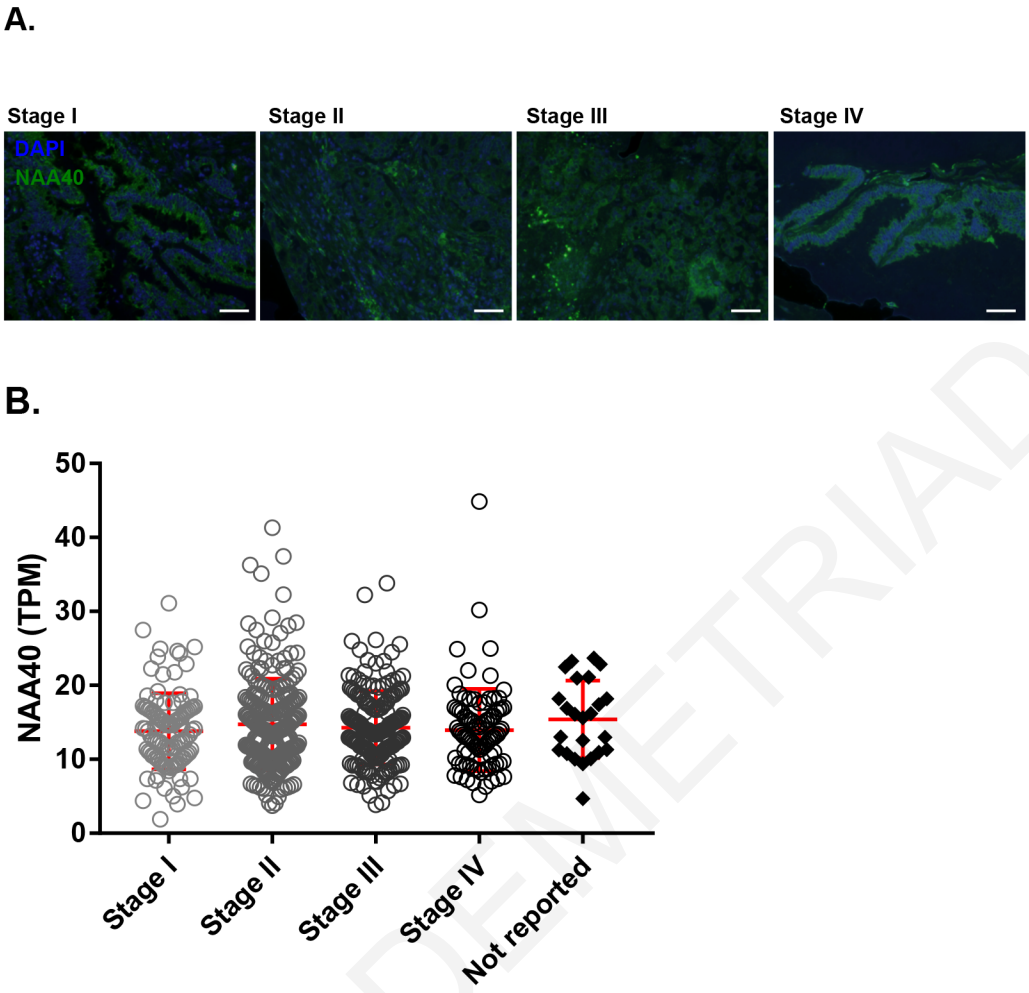

Figure 3.2. NAA40 expression is not correlated with tumor stage. (A) Representative immunofluorescence images of NAA40 staining in CRC patient tissues corresponding to different adenocarcinoma stages (n=232). Green-FITC staining was used against NAA40 and blue DAPI staining was used to visualize cell nuclei. Scale bar, 50 μm. **(B)** Meta-analysis of NAA40 expression levels extracted from the TCGA data portal in CRC adenocarcinoma specimens with different TNM stages (n= 647).

3.2 Loss of NAA40 inhibits the growth of CRC cells *in vitro*

To further evaluate the role of NAA40 in the context of CRC cell growth we constructed an inducible system to downregulate NAA40 upon doxycycline (dox) treatment of HCT116, HT-29, SW480 and SW620 colon cancer cell lines. For this purpose we used two different lentivirus-based shRNA sequences (NAA40-KD1 and NAA40-KD2) targeting two distinct sites of NAA40 mRNA. Dox administration

in all engineered cell lines significantly reduced NAA40 mRNA levels in the NAA40-KD1 and NAA40-KD2 cells compared to the negative scrambled control (SCR) cells as indicated by quantitative real-time PCR (qRT-PCR) (Figure 3.3A). Accordingly, western blot analysis showed substantial decrease of NAA40 protein levels in all four cell lines tested upon dox-mediated induction of both NAA40 shRNAs as opposed to the induction of the control SCR shRNA (Figure 3.3B).

Next, to examine whether NAA40 depletion attenuates CRC cell growth in our cell line model, we used the MTT assay to measure cell viability. In agreement with our previous observations (Pavlou and Kirmizis 2016), exposure of NAA40-KD HCT116, HT-29, SW480 and SW620 cells to different dox concentrations (1-3 μg/ml) exhibited significant loss of viability in contrast to the SCR control cells (Figure 3.4A). Consistently, phase contrast microscopy showed that depletion of NAA40 impeded cell proliferation and resulted in morphological alterations, such as cellular rounding (Figure 3.4B). Taken together, our data show that lack of NAA40 suppresses *in vitro* growth of colon cancer cell lines.

3.3 NAA40 depletion impairs CRC xenograft tumor growth

The effects of NAA40 deficiency on CRC cell proliferation *in vitro* prompted us to examine whether NAA40 regulates CRC tumor growth *in vivo*. To address this speculation, we subcutaneously injected HCT116 and HT-29 cells bearing dox-regulated lentiviral vectors expressing either SCR or NAA40-KD shRNAs into

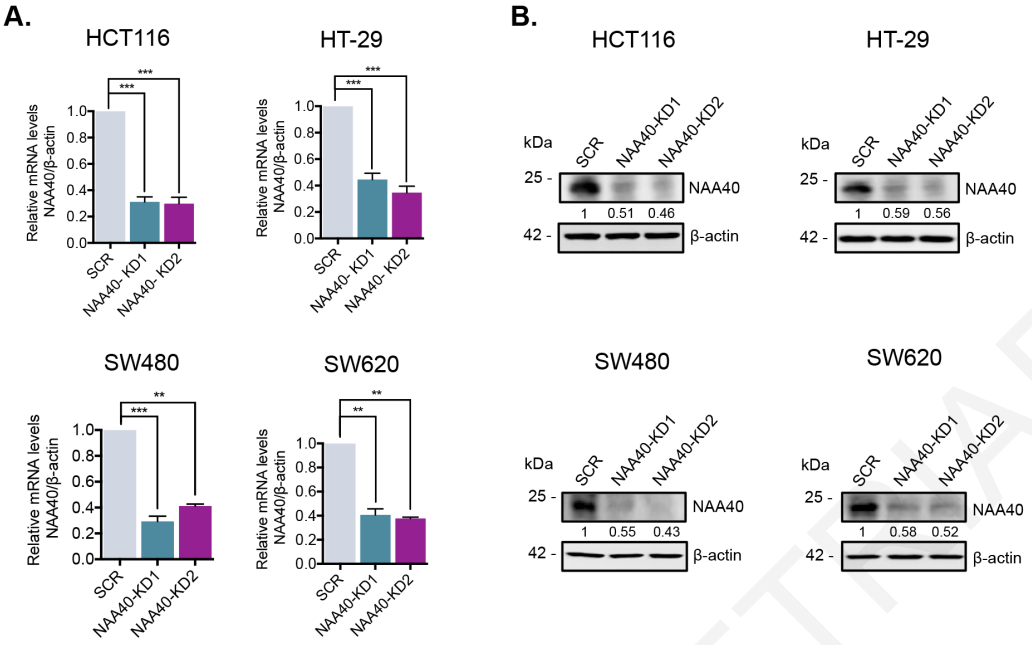

Figure 3.3. Generation of inducible NAA40-KD colon cancer cell lines. (A) Quantitative real-time PCR (qRT-PCR) analysis of NAA40 mRNA levels normalized to β-actin performed in HCT116, HT-29, SW480 and SW620 cell lines expressing doxycycline-inducible scramble shRNA (SCR), or two different shRNA sequences targeting NAA40 mRNA (NAA40-KD1 or NAA40-KD2). The relative values of NAA40 transcripts represent the mean ± s.d. of three independent experiments. Unpaired two-tailed Student's t-test was used (**p<0.01, ***p<0.001). **(B)** Western blot analysis of cell extracts derived from dox treated SCR or NAA40-KD HCT116, HT-29, SW480 and SW620 cells using antibodies against NAA40 and β-actin as loading control. The numbers below each blot indicate densitometry analysis of NAA40 protein levels in NAA40-KD relative to SCR after normalization to the β-actin bands.

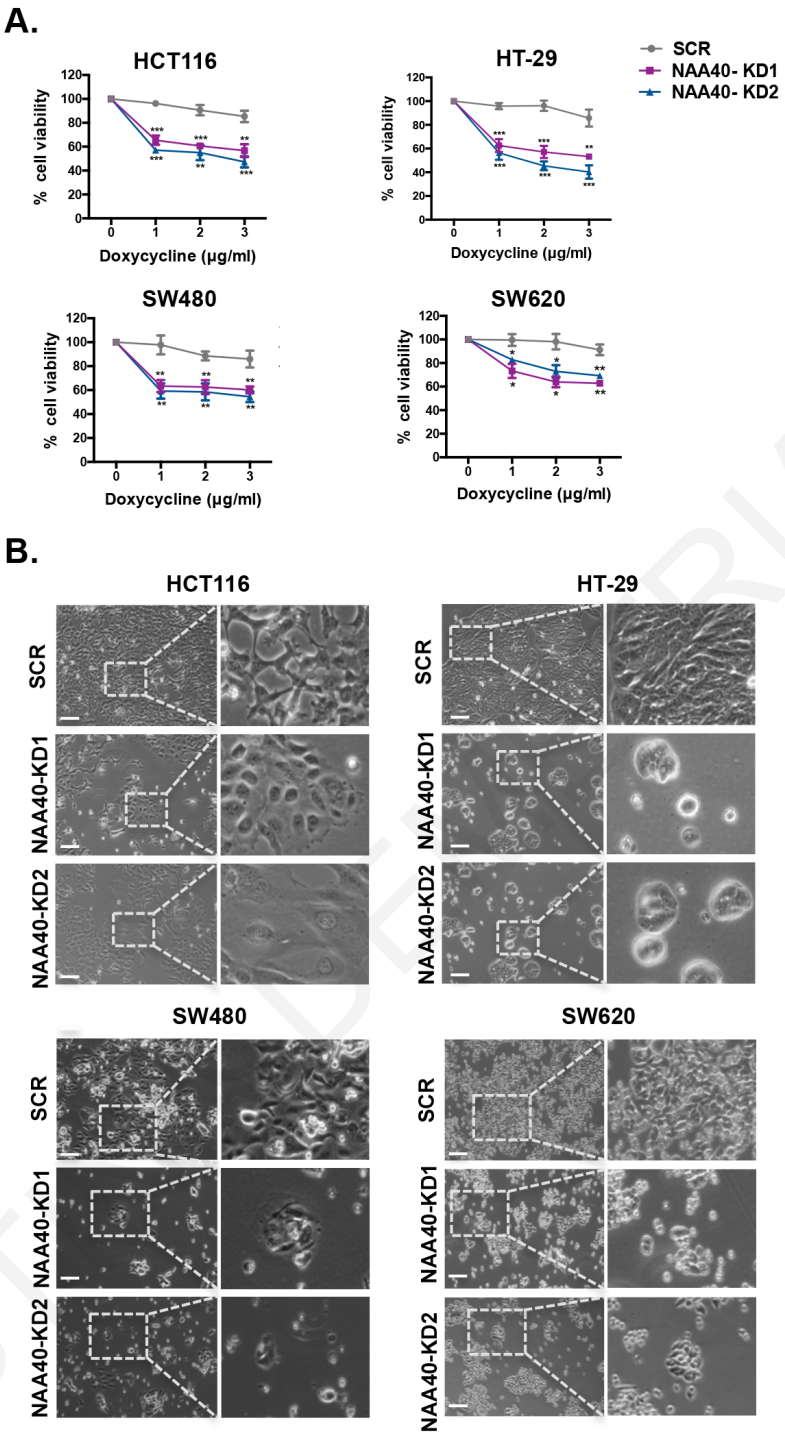

Figure 3.4. NAA40 knockdown reduces CRC cell growth *in vitro*. (A) MTT cell viability assay of SCR and NAA40-KD HCT116, HT-29, SW480 or SW620 cells incubated with various concentrations of dox. Cell viability is shown as a percentage relative to the corresponding dox untreated cells. The data are shown as mean ± s.d. of three replicates. Unpaired two-tailed Student's t-test was used (*p<0.05, **p<0.01, ***p<0.001 compared to SCR control cells). **(B)** Phase contrast microscopy of dox- inducible HCT116, HT-29, SW480 and SW620 engineered cell lines. Dashed rectangles indicate the zoomed-in areas shown in the right panels. Cells were captured in at least five fields of view (x100

magnification). The images are representative microscope fields from at least three independent replicates. Scale bar, 100 μm.

6-week old CD1 nude immunodeficient mice. Notably, NAA40-KD xenograft tumors in mice treated with dox showed significant inhibition in growth relative to the NAA40-KD tumors in mice receiving PBS (-dox), as well as the SCR tumors in mice treated with either dox or PBS (Figure 3.5A). At the end of the experiment, mice were sacrificed and tumors were excised. In agreement to effects observed with tumor volume, the weight of resected tumors from dox-treated NAA40-KD mice was reduced to approximately 33% of the weight in the control groups (Figure 3.5B). The excised tumors representing the four treated groups were aligned for comparison (Figure 3.5C). Histological hematoxylin and eosin (H&E) staining indicated no major morphological changes between tumors from all groups. Interestingly, immunofluorescence Ki67 staining revealed a significant decrease in the fraction of proliferating cancer cells upon NAA40 depletion (Figure 3.5D). Collectively, our findings indicate that NAA40 knockdown significantly decreases the growth of CRC xenografts *in vivo*.

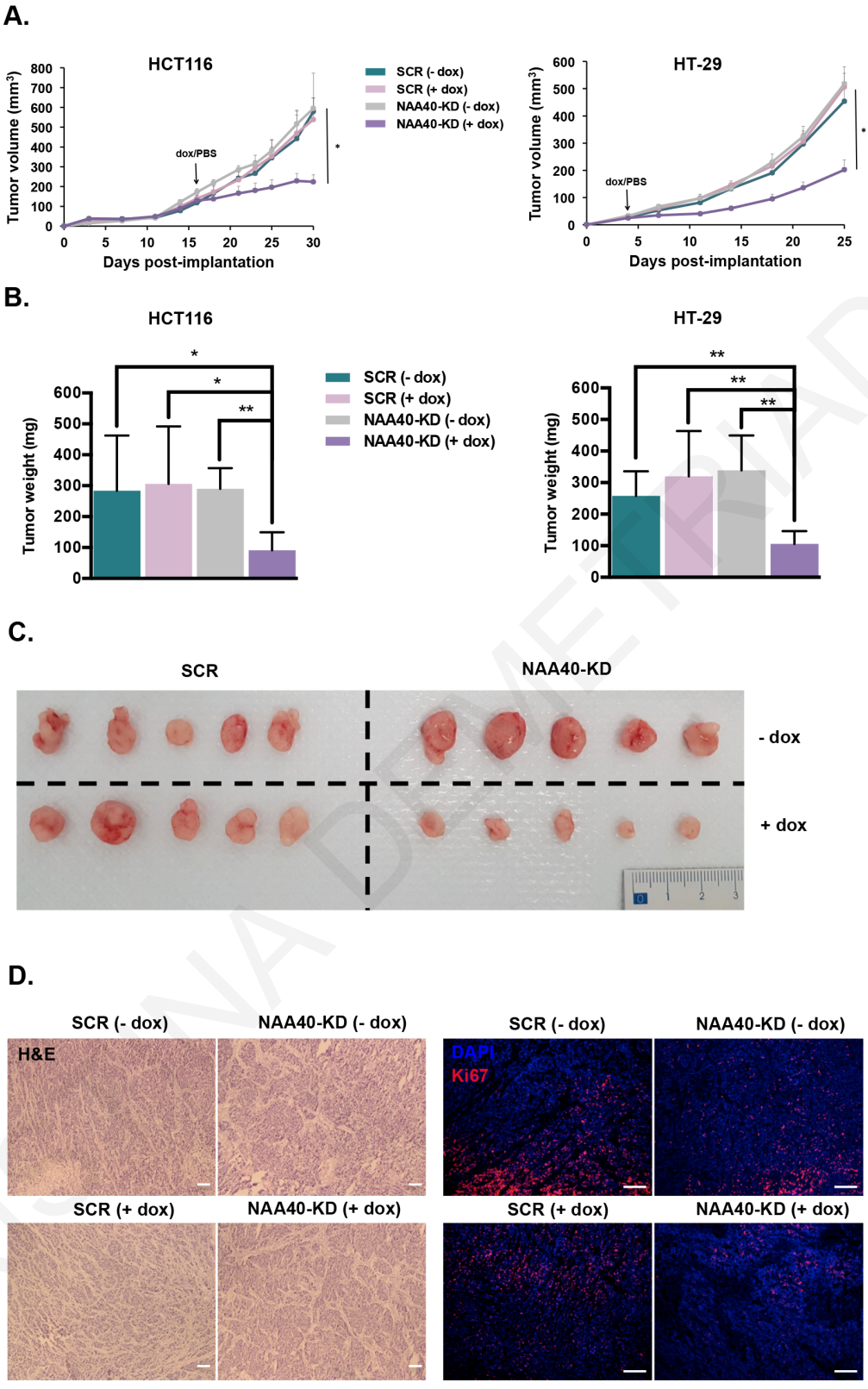

Figure 3.5. NAA40 depletion inhibits CRC cell growth *in vivo*. (A) The mean volume of tumors from the dox-treated (+dox) and PBS-treated (-dox) HCT116 (*left*) or HT-29 (*right*) xenografts harboring the conditionally induced SCR or NAA40-KD2 shRNAs. The tumor volume is shown as mean ± s.d. Unpaired two-tailed Student's t-test was used (*p<0.05). **(B)** At the end of the experiment in (A) mice were sacrificed and tumors were excised and weighted. Error bars represent

mean ± s.d. Unpaired two-tailed Student's t-test was used (*p<0.05, **p<0.01). (**C)** Representative tumors excised from SCR and NAA40-KD mouse xenografts after administration of dox (+dox) or PBS (-dox). **(D)** Representative hematoxylin & eosin (H&E) images (*left*) from tumors derived from SCR and NAA40-KD mouse xenografts after administration of dox (+dox) or PBS (-dox). Scale bar, 200 μm. Representative immunofluorescence Ki67 staining (red) images (*right*) from tumors derived from SCR and NAA40-KD mouse xenografts after administration of dox (+dox) or PBS (-dox). Cell nuclei were visualized using DAPI staining (blue). Scale bar, 100 μm.

3.4 NAA40 stimulates PRMT5 expression in CRC cells

The above findings demonstrated a link between NAA40 expression and CRC cell growth. Therefore, we next sought to determine how NAA40 controls the viability of colon cancer cells. We have previously reported that in yeast cells NAA40-mediated N-terminal acetylation of histone H4 (N-acH4) controls the expression of a specific cohort of genes by regulating the deposition of the adjacent histone H4 arginine 3 asymmetric dimethylation (H4R3me2a) mark (Molina-Serrano et al. 2016; Schiza et al. 2013). Therefore, we wondered if human NAA40 regulates gene expression and thereby cell growth by controlling the deposition of methyl marks at H4R3 in CRC cells. To test this hypothesis, we investigated the global cellular levels of H4R3me modifications in HCT116 cells depleted of NAA40. We found that H4 arginine 3 symmetric dimethylation (H4R3me2s) levels are notably decreased in the absence of NAA40 and of its mediated N-acH4 compared to the SCR and mock control cells. On the other hand, reduction of NAA40 expression did not influence the total levels of monomethylation (H4R3me1) or asymmetric dimethylation (H4R3me2a) at the third residue of histone H4 (Figure 3.6A). Consistently, H4R3me2s levels were reduced upon NAA40 knockdown in SW480 (Figure 3.6B) and SW620 (Figure 3.6C) cells while H4R3me1 and H4R3me2a levels remained unaffected.

In human cells, H4R3 is targeted by various protein arginine methyltransferases (PRMTs) resulting in different methylation states. Specifically, PRMT1 catalyzes asymmetric dimethylation of H4R3 (H4R3me2a), PRMT5 deposits symmetric dimethylation to form H4R3me2s and PRMT7 also mediates

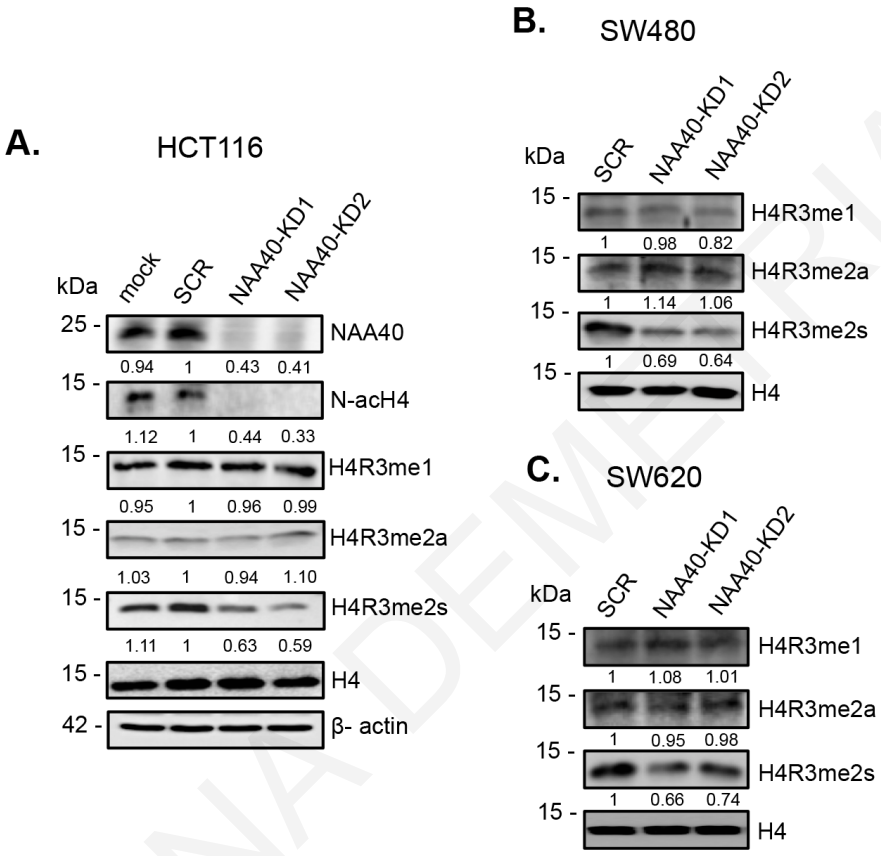

Figure 3.6. NAA40 controls the deposition of H4R3me2s. (A) Western blot analysis of protein extracts from the indicated transiently transfected HCT116 cells using antibodies against NAA40, H4R3me1, H4R3me2a, H4R3me2s, total histone H4 and β-actin as loading control. **(B, C)** Western blot analysis of protein extracts from the indicated SW480 (B) and SW620 (C) engineered cell lines using antibodies against H4R3me1, H4R3me2a, H4R3me2s and total histone H4 as loading control. The densitometry numbers below each blot define the normalized levels of H4R3me1, H4R3me2a and H4R3me2s against H4 relative to SCR cells.

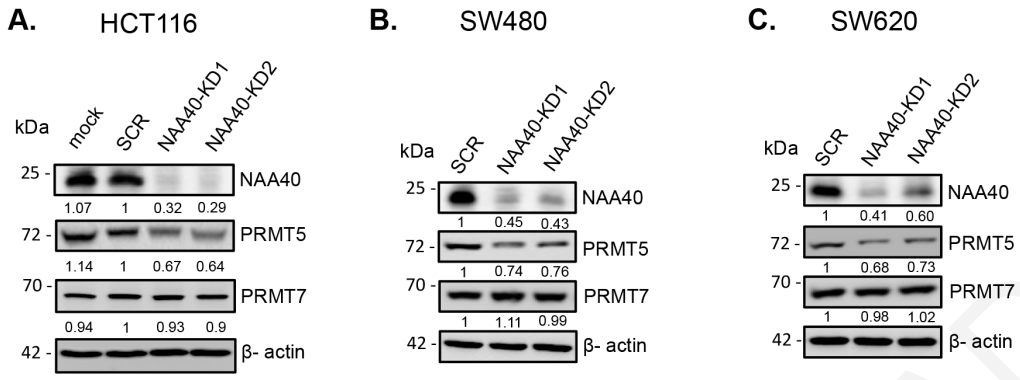

Figure 3.7. NAA40 regulates PRMT5 protein levels *in vitro*. (A) Western blot analysis of protein extracts from the indicated siRNA treated cells using antibodies towards NAA40, PRMT5, PRMT7 and β-actin as loading control. **(B, C)** Western blot analysis of cell extracts derived from dox treated SCR or NAA40-KD SW480 (B) and SW620 (C) cells using antibodies towards NAA40, PRMT5, PRMT7 and β-actin as loading control. The values below each blot were calculated by densitometry analysis of NAA40, PRMT5 and PRMT7 bands relative to SCR control after normalization with β-actin.

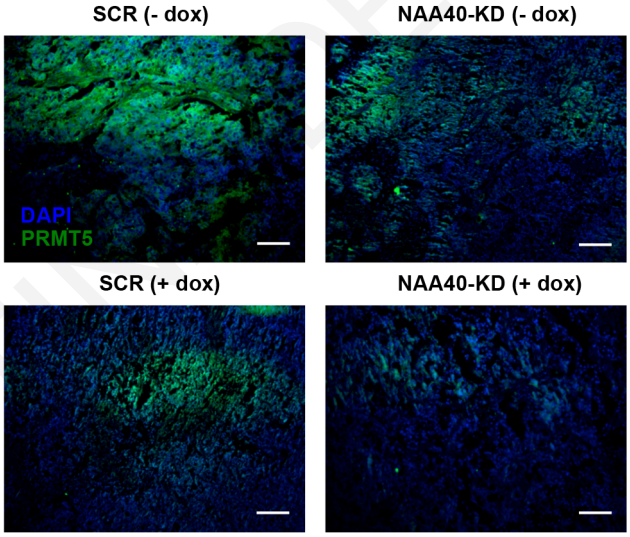

Figure 3.8. NAA40 depletion reduces PRMT5 protein levels in xenograft tumors. Representative immunofluorescence PRMT5 staining (green) images of SCR and NAA40-KD xenograft tumors derived from mice receiving dox (+dox) or PBS (-dox). DAPI staining (blue) was used to visualize cell nuclei. Scale bar, 200 μm.

H4R3me2s but mainly monomethylates this histone residue to form H4R3me1 (Blanc and Richard 2017). Since the H4R3me2s mark is primarily deposited by the PRMT5 arginine methyltransferase, we then examined whether NAA40 knockdown in HCT116 cells affects the levels of this histone-modifying enzyme. We observed that PRMT5 protein levels are reduced in response to NAA40 knockdown as opposed to the SCR and mock controls (Figure 3.7A). No significant differences were noted in PRMT7 protein levels, which is another enzyme mediating H4R3me2s (Figure 3.7A). Moreover, loss of NAA40 decreased PRMT5 but not PRMT7 protein levels in SW480 (Figure 3.7B) and SW620 cells (Figure 3.7C). Accordingly, PRMT5 protein levels are also reduced in NAA40-depleted xenograft tumors (Figure 3.8). To validate this observation, we also examined the mRNA levels of PRMT5 and PRMT7 upon NAA40 depletion. Consistent with the above findings, NAA40 knockdown significantly reduced PRMT5 but not PRMT7 mRNA levels (Figure 3.9A-C), suggesting that NAA40 controls PRMT5 expression at the transcriptional level. In line with this, using chromatin immunoprecipitation (ChIP) assays we detected markedly reduced deposition of N-acH4 and of the transcriptionally activating H3K4me3 modification, while the repressive mark H3K27me3 was significantly enriched, at the PRMT5 gene promoter in HCT116 cells depleted of NAA40 (Figure 3.9D).

To substantiate the association between NAA40 and PRMT5 expression, we next sought to examine the transcription of PRMT5 direct target genes upon NAA40 depletion. We focused our analysis on target genes whose control of

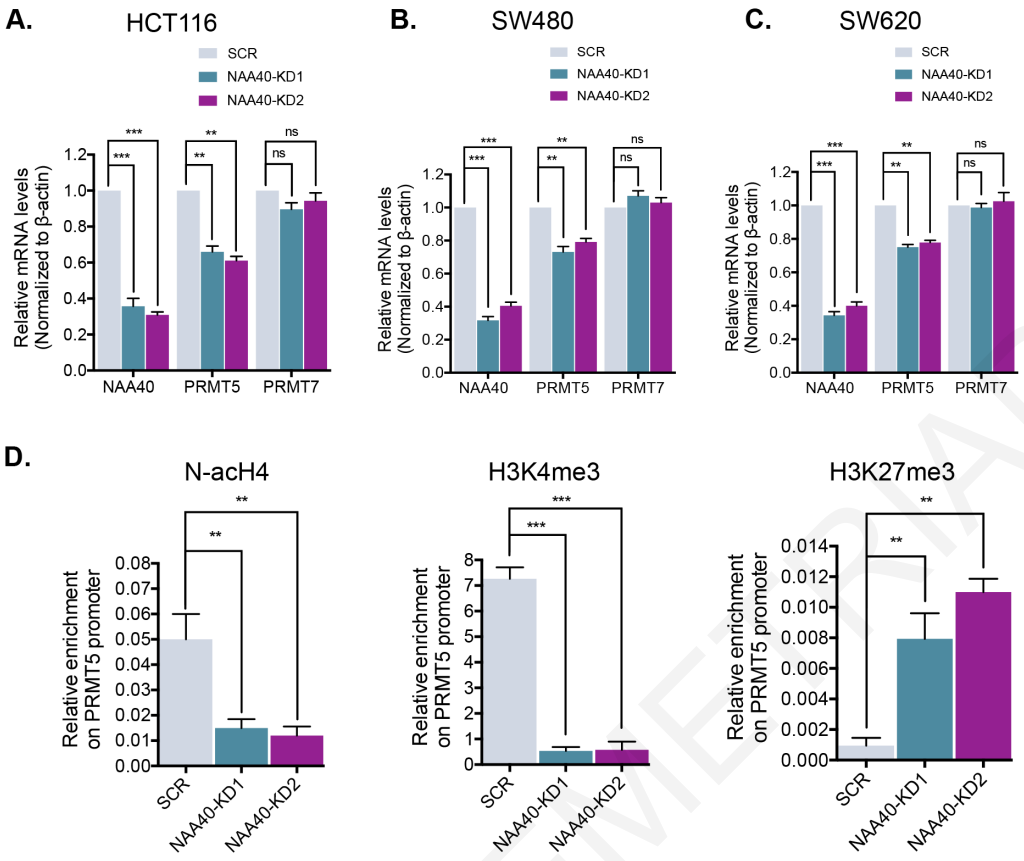

Figure 3.9. NAA40 regulates PRMT5 mRNA levels. (A, B, C) qRT-PCR analysis of mRNA levels of NAA40, PRMT5 and PRMT7 normalized to β-actin in the indicated HCT116 (A), SW480 (B) and SW620 (C) cells. Error bars represent the mean ± s.d of three biological replicates. Unpaired two-tailed Student's t-test was used (ns=no significance, **p<0.01, ***p<0.001). **(D)** ChIP assay monitoring the enrichment of N-acH4, H3K4me3 and H3K27me3 on the PRMT5 gene promoter in HCT116 engineered cells. The enrichment from each antibody was normalized to total histone H3. Results are shown as mean ± s.d. from two independent experiments. Unpaired two-tailed Student's t-test was used (**p<0.01, ***p<0.001).

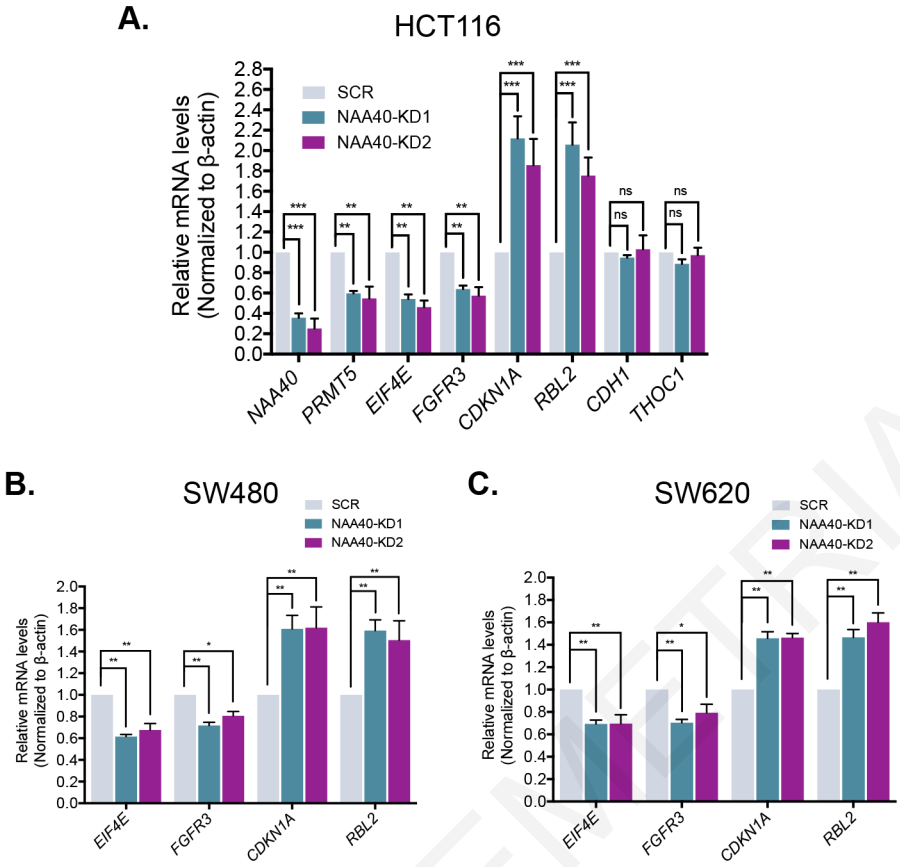

Figure 3.10. NAA40 regulates the expression of PRMT5-target oncogenes and tumour suppressor genes. (A, B, C) qRT-PCR analysis of mRNA levels in HCT116 (A), SW480 (B) and SW620 (C) cells for the indicated genes. The results were normalized to β-actin mRNA and represent the average from three independent experiments. Unpaired two-tailed Student's t-test was used (ns = no significance, *p<0.05, **p<0.01, ***p<0.001).

expression by PRMT5 has been previously linked to colorectal cancer growth (Zhang et al. 2015). Accordingly, we found that NAA40 reduction and subsequent downregulation of PRMT5 results in decreased expression of Fibroblast Growth Factor Receptor 3 (FGFR3) and Eukaryotic Translation Initiation Factor 4E (EIF4E) oncogenes and derepression of RB Transcriptional Corepressor Like 2 (RBL2) and Cyclin Dependent Kinase Inhibitor 1A (CDKN1A) tumor suppressors, which, respectively, are activated and repressed by PRMT5 in proliferating CRC

cells (Figure 3.10). Conversely, there was no significant change in the expression of cadherin-1 (CDH1) and THO complex 1 (THOC1) control genes (Figure 3.10A). Altogether, these results suggest that NAA40 promotes PRMT5 transcriptional activation, which in turn influences the expression of vital cancer-associated genes in CRC cells.

3.5 PRMT5 upregulation restores viability in NAA40-depleted CRC cell

The data shown above indicate that NAA40 knockdown reduces PRMT5 expression in colon cancer cells. To investigate whether PRMT5 downregulation is important for the decreased CRC cell viability mediated by NAA40 depletion we performed MTT assay in NAA40-knockdown cells that overexpressed PRMT5. Notably, ectopic expression of PRMT5 restored to a great extent the viability of HCT116 cells that were depleted of NAA40 (Figure 3.11), suggesting that PRMT5 contributes to NAA40-dependent CRC cell growth. In support of this relationship, meta-analysis of RNA-seq data from TCGA showed that PRMT5 is significantly upregulated in CRC patient samples compared to the non-cancerous specimens, as previously seen for NAA40 (compare Figure 3.12A to 3.1C). Furthermore, similarly to NAA40, PRMT5 expression levels are also increased in all tumor stages in CRC patients (Figure 3.12B). More importantly, we found a significant positive correlation ($r=0.388$, $p<0.0001$) between the mRNA levels of NAA40 and PRMT5 in CRC patient samples (Figure 3.12C). In contrast, there was no significant association ($r=0.050$, $p=0.201$) between NAA40 and PRMT7 mRNA levels in these CRC samples (Figure 3.12D), consistent with the fact that NAA40-depletion does not affect the levels of PRMT7 (Figures 3.9A-C). Thus, overall

these findings suggest that NAA40 facilitates survival of colon cancer cells partly through upregulation of PRMT5 expression.

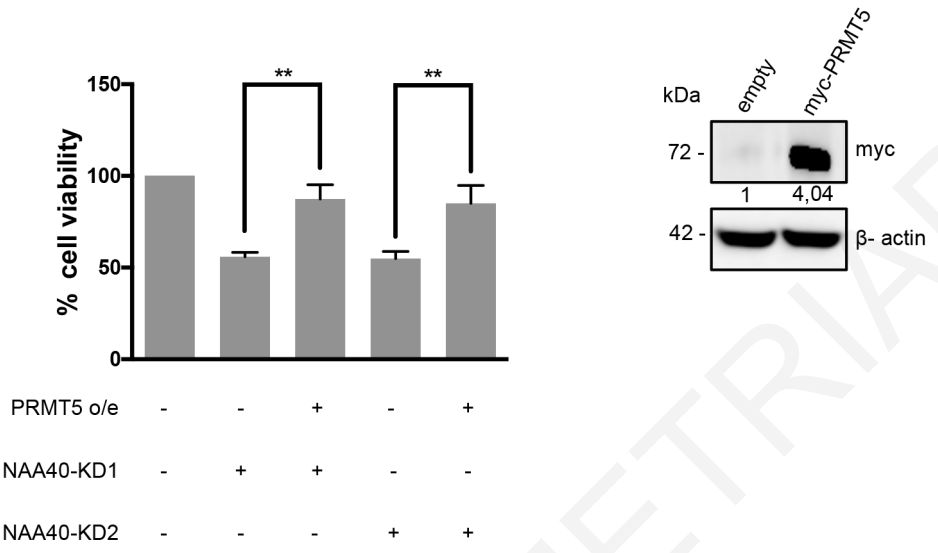

Figure 3.11. PRMT5 upregulation restores viability in NAA40-depleted CRC cells. MTT assay of HCT116 colon cancer cells expressing an empty vector (-) or a vector containing myc-tagged PRMT5 (+) in SCR (-) or NAA40-KD (+) conditions. Error bars represent the mean ± s.d of three biological replicates. Unpaired two-tailed Student's t-test was used (**p<0.01). Western blot analysis (*right panel*) was performed to detect ectopic expression of tagged PRMT5 using an antibody against myc. β-actin was used as a loading control. The values below the blot were determined by densitometry analysis.

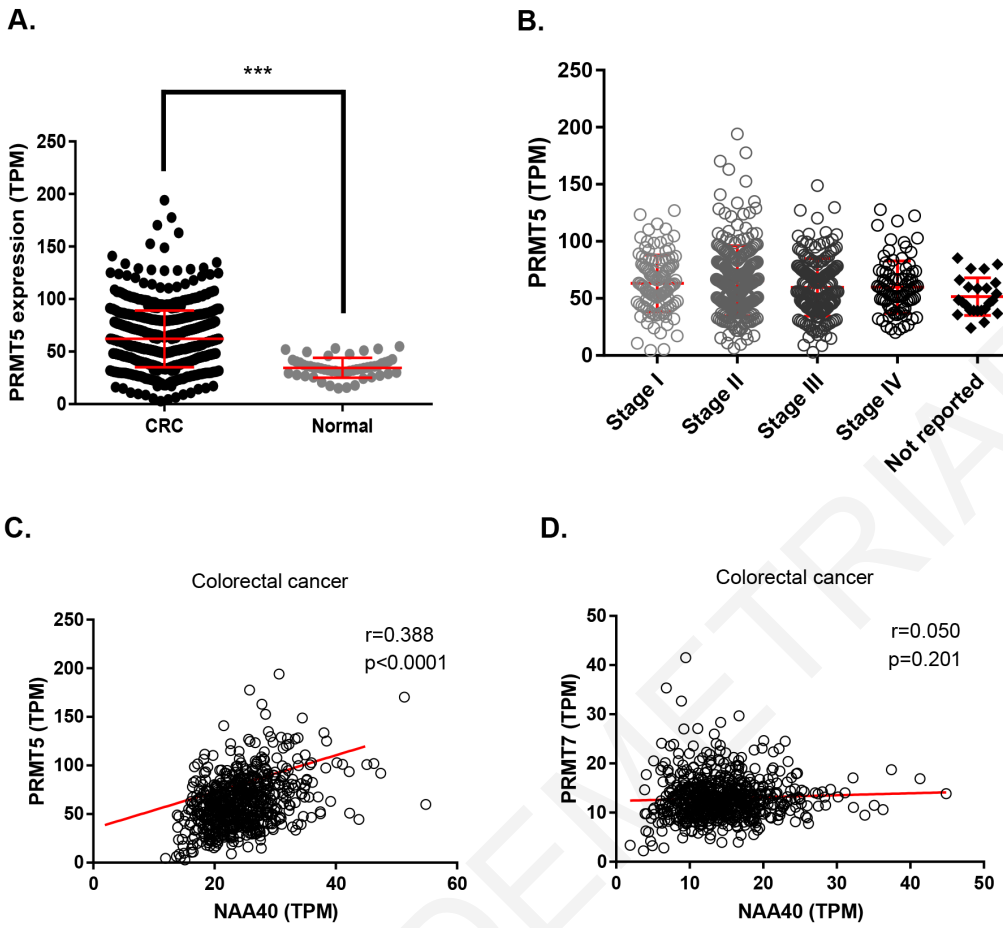

Figure 3.12. NAA40 and PRMT5 are positively correlated in human CRC tissues. (A) Meta-analysis of PRMT5 expression levels extracted from the TCGA data portal in 647 colorectal cancer (CRC) and 51 normal patient samples. The Mann Whitney test was used for the statistical analysis (***p<0.001). **(B)** Meta-analysis of PRMT5 expression levels extracted from the TCGA data portal in CRC adenocarcinoma specimens with different TNM stages (n= 647). **(C)** and **(D)** Scatter plots illustrating the correlation between the expression of *NAA40* and PRMT5 (C) or between NAA40 and PRMT7 (D) in 647 colorectal cancer (CRC) patient samples extracted from the TCGA database. The red line indicates the linear regression slope. Statistical analysis was performed using Pearson's rank correlation coefficient (r).

CHAPTER 4

RESULTS OF AIM 2

4.1 NAA40 regulates one-carbon metabolism in colorectal cancer cells

As described above we have demonstrated that NAA40 is upregulated in CRC and sustains tumour growth by controlling the expression of PRMT5 gene identified through individual gene analysis. However, given the abundance of N-acH4 in the proteome (Tweedie-Cullen et al. 2012), we anticipate that PRMT5 is not the sole player facilitating NAA40-mediated survival of CRC cells. This is also supported by the fact that PRMT5 upregulation cannot fully restore the loss of CRC cell viability upon NAA40 knockdown (Figure 3.11). Consequently, to fully comprehend the regulatory network of NAA40 in CRC, we conducted RNA-seq analysis using the inducible shRNA-mediated knockdown cell line models that were previously constructed and described (Figure 3.3). Comparison of doxycycline treated Scramble (SCR) and NAA40-knockdown (NAA40-KD) HCT116 stable cells revealed that NAA40 depletion leads to altered expression of 2102 genes, with differential expression determined at a threshold of p-value < 0.05 and an absolute log fold change > 1 (Figure 4.1A). Gene Ontology (GO) analysis of the differentially expressed genes illustrated that loss of NAA40 alters sets of genes involved in cancer-related processes in support of our previous finding (Figure 3.4 and Figure 4.1B). Specifically, some of the most significantly enriched GO terms included DNA replication, DNA damage and repair pathways, as well as cell cycle phase transition (Figure 4.1B). In line with these findings, we observed that cells deprived of NAA40 are restricted in the G1/S phase of the cell cycle (Figure 4.1C), further supporting the oncogenic potential of NAA40. Intriguingly, among the most notably enriched GO terms were ones pointing to a connection with metabolism

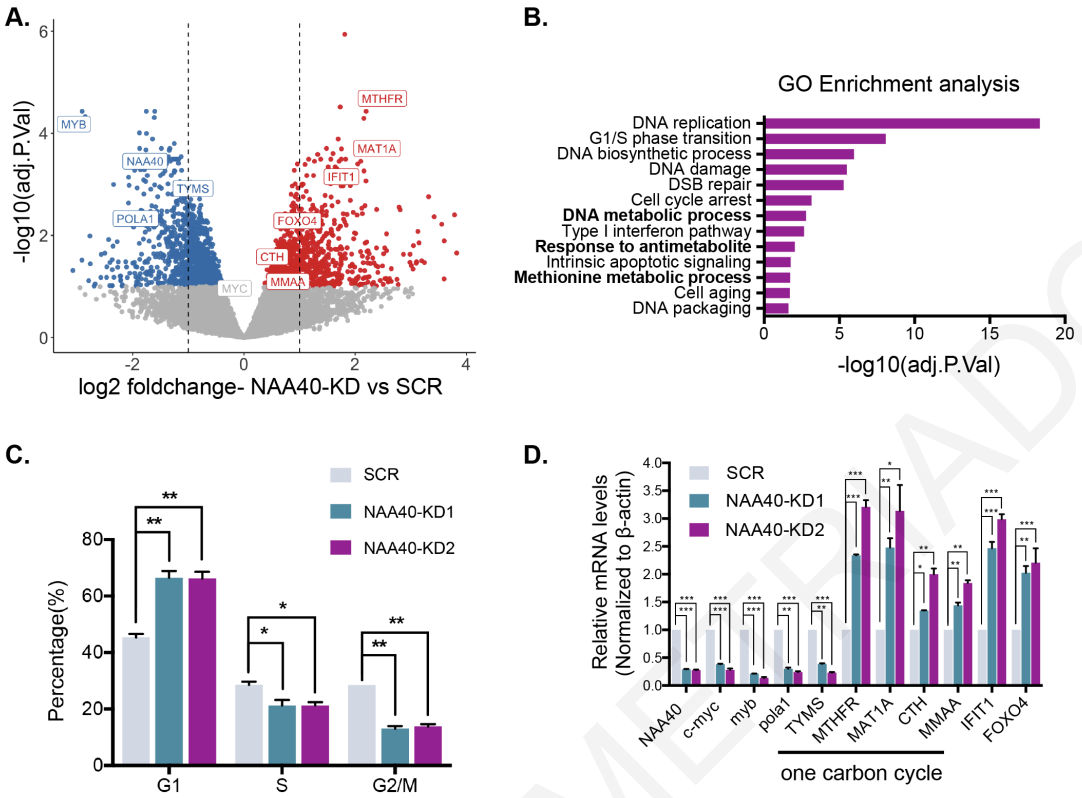

Figure 4.1. NAA40 regulates the levels of key 1C metabolic genes. (A) Volcano plot comparing mRNA levels between NAA40 depleted and SCR control HCT116 cells as determined by RNA-seq analysis. Upregulated genes upon loss of NAA40 are shown in red (adjusted P-value<0.01 and logFC>1) and downregulated genes in blue (adjusted P- value<0.01 and logFC<-1). **(B)** Gene ontology analysis of all differentially expressed genes showing enriched biological processes following depletion of NAA40. **(C)** Flow cytometry analysis (mean ± s.d., N=2) of HCT116 cells stably transfected with doxycycline-inducible SCR or NAA40-KD constructs upon treatment with 1 μg/ml dox for 96 h. Unpaired two-tailed Student's t-test was used (*p<0.05, **p<0.01). **(D)** Quantitative real-time PCR (qRT-PCR) analysis (mean ± s.d., N=3) of the indicated genes normalized to β-actin mRNA levels in dox-treated SCR and two independent NAA40-KD lines in HCT116 cells. All statistical analyses were performed using unpaired two-tailed Student's t-test (*p<0.05, **p<0.01, ***p<0.001).

such as the methionine metabolic pathway, regulation of DNA metabolic process and response to anti-metabolite therapy (Figure 4.1B). Key genes within these categories included methylenetetrahydrofolate reductase (MTHFR), methionine adenosyltransferase 1A (MAT1A), cystathionine gamma-lyase (CTH) and metabolism of cobalamin associated A (MMAA) which were significantly upregulated, while thymidylate synthase (TYMS) was markedly downregulated in the absence of NAA40 (Figure 4.1A). The expression of these and other genes identified during our transcriptomic study was also validated through quantitative real time PCR (qRT-PCR) analysis (Figure 4.1D).

The above identified differentially expressed genes control important reactions within the 1C-metabolic network, which interconnects the methionine, folate and trans-sulfuration cycles (Figure 4.2A), circulating 1C-units to support a multitude of fundamental cellular activities, including nucleotide synthesis and the production of the universal methyl donor SAM (Serefidou et al. 2019; Locasale 2013). Since NAA40 knockdown influenced the transcription of important one-carbon metabolic genes, we next examined the impact of NAA40 on the metabolome of CRC cells. To address this, we performed targeted metabolomic analysis using a liquid chromatography/mass spectrometry (LC/MS) approach to identify metabolites whose abundance displays significant change in cells devoid of NAA40 compared to doxycycline-treated control cells. In accordance with our transcriptomic data, enrichment analysis of deregulated metabolites in NAA40 depleted cells revealed cysteine and methionine metabolism as the most significantly modulated metabolic pathway (Figure 4.2B). Specifically, NAA40 deficiency resulted in a substantial increase of intracellular SAM pools and a smaller increase in the abundance of S-adenosyl-L-homocysteine (SAH), homocysteine, methylene- tetrahydrofolate (me-THF) and glycine intermediary

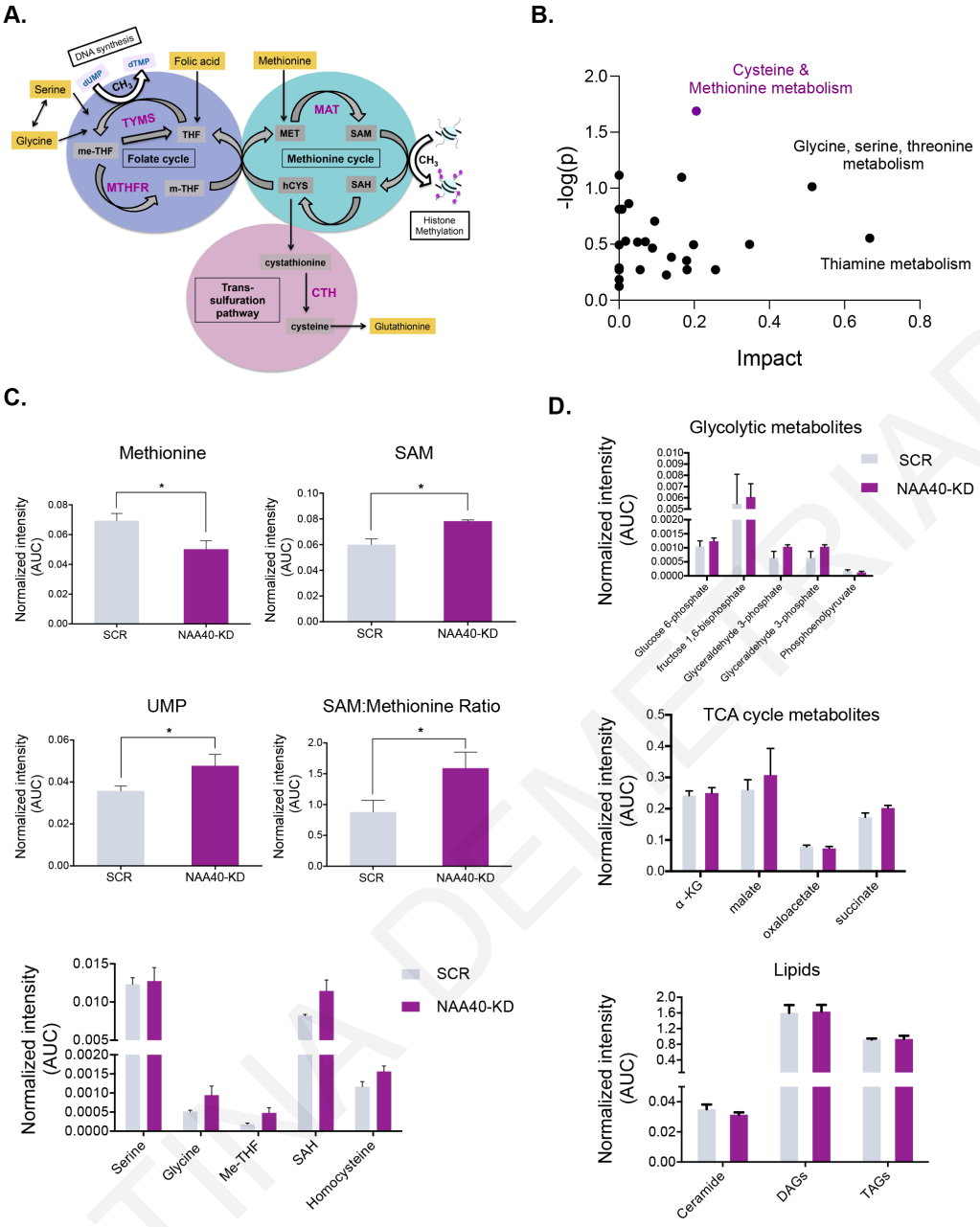

Figure 4.2. NAA40 regulates the abundance of 1C metabolites. (A) Schematic of the folate, methionine and trans-sulfuration cycles of the one-carbon metabolic network depicting key enzymes and intermediate metabolites. **(B)** Enrichment analysis of altered metabolic pathways based on detected metabolites by UPLC-MS in NAA40-KD versus SCR control cells. Impact represents the enrichment ratio; the number of total compounds in the pathway divided by the number of hits **(C)** Intracellular levels of the indicated one-carbon metabolites or their ratios (mean ± s.e., N=3) in dox-treated SCR and NAA40-KD HCT116 cells. **(D)** Intracellular levels of the indicated metabolites found in glycolysis, TCA cycle and lipid synthesis measured by UPLC-MS (mean ± s.d., N=3) in HCT116 SCR and NAA40-KD cells treated with doxycycline. All statistical analyses were performed using unpaired two-tailed Student's t-test (*p<0.05).

metabolites, whereas methionine levels were significantly lower relative to SCR control cells (Figure 4.2C). These results are consistent with the induction of MTHFR and MAT1A, and repression of TYMS observed in the gene expression analysis (Figures 4.1A and 4.1D). Notably, NAA40 depletion led to increased SAM/methionine ratio and accumulation of UMP which is the central precursor for thymidine synthesis (Figure 4.2C), suggesting that NAA40 depleted cells may therefore possess an enhanced capacity for methylation reactions. In contrast, at this stage we do not detect major changes in metabolite levels of other central metabolic pathways, such as glycolysis, tricarboxylic acid (TCA) cycle and fatty-acid synthesis, indicating that the effects of NAA40 knockdown are specific towards 1C-metabolism (Figure 4.2D). Altogether, these findings establish a role for NAA40 histone acetyltransferase in the regulation of one-carbon metabolism in CRC cells.

4.2 Regulation of one-carbon metabolism by NAA40 rewires global histone methylation

Previous studies have linked fluctuations in the availability of the principal methyl donor SAM with bulk changes in chromatin methylation (Mentch et al. 2015; Roy et al. 2020; Shiraki et al. 2014; Shyh-Chang et al. 2012). Since NAA40 controls SAM levels, we next sought to investigate whether NAA40 depletion impacts the epigenome by affecting histone methylation levels. Initially, we validated NAA40 depletion through loss of its associated acetyltransferase activity towards histone N-termini by examining the appearance of its previously reported antagonistic phosphorylation mark at serine 1 (Figure 4.3A) (Ju et al. 2017a). This was necessary because the previously used antibody for detecting histone N-terminal

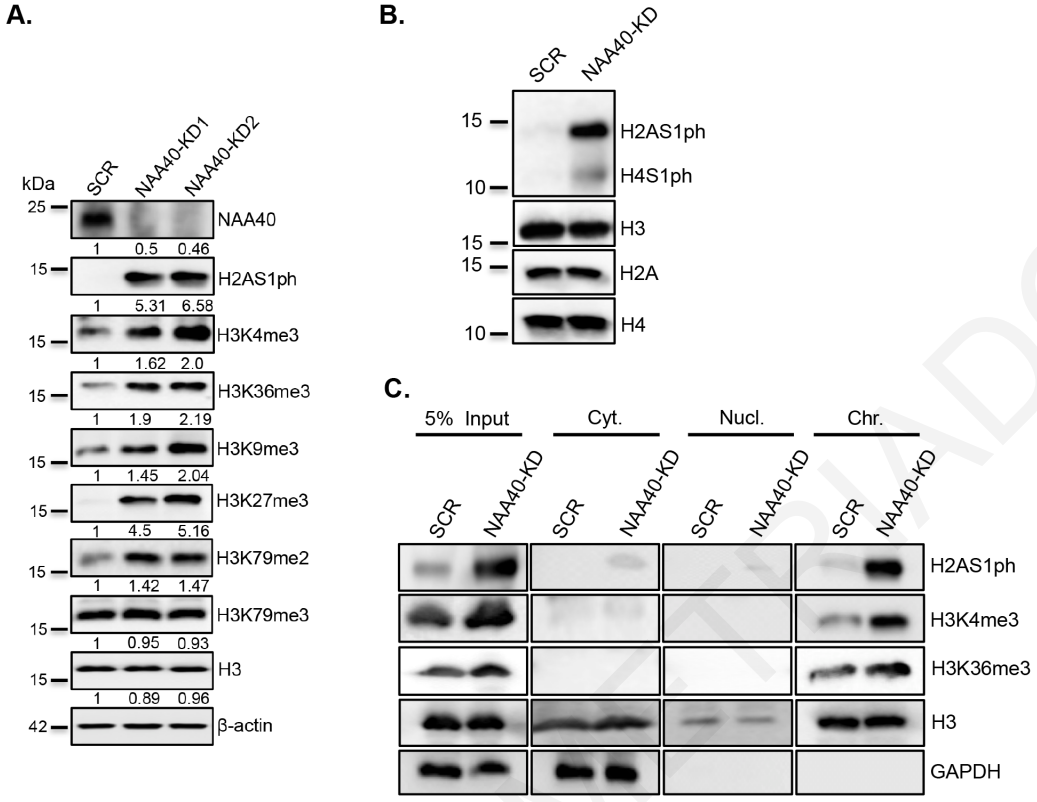

Figure 4.3. NAA40 impacts global histone methylation. (A) Representative western blot analysis (N=3) of cell extracts derived from dox-treated SCR or NAA40-KD HCT116 cells using the indicated antibodies. The numbers below each blot indicate densitometry analysis of protein levels in NAA40-KD relative to SCR after normalization to the β-actin bands. **(B)** Western blot analysis (N=3) of acid extracted histones from dox-treated SCR and NAA40-KD using antibodies against H2A/H4S1ph, H3, H2A and H4. **(C)** Western blot analysis (N=2) in whole cell (5% Input), cytoplasmic (S2), nucleoplasmic (S3) and chromatin-bound (P3) protein extracts derived from biochemical fractionation of dox-treated SCR or NAA40-KD cells.

acetylation (Figure 3.6A) was expended and no longer available. Specifically, we found that loss of NAA40 in HCT116 cells dramatically potentiated serine 1 phosphorylation at both histones H2A (H2AS1ph) and H4 (H4S1ph) with the signal at the former being more readily detected (Figure 4.3B). Once we validated that NAA40 function was efficiently diminished, we then monitored the levels of several histone methylation marks. Remarkably, attenuation of NAA40 results in robust increase in the total levels of various histone methylation marks associated with transcription, including both permissive (H3K4me3, H3K36me3 and H3K79me2) and repressive (H3K9me3 and H3K27me3) methylations (Figure 4.3A), which is consistent with the detected accumulation in SAM levels (Figure 4.2C). However, this increase was not universal since the levels of other methylation marks, such as H3K79me3, remained unaffected (Figure 4.3A). In support of this observation, recent evidence confirms that fluctuations in SAM abundance do not impact all methylated histone sites, but rather directed to specific residues in a context-dependent manner (Shyh-Chang et al. 2012; Ulanovskaya et al. 2013; Ye et al. 2017). Moreover, subcellular fractionation experiments illustrated that the induction of histone methylation occurs mainly on chromatin-associated histone proteins (Figure 4.3C). Hence, we then reasoned to exploit the precise genomic locations at which these modification changes occur by chromatin immunoprecipitation followed by deep sequencing (ChIP-seq). To our surprise, the genome-wide distribution of the various tested histone methylation marks was highly preserved in the absence of NAA40 since no differences were observed in the total peak number, feature distribution or the peak enrichment relative to the transcription start site (TSS) between doxycycline-treated SCR and NAA40-KD cells (Figure 4.4A-C). Given that SAM is also used by DNMTs, we next examined cytosine methylation between doxycycline-treated SCR and NAA40-KD cells using DNA

methylation microarrays. In contrast to the robust histone methylation response detected by western blot, no significant differences were seen in global DNA methylation following NAA40 depletion (Figure 4.4E). The minor changes detected with some probes were similar to those observed when we compared the two biological replicates of SCR control cells indicating that those differences are probably due to technical variability (Figure 4.4E, compare top and bottom plots).

To gain further insight into NAA40-mediated regulation of one carbon metabolism and its connection with histone methylation changes, we then monitored the temporal dynamics of these alterations. To achieve this, SCR and NAA40-KD cells were treated with doxycycline and examined at various time points (6, 16, 24, 48, 72, 96 h). Significant NAA40 depletion was detected from 16h after dox treatment and progressively increased based on both NAA40 mRNA and protein levels as well as the appearance of its antagonistic histone mark H2AS1ph. Induction of one-carbon metabolic genes MTHFR and MAT1A followed NAA40 depletion since it was detected at 24h after dox treatment and progressively increased until 96h (Figure 4.5A). Importantly, this gene induction was concurrent to the rising levels of H3K4me3 and H3K36me3 (Figure 4.5B). Comparison of all these alterations clearly indicates that the expression changes in one-carbon metabolic genes occur shortly after NAA40 depletion and coincide temporally with the histone methylation changes (Figure 4.5C). Because we have previously shown that NAA40-knockdown results in reduced viability of CRC cells (Figure 3.4), we wanted to exclude the possibility that the observed coordinated changes in metabolic gene expression and histone methylation are occurring as a response to growth retardation signals. We found that these chromatin changes

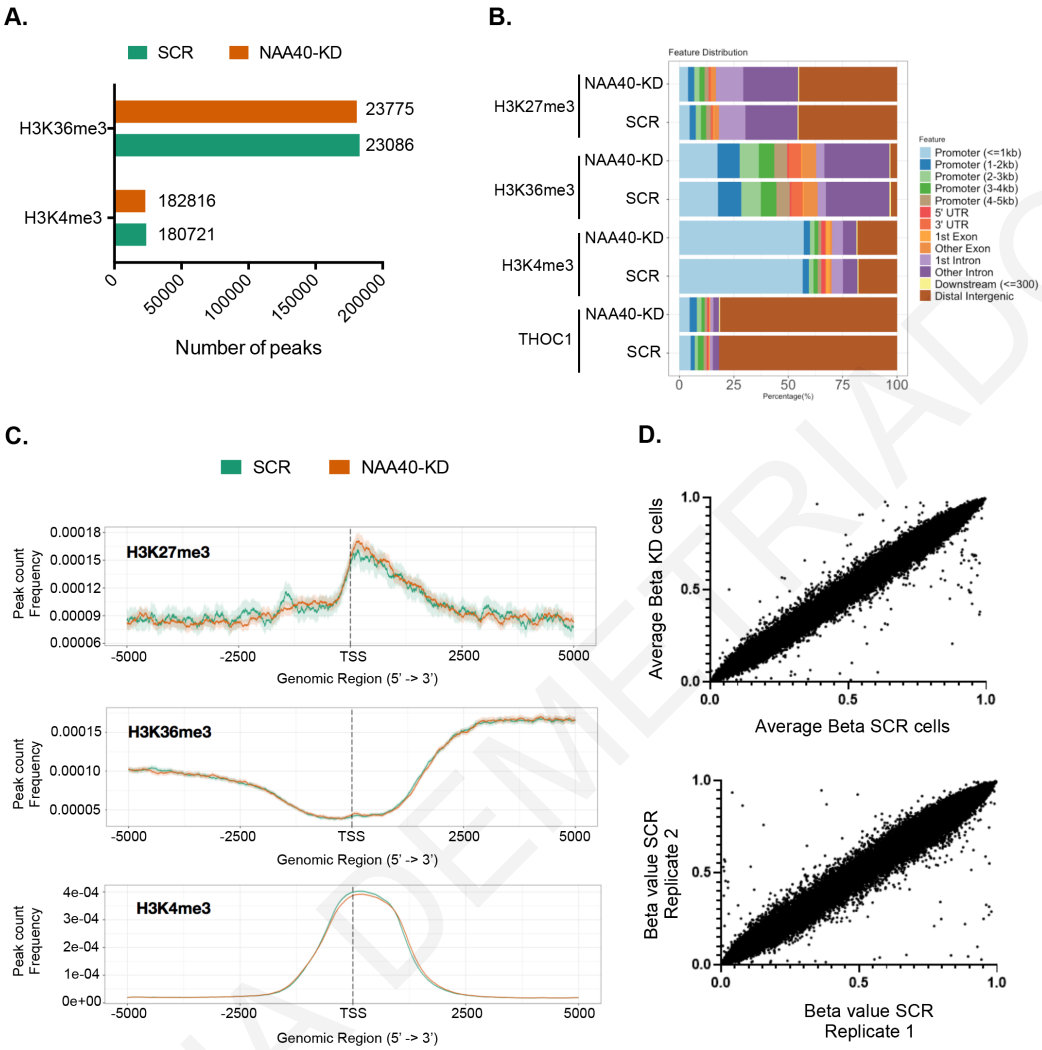

Figure 4.4. NAA40 depletion does not alter the genome-wide distribution of histone and DNA methylation marks. (A, B, C) ChIP-seq analysis showing the total number of peaks (A), feature distribution (B) and peak enrichment relative to TSS (C) of different activating and repressive histone marks normalized to total histone H3 in dox-treated SCR and NAA40-KD HCT116 cells. **(D)** Scatter plots representing the average beta-values of each CpG probe between dox-treated SCR and NAA40-KD cells (top plot) or the two biological replicates of SCR cells as a control for technical variability (bottom plot).

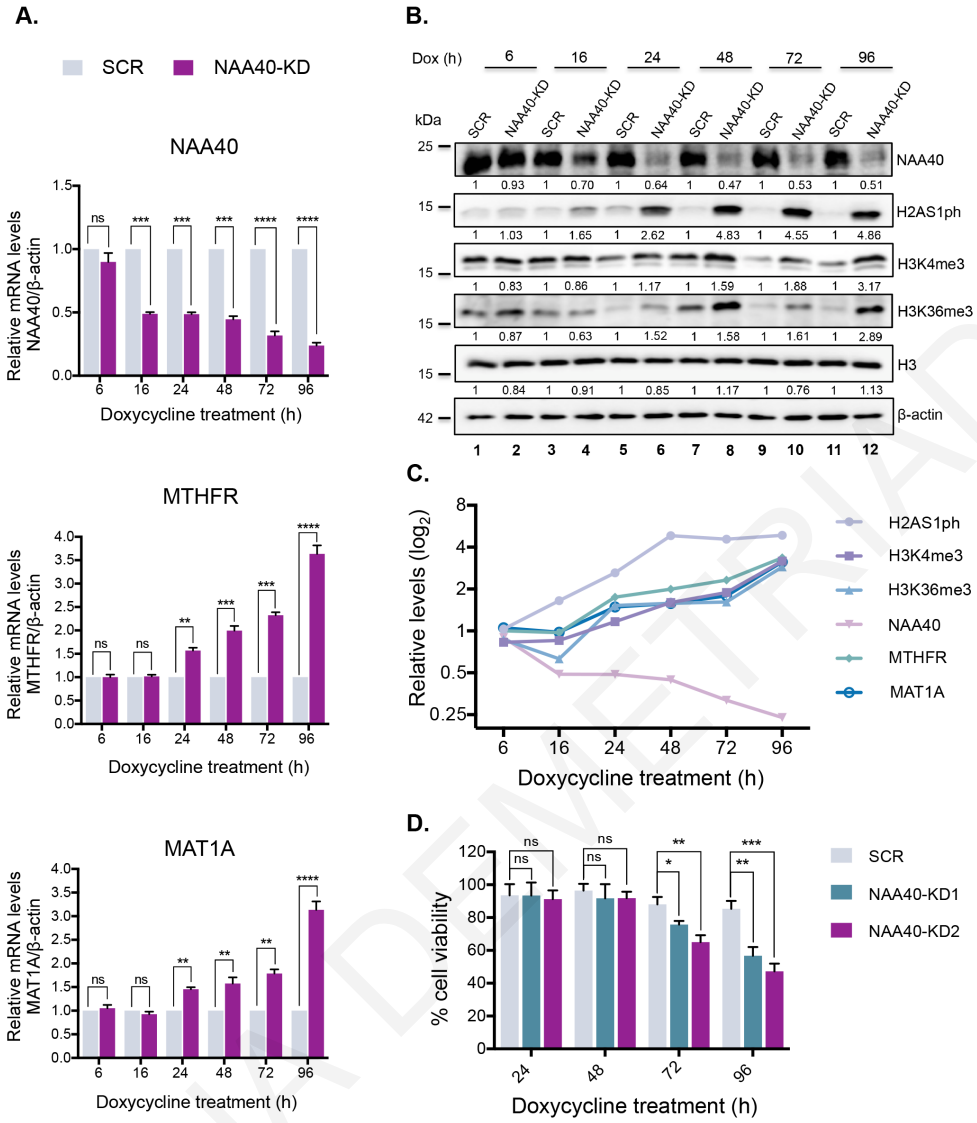

Figure 4.5. NAA40 effects on histone methylation and one-carbon metabolism are dynamically regulated. (A) qRT-PCR analysis (mean ± s.d., N=3) of NAA40, MTHFR and MAT1A mRNA levels normalized to β-actin performed in SCR or NAA40-KD HCT116 cells treated with doxycycline for the indicated time points. **(B)** Representative western blot analysis (N=3) in proteins extracted at different time points from dox-treated HCT116 SCR and NAA40-KD cells using the indicated antibodies. The densitometry numbers below each blot define the normalized levels of each protein against β-actin relative to SCR cells. **(C)** Relative changes in modification (H2AS1ph, H3K4me3 and H3K36me3) or mRNA (NAA40, MTHFR and MAT1A) levels following NAA40 depletion for the indicated time points. **(D)** MTT assay (mean ± s.d., N=3) of SCR and NAA40-KD HCT116 cells incubated with dox for the indicated time points. Cell viability is shown as a percentage relative to the corresponding dox untreated cells. All statistical analyses were performed using unpaired two-tailed Student's t-test (ns=no significance, *p<0.05, **p<0.01, ***p<0.001, ****p<0.0001).
(Figure 4.5A, top plot and Figure 4.5B).

precede the effects on cell viability, since reduction in cell survival was only apparent after 72 h of NAA40 depletion (Figure 4.5D). These findings overall show that the effects of NAA40 knockdown on metabolic rewiring and its corresponding epigenome changes are not prompted by a cell growth defect and suggest that NAA40-dependent transcriptional effects in one-carbon metabolism drive histone methylation changes.

Interestingly, LC/MS analysis at 96h of dox treatment, during which severe depletion of NAA40 mRNA and protein levels is achieved, revealed significant accumulation of Acetyl-CoA, the obligatory co-factor for N-terminal acetylation (Figure 4.6A). Further lipidomics analysis revealed that the enhanced Acetyl-CoA abundance was accompanied by marked induction of cholesterol and diacyglycerols (DG [34:0], DG [36:1] and DG [36:2] species) (Figures 4.6B and 4.6C). These data indicate that increased Ac-CoA accumulation after 96 h of dox treatment might be used for lipid synthesis. On the contrary, no significant changes in cholesterol and DAG levels were observed at 24 h of dox treatment where Ac-CoA abundance was not affected significantly (Figure 4.6).

To support the above notion that NAA40 driven metabolic gene expression changes are responsible for the increased histone methylation phenotype, we next depleted MTHFR using siRNA transfection experiments to attenuate one-carbon metabolism (Figure 4.7A). Unlike the control siRNA which had no effect (Figures 4.7B-D), MTHFR siRNA specifically prevented the induction of histone methylation (Figure 4.7B, compare lanes 7 and 8 with lanes 5 and 6), and rescued the cell viability defect caused by NAA40 depletion (Figures 4.7C and 4.7D bottom images). To ensure that MTHFR is acting downstream of NAA40, we repeated these experiments in SCR and NAA40-KD cells without dox treatment which maintain NAA40 expression (Figure 4.7A, left plot). As expected, MTHFR was

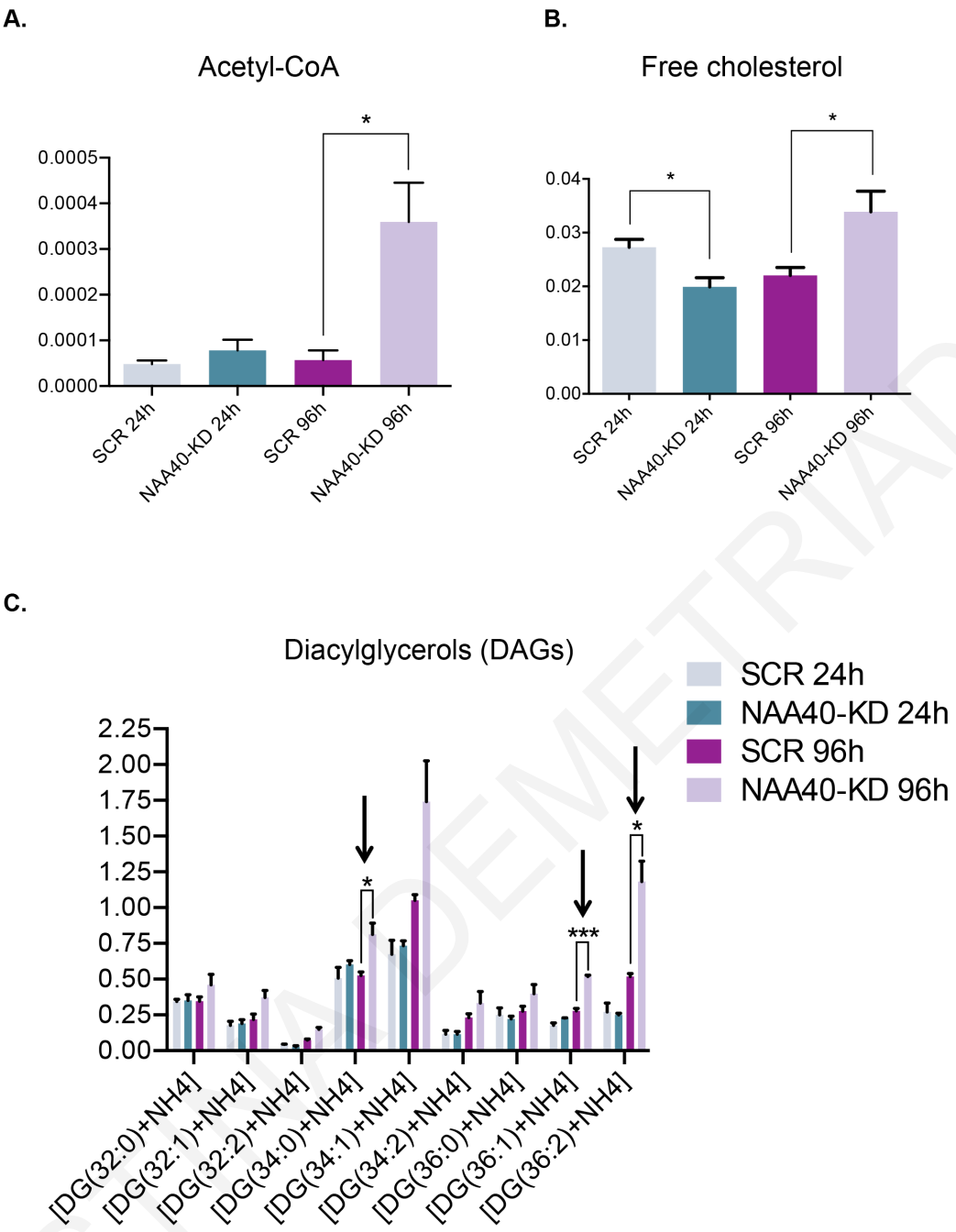

Figure 4.6. NAA40 affects acetyl-CoA pools and lipid synthesis. (A, B, C) Intracellular levels of acetyl-CoA (A), cholesterol (B) and diacylglycerols (C) measured by UPLC-MS (mean ± s.e., N=3) in HCT116 SCR and NAA40-KD cells treated with doxycycline for 24 h and 96 h. All statistical analyses were performed using unpaired two-tailed Student's t-test (*p<0.05, ***p<0.001).

again depleted (fig. 4.7A, right plot) but we did not detect any dramatic changes in either histone methylation or CRC cell growth and viability (Figure 4.7B, compare lanes 3 and 4 with lanes 1 and 2, Figure 4.7C and Figure 4.7D top images). These results reinforce the idea that the effects on histone methylation levels are dependent on NAA40-mediated regulation of one-carbon metabolism and may impinge on CRC cell survival.

Finally, to examine whether the effects of NAA40 on histone methylation occur universally in colon cancer cells we examined three additional CRC cell lines (HT-29, SW480 and SW620). In line with the results observed in HCT116 cells, the bulk levels of histone methylation were elevated in all three different cell lines upon NAA40 knockdown (Figure 4.8A). The increase in histone methylation seen in doxycycline treated NAA40-KD cells was accompanied by transcriptional upregulation of MTHFR one-carbon metabolic gene (Figure 4.8B) and consistently the viability of these cells declines in the absence of NAA40 (Figure 3.4). On the contrary, global histone methylation, MTHFR expression and cell viability remained largely unaffected in non-malignant, immortalized HEK-293 cells lacking NAA40 (Figure 4.9). Collectively, these data suggest that in colorectal cancer cells NAA40-mediated regulation of one-carbon metabolic gene expression controls the global levels of different histone methylation marks.

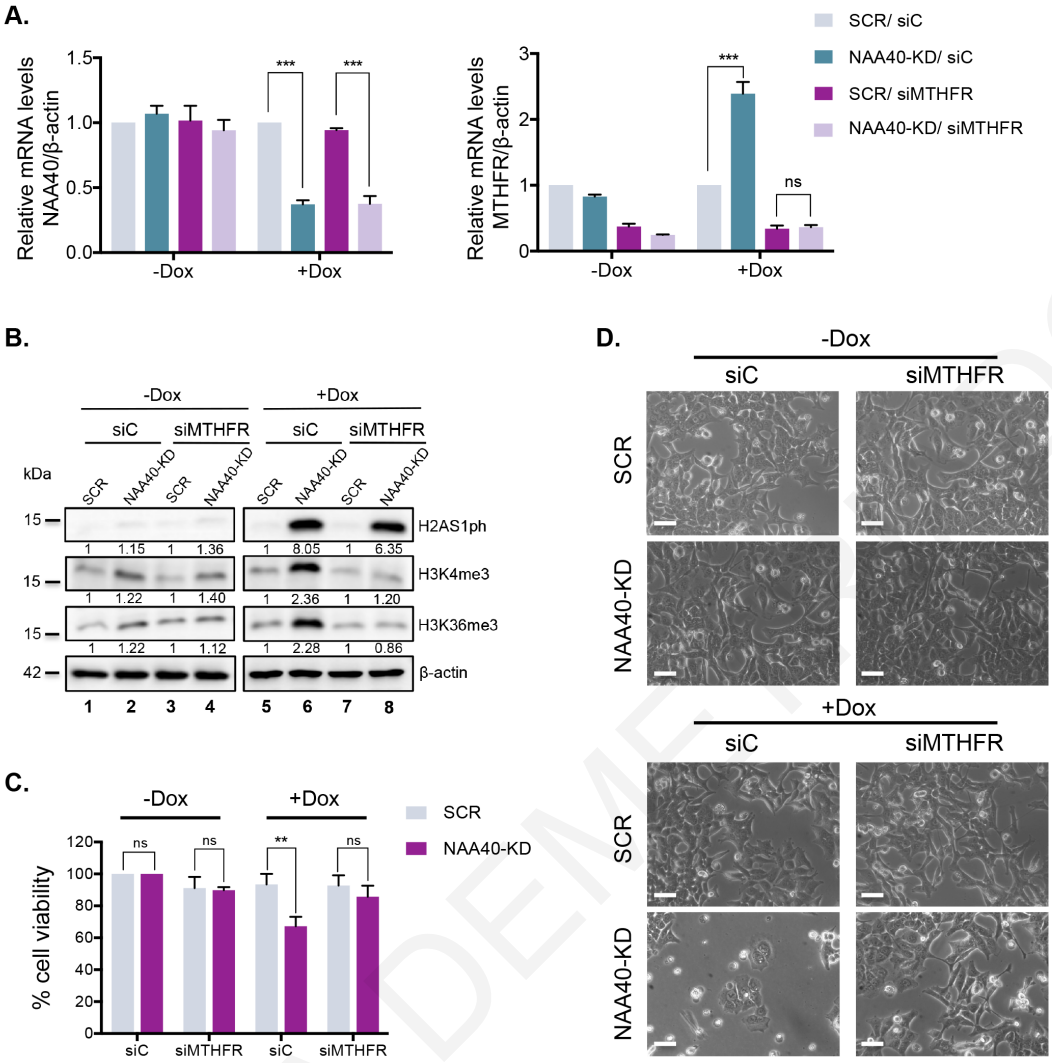

Figure 4.7. The effect of NAA40 on histone methylation is driven through one-carbon metabolism. (A) qRT-PCR analysis (mean ± s.d., N=3) monitoring NAA40 (*left*) and MTHFR (*panel*) mRNA levels normalized to β-actin of HCT116 SCR or NAA40-KD cells transiently transfected with MTHFR-specific (siMTHFR) or control (siC) siRNAs in the presence or absence of dox treatment. **(B)** Representative western blot analysis (N=3) of proteins extracted from siC or siMTHFR transfected SCR and NAA40-KD HCT116 cells treated with or without dox using the indicated antibodies. The values were calculated by densitometry analysis of each protein band relative to the corresponding SCR control after normalization with β-actin. **(C)** MTT assay (mean ± s.d., N=3) in dox-treated or untreated SCR and NAA40-KD cells that were transiently transfected with siC or siMTHFR. **(D)** Phase contrast microscopy of dox-inducible HCT116 SCR and NAA40-KD cells transfected with siC or siMTHFR. Cells were captured in at least five fields of view (100X magnification). The images are representative fields from at least three independent replicates. Scale bar, 100 μm. Unpaired two-tailed Student's t-test was used (ns=no significance, **p < 0.01, ***p < 0.001).

4.3 NAA40 regulates one-carbon metabolism through its histone acetyltransferase activity

Next, we sought to investigate whether the above described NAA40-dependent outcomes are indeed specific to the loss of NAA40 and mediated through its acetyltransferase activity, reported to act selectively on histones (Magin et al. 2015b). To this end, we devised RNAi-rescue experiments by engineering doxycycline-inducible NAA40-KD cells that ectopically express either i) a wild type

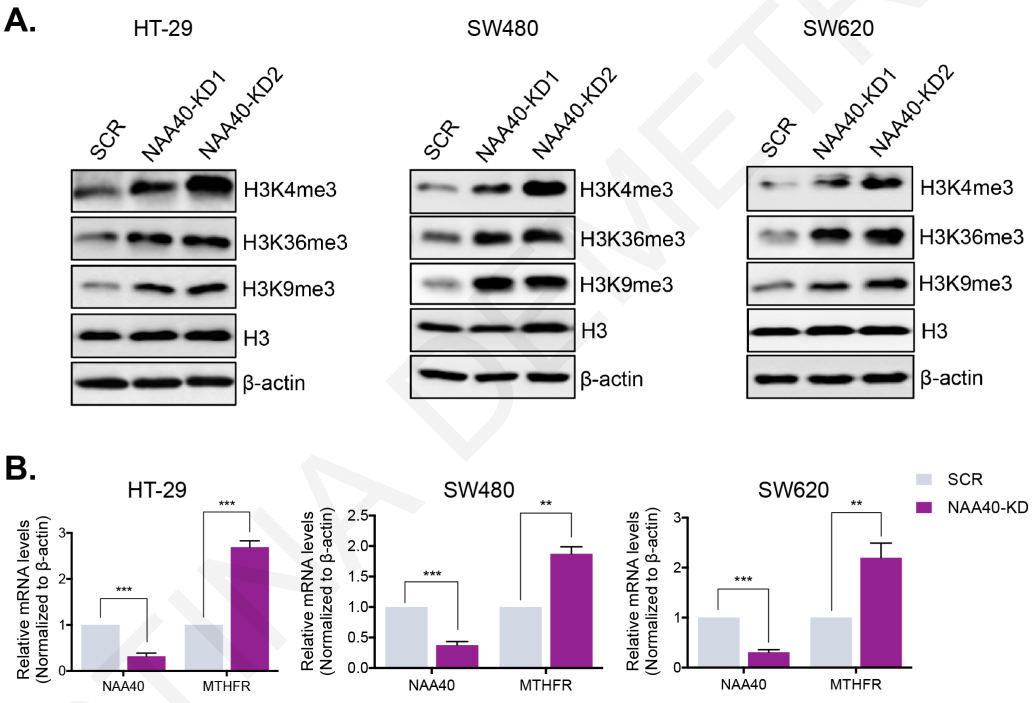

Figure 4.8. NAA40 universally affects one-carbon metabolism and histone methylation in different CRC cell lines. (A) Western blot analysis (N=3) of cell extracts derived from dox-treated SCR or NAA40-KD HT-29, SW480 and SW620 colorectal cancer cells. **(B)** qRT-PCR analysis (mean ± s.d., N=3) of NAA40 and MTHFR mRNA levels normalized to β-actin performed in dox-treated HT-29, SW480 and SW620 engineered to express SCR or NAA40-KD. Student's t-test was used (**p < 0.01, ***p < 0.001).

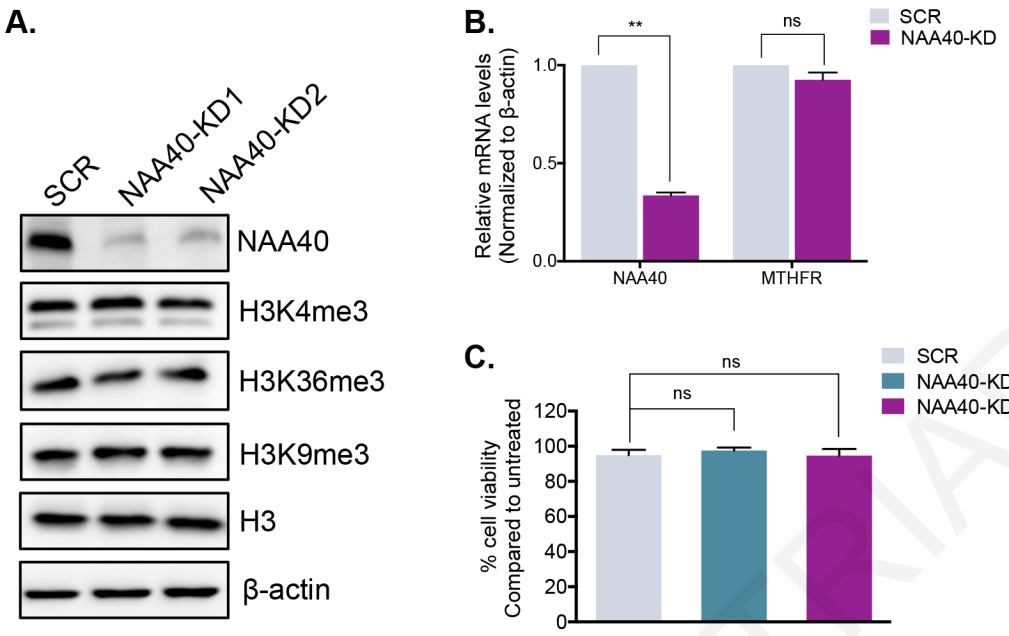

Figure 4.9. NAA40 depletion in HEK293 cells does not affect histone methylation, one-carbon metabolism and cell viability. (A) Representative western blot analysis (N=3) of cell extracts derived from dox-treated SCR or NAA40-KD HEK293 cells using the indicated antibodies. **(B)** qRT-PCR analysis (mean ± s.d., N=3) of NAA40 and MTHFR mRNA levels normalized to β-actin performed in dox-treated HEK293 cells engineered to express SCR or NAA40-KD. **(C)** MTT assay (mean ± s.d., N=3) in HEK293 SCR and NAA40-KD cells treated with dox for 96h. All statistical analyses were performed using unpaired two-tailed Student's t-test (ns=no significance, **p < 0.01).

V5-tagged NAA40 mRNA that was still targeted by shRNAs (Sensitive NAA40(WT)-V5), ii) a wild type NAA40-V5 mRNA that was resistant to shRNA-mediated depletion (Resistant NAA40(WT)-V5), or iii) a resistant catalytically inactive version of NAA40-V5 (Resistant NAA40(E139Q)-V5) (Hole et al. 2011; Magin et al. 2015b). We initially validated our engineered system showing that in the shRNA-sensitive cell line exogenous NAA40(WT)-V5 was efficiently depleted upon dox treatment and, as expected, this was also accompanied with the appearance of the antagonistic histone mark H2AS1ph due to the lack of histone N-terminal acetylation (Figure 4.10A, compare lane 3 with 4). In contrast, the shRNA-resistant NAA40(WT)-V5 cells maintain expression of exogenous

NAA40(WT)-V5 under dox treatment and as a result there is no accumulation of the opposing mark H2AS1ph, showing that the exogenous NAA40(WT)-V5 could complement the function of the endogenous NAA40 enzyme (Figure 4.10A, compare lanes 5 with 6). Most importantly, the exogenous shRNA-resistant catalytically inactive NAA40(E139Q)-V5 remains unchanged under dox treatment, but the antagonistic mark H2AS1ph accumulates indicating that this inactive version of NAA40 is unable to modify histone N-termini and thus cannot complement the catalytic function of the endogenous enzyme (Figure 4.10A, compare lane 7 with 8).

Having validated this complementation system, we then examined how the levels of histone methyl marks and cell viability are affected in these various engineered cells. Consistent with the above results, the increase of H3K4me3 and H3K36me3 was again detected upon depletion of both the endogenous and exogenous shRNA-sensitive NAA40(WT)-V5 version (Figure 4.10A, lanes 3-4). However, this histone methylation enhancement was rescued by exogenous expression of the resistant NAA40(WT)-V5 (Figure 4.10A, lanes 5-6), reinforcing the notion that this effect is mediated by specific loss of NAA40. Of note, the shRNA-resistant enzymatically inactive NAA40(E139Q)-V5 was unable to reduce the levels of H3K4me3 and H3K36me3 under dox treatment suggesting that these effects are driven by the acetyltransferase activity of NAA40. Accordingly, overexpression of the exogenous shRNA-sensitive NAA40(WT)-V5 showed reduced viability upon dox treatment, similarly to cells lacking the endogenous enzyme (Figure 4.10B). On the other hand, the resistant NAA40(WT)-V5 rescued cell viability almost fully while the catalytically dead NAA40(E139Q)-V5 failed to

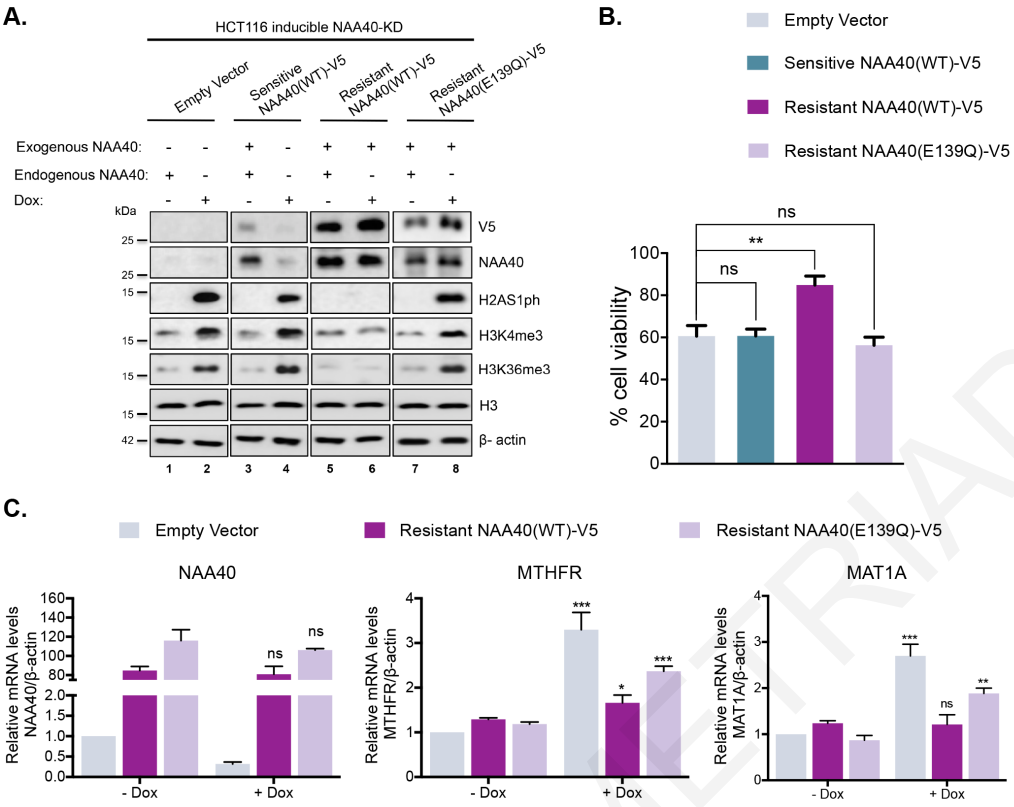

Figure 4.10. NAA40-mediated regulation of one-carbon metabolism, histone methylation and cell viability are dependent on its acetyltransferase activity. **(A)** Western blot analysis (N=3) of HCT116 inducible NAA40-KD cells transduced with Empty vector, shRNA-Sensitive NAA40(WT)-V5, shRNA-Resistant NAA40(WT)-V5 or shRNA-Resistant NAA40(E139Q)-V5 plasmids and treated with or without doxycycline using antibodies against the specified antibodies. **(B)** MTT assay (mean ± s.d., N=3) to assess cell viability in dox-treated HCT116 inducible NAA40-KD cells expressing the indicated proteins. **(C)** qRT-PCR analysis (mean ± s.d., N=3) demonstrating the mRNA levels of NAA40, MTHFR and MAT1A normalized to β-actin in HCT116 inducible NAA40-KD cells transduced with the indicated plasmids in the presence or absence of dox treatment. All statistical analyses were performed using unpaired two-tailed Student's t-test (ns=no significance, *p < 0.05, **p < 0.01, ***p < 0.001).

restore CRC cell viability in the absence of the endogenous enzyme showing once again that this inactive form cannot complement the function of intact NAA40 (Figure 4.10B).

Lastly, we found that overexpression of the shRNA-resistant NAA40(WT)-V5 prevented robust upregulation of MTHFR and MAT1A under dox conditions and this was consistent with the absence of H3K4me3 and H3K36me3 enhancement (compare Figures 4.10A and 4.10C). Nevertheless, forced expression of the shRNA-resistant catalytically dead NAA40(E139Q)-V5 failed to block MTHFR and MAT1A induction after depletion of endogenous NAA40 by dox treatment, which was again consistent with the detected increase in histone methylation marks (compare Figures 4.10A and 4.10C). Altogether, these results demonstrate that the function of NAA40 in regulating one-carbon metabolic gene expression, global histone methylation as well as CRC cell viability is specifically attributed to its acetyltransferase activity.

4.4 NAA40 is localized in the nucleus and interacts with chromatin

Although NAA40 is known to predominantly acetylate histones H4 and H2A co-translationally, previous evidence depicts a nuclear localization for this epigenetic modifier (Hole et al. 2011; Poledova et al. 1999; Jonckheere and Van Damme 2021). Since NAA40 acetyltransferase activity towards histone proteins is required for the molecular and phenotypic effects of CRC cells we then explored the subcellular distribution of this epigenetic modifier. In addition to immunoblot analysis (Figure 4.10A), the expression and localization of exogenous NAA40

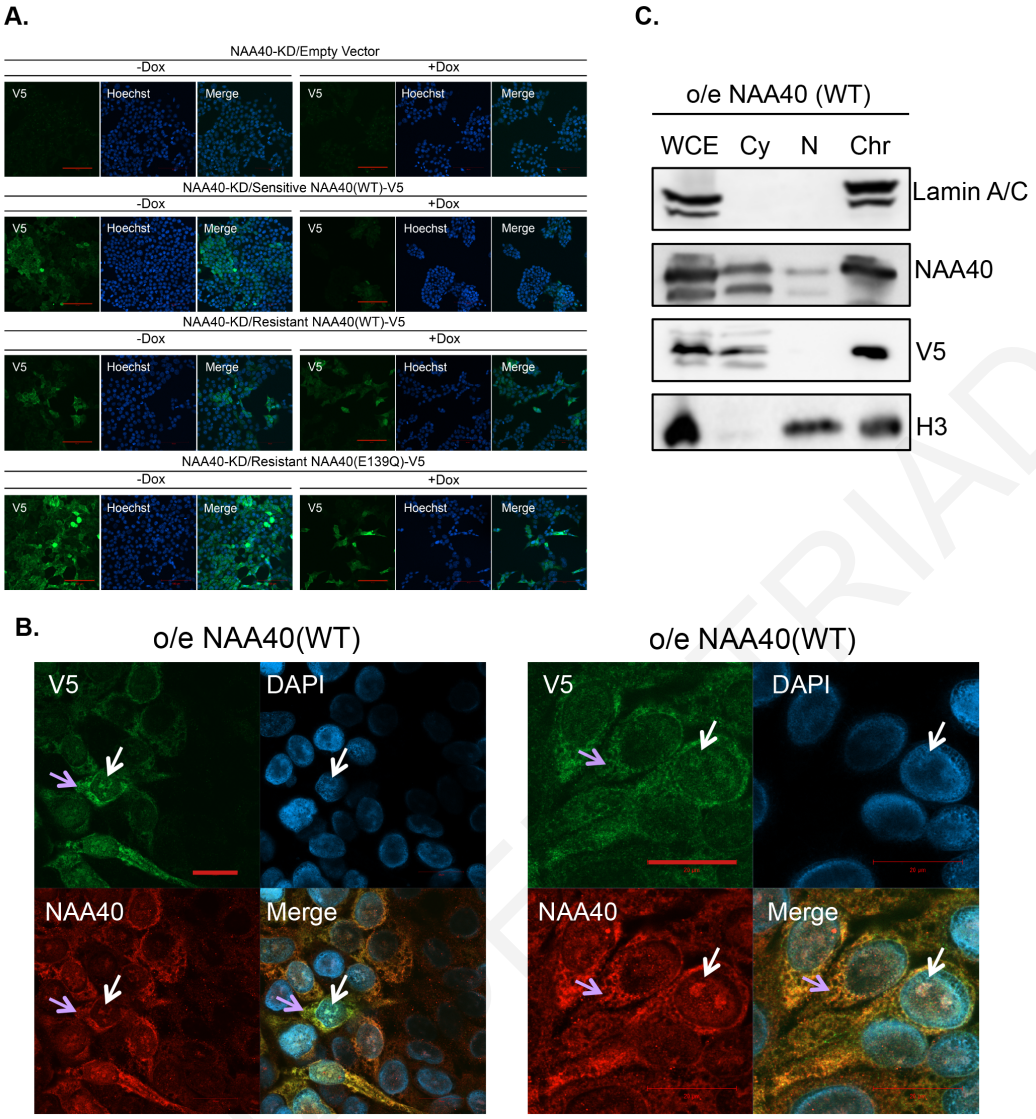

Figure 4.11. NAA40 is localized in the cytoplasm and nucleus. (A) Representative confocal images of V5-tag (green) or Hoechst (blue) in the indicated stable cell lines treated with or without doxycycline. Scale bar, 100 μm. **(B)** Representative confocal images of NAA40-V5 overexpressing HCT116 cells (o/e NAA40(WT)) stained with V5-tag (green), NAA40 (red) or Hoechst (blue). Scale bars, 20 μm. **(C)** Immunoblot analysis (N=3) using the indicated antibodies in whole cell (WCE), cytoplasmic (Cy), nucleoplasmic (N) and chromatin-bound (Chr) protein extracts derived from biochemical fractionation of HCT116 cells overexpressing the wild type NAA40-V5 protein (o/e NAA40(WT)).

protein among the different engineered cell lines in the presence or absence of doxycycline was validated using confocal immunofluorescence microscopy (Figure 4.11A). As expected, we determined a predominant cytosolic localization of NAA40, which is consistent with its previously reported co-translational function (Figure 4.11B, see purple arrows). Interestingly, we also observed a fraction of NAA40 within the nucleus and more specifically at chromatin regions as indicated by DNA staining, suggesting a novel chromatin-bound activity for NAA40 (Figure 4.11B, see white arrows). Consistently, cell fractionation experiments confirmed the enrichment of exogenous NAA40 protein in both cytoplasmic and chromatin-bound fractions further supporting its potential post-translational activity within the nucleus (Figure 4.11C).

4.5 Regulation of one-carbon metabolism by NAA40 renders CRC cells resistant to antimetabolite drug 5-FU

Apart from its role in methyl group biogenesis to support methylation reactions, one-carbon metabolism is also essential for nucleotide synthesis (Locasale 2013). Specifically, TYMS is a key 1C metabolic enzyme converting deoxyuridine monophosphate (dUMP) to deoxythymidine monophosphate (dTMP) by competing with the MTHFR enzyme for the one-carbon unit methylenetetrahydrofolate (me-THF) (Figure 4.2A). The antimetabolite drug 5-Fluorouracil (5-FU), targets TYMS by antagonizing dUMP binding on its catalytic domain inhibiting dTMP synthesis (Figure 4.12A). Although 5-Fluorouracil (5-FU) is the most widely used chemotherapeutic agent for the treatment of CRC, resistance to 5-FU is an important reason for treatment failure (Hammond et al. 2016). Of note, TYMS expression levels have been shown to predict response of malignant cells to 5-FU

therapy (Varghese et al. 2019; Wakasa et al. 2015) but the mechanism underlying TYMS regulation remains largely unexplored.

Given that we identified TYMS to be significantly downregulated upon NAA40-knockdown (Figures 4.1A and 4.1D), we speculated that NAA40 could be a novel regulator of TYMS affecting the response of CRC cells to 5-FU. To test this hypothesis, we initially sought to verify that TYMS expression is indeed responsive to NAA40 levels. Conversely to the observed downregulation of TYMS in NAA40-depleted cells, we found that TYMS levels are increased in cells ectopically overexpressing a wild-type but not a catalytically inactive NAA40 relative to empty vector control cells (Figure 4.12B), further supporting the regulatory link between NAA40 and TYMS expression.

In light of the above results, we then investigated the effects of NAA40-mediated TYMS regulation on the response of CRC cells to 5-FU. We initially examined the response of HCT116 cells overexpressing NAA40 to 5-FU by monitoring cell viability. Interestingly, the viability of cells overexpressing wild-type NAA40-V5 was significantly less affected by the 5-FU treatment compared to non-overexpressing cells carrying an empty vector control (Figure 4.12C, right plot). However, TYMS knockdown by transient siRNA (Figure 4.12C, left plot) reversed the acquired 5-FU resistance of NAA40(WT)-V5 overexpressing cells, indicating that TYMS upregulation is required for NAA40-mediated 5-FU resistance (Figure 4.12C, right plot). In support of this result, dox-induced depletion of NAA40 protein which leads to TYMS downregulation (Figure 4.1A and 4.1D), renders CRC cells more vulnerable to 5-FU when compared to treatment of cells with intact NAA40 (5-FU alone) (Figure 4.12D). However, combinatorial supplementation of doxycycline and 5-FU in cells overexpressing the shRNA-resistant wild-type NAA40 overexpressing the shRNA-resistant wild-type NAA40 did not display

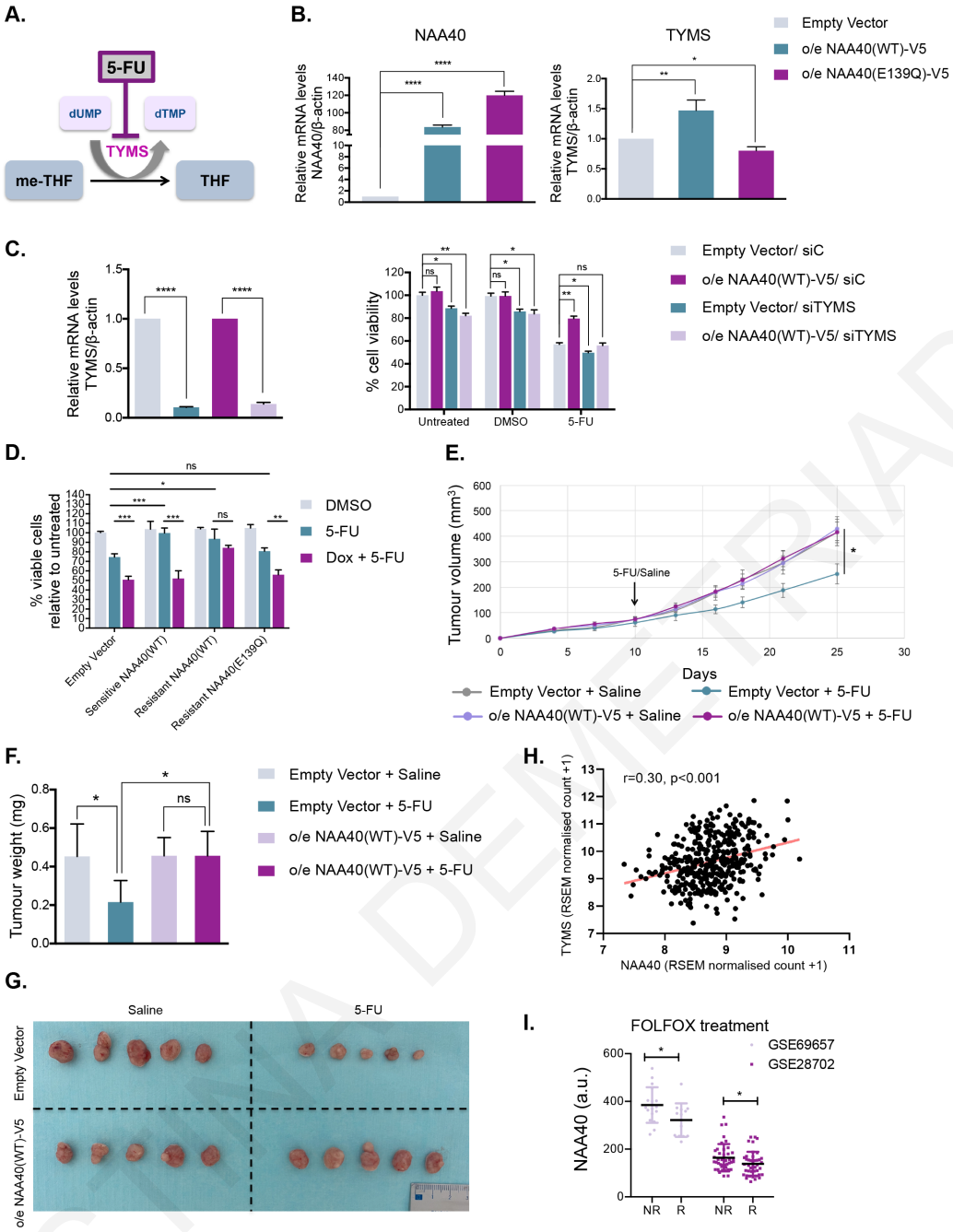

Figure 4.12. NAA40 confers 5-FU resistance through activation of the one-carbon metabolic gene TYMS. (A) Schematic of the metabolic reaction catalyzed by TYMS enzyme which is targeted by 5-FU. **(B)** qRT-PCR analysis (mean ± s.d., N=3) of the indicated HCT116 overexpression cell lines using specific primers for NAA40 and TYMS. The presented values are normalized to β-actin mRNA. **(C)** qRT-PCR analysis (mean ± s.d., N=3) of TYMS mRNA levels normalized to β-actin in HCT116 cells stably overexpressing NAA40(WT)-V5 or empty vector that are transiently transfected with control (siC) or TYMS-specific (siTYMS) siRNAs (*left panel*). MTT assay in HCT116 carrying empty vector control or NAA40(WT)-V5 overexpressing plasmid that are then transfected with siC or siTYMS and cultured in medium containing 5-FU, DMSO or untreated control (*right panel*). **(D)** MTT assay (mean ± s.d., N=3) in HCT116 doxycycline inducible NAA40-KD cells transduced with the indicated plasmids and grown in DMSO, 5-FU or Dox+5-FU. **(E)** Mean tumour volume from 5-FU or saline treated HCT116 xenografts stably

overexpressing (o/e) NAA40(WT)-V5 or carrying an empty vector control. The tumour volume is shown as mean ± s.e. **(F)** Tumour weight and **(G)** representative images of excised empty vector control or o/e NAA40 (WT)-V5 xenograft tumours from mice receiving 5-FU or saline. **(H)** Correlation between the expression of NAA40 and TYMS in 380 primary colorectal cancer tissues extracted from the TCGA database. The orange line demonstrates the regression slope. Statistical analysis was performed using Pearson's rank correlation coefficient (r). **(I)** Relative NAA40 mRNA levels from two independent datasets extracted from GEO omnibus of patients responding to FOLFOX treatment ("R") and patients not responding ("NR"). The p values were calculated using Fisher method (*p < 0.05). All other statistical analyses in the figure were performed using unpaired two-tailed Student's t-test (ns=no significance, *p < 0.05, **p < 0.01, ***p < 0.001, ****p < 0.0001)**.**

sensitivity to 5-FU but conversely conferred resistance to this drug (Figure 4.12D), in line with the previous finding (Figure 4.12C, right plot). Most importantly, cells overexpressing an exogenous shRNA-resistant catalytically inactive NAA40 remained sensitive to 5-FU upon doxycycline treatment (Figure 4.12D). This result indicates that NAA40 histone acetyltransferase activity is driving 5-FU resistance, in agreement with the fact that this activity is implicated in TYMS expression (Figure 4.12B).

Following the above *in vitro* findings, we next wanted to determine if NAA40 controls the response of CRC cells to 5-FU in an *in vivo* model. Therefore, we inoculated HCT116 cells either stably overexpressing wild-type NAA40-V5 or transfected with the empty vector control into nude immunodeficient mice, followed by treatment with 5-FU or vehicle (saline) control through intraperitoneal injection. As expected, the growth of empty vector control tumours was significantly reduced when treated with 5-FU compared to saline control. In contrast, xenograft tumours overexpressing NAA40-V5 developed with similar growth rate in mice receiving either 5-FU or saline control (Figure 4.12E), demonstrating that NAA40 confers 5-FU resistance to CRC tumours similarly to the aforementioned cell-based assays. In addition to the delayed tumour growth, NAA40 overexpressing explants in mice

treated with 5-FU showed increased tumour weight and size compared to the empty vector tumours in the equivalent treatment group (Figure 4.12F and 4.12G). It is worth noting that, in agreement with our *in vitro* studies (Figure 4.12C), the tumour volume of empty vector grafts was vastly similar to that of NAA40 overexpressing tumours receiving saline control, suggesting that NAA40 overexpression alone is not sufficient to promote additional growth advantage to CRC cells (Figure 4.12E). Overall, the data from mouse models combined with our *in vitro* findings indicate that NAA40 promotes 5-FU drug resistance by controlling one-carbon metabolism and particularly TYMS expression.

Finally, we explored the clinical relevance of NAA40 regulating TYMS transcription and 5-FU drug response. The current study along with previous reports showed that NAA40 and TYMS expression levels are elevated in colorectal cancer patients as opposed to normal colon tissues (Varghese et al. 2019). To this end, we performed *in silico* analysis of 380 primary colorectal tumour tissues retrieved from The Cancer Genome Atlas (TCGA) database and found that NAA40 transcript levels in these patients are positively correlated ($r=0.30$, $p<0.001$) with the expression of TYMS (Figure 4.12H), consistent with the above-described regulatory link within CRC cells. Moreover, analysis of microarray data derived from two independent cohorts showed that CRC patients defined as non-responders to 5-FU based chemotherapy display higher NAA40 expression levels relative to those who responded well to 5-FU treatment (Figure 4.12I), suggesting that NAA40 upregulation in human cancers is associated with resistance to antimetabolite chemotherapy. Altogether, these results indicate that NAA40-mediated regulation of TYMS expression affects the response to 5-FU based chemotherapy, providing insight on a new molecular link implicated in CRC drug resistance.

4.6 The NAA40 antagonizing mark H2A/H4S1ph is enriched at the nuclear lamina and mediates TYMS repression

The above results indicate that TYMS expression strongly correlates with NAA40 activity and drug response. Thus, we next looked into possible mechanisms through which NAA40 could mediate transcriptional regulation of TYMS. Because NAA40 affects TYMS activation through its acetyltransferase activity (Figure 4.12B) that is known so far to selectively target histones (Magin et al. 2015b), we turned our focus on the NAA40 antagonizing mark H2A/H4S1ph which has been previously implicated in transcriptional repression (Ju et al. 2017a; Zhang et al. 2004). ChIP analysis showed higher occupancy of H2A/H4S1ph on the TYMS gene in NAA40-knockdown cells (2.5-fold increase) compared to SCR control cells (Figure 4.13A), which is consistent with TYMS downregulation under these conditions (Figure 4.1A and 4.1D). To further support the connection between H2A/H4S1ph and TYMS repression, we examined its expression after exposing doxycycline-treated SCR and NAA40-KD cells to CX-4945 (Silmitasertib), a selective inhibitor of CK2α kinase which mediates H2A/H4S1ph. Importantly, we found that treatment of NAA40-depleted cells with CX-4945 reduced the levels of both H2A and H4 serine 1 phosphorylation and this was accompanied by restoration of TYMS expression (Figure 4.13B and 4.13C).

To define how H2A/H4S1ph could mediate transcriptional silencing upon NAA40 knockdown, we next examined the sub-nuclear localization of this repressive histone mark by super-resolution confocal microscopy. Remarkably, upon NAA40 depletion H2A/H4S1ph re-localizes from the nuclear interior to a prominent ring-like distribution around the inner nuclear membrane of the nuclear envelope where it colocalizes with Lamin A/C (Figure 4.13D, compare left with

right panel), a compartment typically associated with transcriptionally repressive heterochromatin (Buchwalter et al. 2018). To corroborate the association between H2A/H4S1ph and Lamin A/C, we also performed co-immunoprecipitation (co-IP) experiments through which we detected enhanced interaction between Lamin A/C and H2AS1ph upon doxycycline-induced depletion of NAA40 (Figure 4.13E, compare lane 2 with 5).

Consistent with TYMS de-repression seen upon CX-4945 treatment (Figure 4.13C), the ring-like enrichment of H2A/H4S1ph at the nuclear periphery in NAA40-depleted cells was suppressed after inhibition of CK2α but not in control DMSO-treated cells (Figure 4.13F, compare upper with bottom panels). These results suggest that since H2A/H4S1ph becomes enriched at the nuclear periphery upon NAA40 knockdown then TYMS might also become associated with the nuclear lamina. Hence, we next examined the occupancy of Lamin A/C at the TYMS genomic locus in cells expressing or lacking NAA40. ChIP analysis revealed significantly increased occupancy of Lamin A/C at the TYMS gene upon loss of NAA40 but not in SCR control cells, whereas no significant binding was detected at the control JUN promoter (Figure 4.13G) (Salvarani et al. 2019). Taken together, these data highlight a role for NAA40 in controlling the abundance and localization of its antagonizing H2A/H4S1ph mark at the heterochromatin-associated nuclear lamina thus preventing TYMS transcriptional silencing.

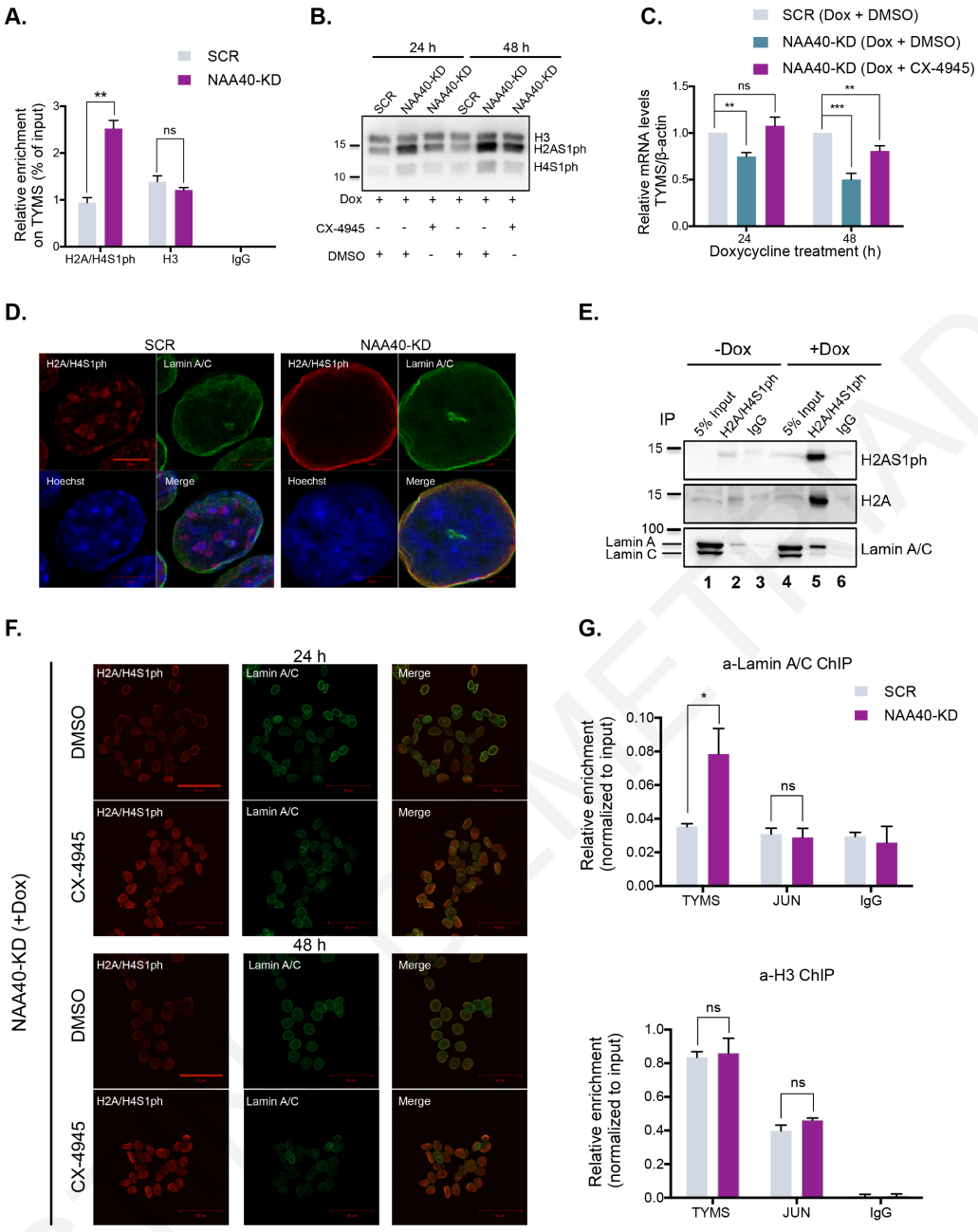

Figure 4.13. The NAA40 antagonizing mark H2AS1ph is localized at the nuclear periphery and silences TYMS expression. (A) ChIP-qPCR (mean ± s.d., N=3) in dox-treated SCR and NAA40-KD cells monitoring the enrichment of H2AS1ph, H3 and IgG on TYMS gene relative to input. **(B)** Western blot analysis (N=3) and **(C)** qRT-PCR analysis (mean ± s.d., N=3) in dox-treated SCR and NAA40-KD HCT116 cells cultured with CX-4945 or DMSO for 24 h and 48 h. **(D)** Representative super-resolution confocal images of H2A/H4S1ph (red) and Lamin A/C (green) in SCR and NAA40-KD cells treated with doxycycline for 72 h. Scale bar, 5 μm. See also Figure S7. **(E)** Immunoprecipitation followed by immunoblot analysis (N=3) of H2A/H4S1ph probed with the indicated antibodies in inducible NAA40-KD cells treated or not with doxycycline for 72 h. **(F)** Confocal IF images of H2A/H4S1ph (red) and Lamin A/C (green) in HCT116 inducible NAA40-KD cells following treatment with doxycycline and CX-4945 or DMSO control for 24 h or 48

h. Scale bar, 50 μm **(G)** ChIP-qPCR analysis on TYMS and JUN genomic location using antibodies against Lamin A/C, H3 or IgG control in SCR and NAA40-KD treated with dox for 72 h. The enrichment for each antibody was normalized to input. All statistical analyses were performed using unpaired two-tailed Student's t-test (ns=no significance, *p < 0.05, **p < 0.01, ***p < 0.001, ****p < 0.0001)**.**

CHAPTER 5

DISCUSSION

5.1 NAA40 contributes to colorectal cancer growth by controlling PRMT5 expression

Emerging evidence shows that impaired levels of epigenetic modifiers and their corresponding histone marks alter gene expression and affect cell growth leading to carcinogenesis. Recently, deregulation of the evolutionarily conserved NAA40 enzyme towards N-terminal acetylation on histone H4 has been implicated in different types of cancer (Ju et al. 2017b; Liu et al. 2009b; Pavlou and Kirmizis 2016). Although we have previously linked NAA40 to CRC (Pavlou and Kirmizis 2016) it remained unclear whether NAA40 contributes to colorectal oncogenesis. Interestingly, we show that NAA40 expression is significantly higher in patient-derived CRC primary tissues than in non-cancerous specimens. Additionally, our findings illustrate that conditional depletion of NAA40 blocks the growth of multiple CRC cell lines and inhibits xenograft tumor formation in mice. Moreover, we provide evidence showing that NAA40 depletion and loss of N-acH4 significantly reduce the global levels of the adjacent histone mark H4R3me2s through transcriptional repression of PRMT5 which in turn alters the expression of its own cancer-associated target genes (Figure 5.1). Consistent with this link between NAA40 and PRMT5, we show that enforced PRMT5 expression partly restores the survival of NAA40 depleted cells and NAA40 expression levels are positively correlated to those of PRMT5 in CRC patient tissues. Taken together, we speculate that NAA40 is crucial for CRC cell growth by acting as a modulator of the PRMT5 oncogene.

Arginine methylation of H4R3 is known to either activate or silence gene expression depending on the symmetric or asymmetric configuration of its dimethylated state. In yeast cells, H4R3me2a is considered to mediate

transcriptional silencing, while H4R3me2s is an activating mark (Low and Wilkins 2012). Conversely in humans, H4R3me2a activates gene expression whereas H4R3me2s is linked to transcriptional repression (Wang et al. 2001; Zhao et al. 2009). Intriguingly, our previous reports together with our findings here point towards an interplay of N-acH4 with the silencing versions of dimethylated H4R3 in yeast (H4R3me2a) and human (H4R3me2s) cells respectively (Schiza et al. 2013). The current study is specifically focused on monitoring N-acH4 since we have previously demonstrated in yeast that NAA40 regulates H4R3me2a through histone H4 but not histone H2A (Schiza et al. 2013). However, it would be intriguing to investigate in future work whether N-acH2A affects respectively the PRMT5-mediated deposition of H2AR3me2s since, in contrast to yeast, human histones H2A and H4 are identical (Hole et al. 2011; Deng et al. 2017). Additionally, in budding yeast, NAA40-mediated N-acH4 directly inhibits the activity of the HMT1 methyltransferase towards H4R3 thus, blocking the deposition of H4R3me2a and activating rDNA expression (Schiza et al. 2013). On the contrary, the current study reveals that N-acH4 in human cells indirectly cross-talks with H4R3me2s through NAA40-mediated transcriptional activation of PRMT5. Consistent with this indirect crosstalk in human cells, a recent biochemical study has demonstrated that N-acH4 has no direct influence on the PRMT5 methyltransferase activity (Fulton et al. 2017). Interestingly, the unique $Arg3_p$ pocket in the structure of NAA40 which is required for substrate recognition specificity raises the possibility that PRMT5-mediated Arg3 methylation might block peptide binding and N-terminal acetylation in a negative feedback loop.

PRMT5 has been extensively characterized as an oncogene that epigenetically silences the expression of vital tumor suppressor genes (Chung et al. 2013; Kaushik et al. 2018; Tae et al. 2011; Wang et al. 2008). Paradoxically,

PRMT5 was recently shown to enhance the transcription of important oncogenes despite depositing silencing histone marks (Deng et al. 2017; Zhang et al. 2015). As a result, PRMT5 deficiency can either restore the expression of tumor suppressor genes or reduce the transcription of oncogenes to block cancer cell growth. Previous data show that PRMT5-mediated histone methylation directly controls the expression of certain cancer-related genes to promote colorectal oncogenesis (Zhang et al. 2015). Consistently, we show here that depletion of NAA40 and subsequent downregulation of PRMT5 leads to induction of the RBL2 and CDKN1A tumor suppressor genes and repression of the EIF4E and FGFR3 oncogenes. These data indicate that PRMT5 plays a key role in NAA40-mediated cancer cell growth. Although the evidence connecting NAA40 to PRMT5 transcriptional activation and downstream expression of its target genes are indirect, the presence of N-acH4 at the PRMT5 promoter suggests that histone N-terminal acetylation may have a direct role in transcription.

5.2 The role of NAA40 in modulating cancer cell metabolism

Metabolic dysfunction is one of the major hallmarks of cancer and emerging studies are highlighting that epigenetic mechanisms could prompt this metabolic dysregulation (Carrer and Wellen 2015; Wong et al. 2017; Campbell and Wellen 2018). However, the contribution of this cross-regulation in therapeutic resistance is underexplored. Here, we have established a new function for this enzyme in bridging epigenetic regulation and metabolism that is exploited by cancer cells to counteract anti-metabolite drug therapy. It is important to note that the principle of resistance established here might have broader implications in other cancers since NAA40 is upregulated in various types of tumours (Koufaris and Kirmizis 2020),

many of which are routinely treated by chemotherapy regimens encompassing antimetabolite agents and may develop chemoresistance (Marine et al. 2020; Shuvalov et al. 2017).

During this study, we combined transcriptomics and metabolomics analysis to reveal that NAA40 modulates two inter-connected parts of the one-carbon metabolic network which impact on one side methylation reactions and on the other side nucleotide biosynthesis. Specifically, among the deregulated genes found in our RNA-seq analysis we identified a set of genes encoding metabolic enzymes implicated within the methionine cycle. Subsequently, LC/MS analysis demonstrated that NAA40 depletion profoundly affects the abundance of critical intermediary methionine and one carbon cycle metabolites, such as methionine, SAM and UMP, which are intimately connected to the deregulated enzymes. Accordingly, 1C metabolic rewiring in response to loss of NAA40 or its histone acetyltransferase activity induces global histone methylation which attenuates CRC cell growth. Importantly this rewiring can be reverted if the methionine and folate cycles are uncoupled by preventing MTHFR expression. This finding strongly suggests that NAA40 upregulation in colorectal cancer cells serves to dampen SAM production and associated chromatin methylation in order to sustain malignant properties (Figure 5.2). In particular, elevated SAM abundance upon NAA40 knockdown is associated with a pronounced increase in various histone methylation marks since we have demonstrated enhancement in the total levels of H3K4me3, H3K36me3, H3K79me2, H3K9me3 and H3K27me3, whereas H3K79me3, H4R3me2a and H4R3me1 remained unaffected. In line with this, it was previously reported that alterations in SAM abundance mediated either by dietary interventions or disruption of relevant metabolic enzymes, such as Nicotinamide N-methyltransferase (NNMT), impacts several methylated histone

residues but the effects are not widespread (Shyh-Chang et al. 2012; Ulanovskaya et al. 2013). It was suggested that this diverse response to SAM abundance could stem from the different affinities (K_m values) of particular methyltransferase enzymes for SAM or the diverse turnover rates of individual histone methylation marks (Dai et al. 2020). Generally, H3K4me3, H3K36me3, H3K9me3, H3K27me3 and H3K79me2 have been shown to be highly sensitive to changes in SAM levels, whereas H3K79me3 and H3R17me2a were found to be less responsive to such metabolic alterations (Shyh-Chang et al. 2012; Ulanovskaya et al. 2013). Also, the response of histone methylation marks to SAM changes could be affected by the altered expression of certain methyltransferase enzymes. For instance, despite SAM accumulation in the absence of NAA40, H4R3me2s levels are reduced due to concomitant downregulation of the PRMT5 methyltransferase.

In contrast to the bulk histone methylation changes, ChIP-seq analysis of histone methylation marks upon NAA40 depletion displayed no significant changes in their genome-wide distribution. One possible reason for this could be that bulk signal alterations which occur in equal trends throughout the genome might be lost after normalization of the signal as a percentage to all mapped sequencing reads. Additionally, a previous study revealed that methionine restriction despite reducing the global levels of H3K4me3, maintains its genomic distribution largely unaffected. Conversely, they showed that limitations in SAM availability decrease H3K4me3 peak width which in turn regulates gene expression (Dai et al. 2018). Our studies further demonstrated that regulation of one-carbon metabolism by NAA40 does not impact global DNA methylation. Methylation of DNA in response to SAM perturbations is highly controversial with some studies demonstrating predominant effects on cytosine methylation and others revealing no significant alterations compared to histone methylation (Maddocks et al. 2016; Ulanovskaya

et al. 2013; Kottakis et al. 2016).

The impact of global changes in SAM availability on the activity of certain chromatin-modifying enzymes and whether or how alterations at the bulk levels of methylated histone residues modulate specific gene expression programs is an active area of research. It is possible that methyltransferase/demethylase enzymes which are sensitive to SAM availability are recruited to specific chromatin regions through their interaction with transcription factors. Another possibility is that SAM synthesizing enzymes may translocate in the nucleus and recruited to specific genomic loci altering local SAM levels (Schvartzman et al. 2018). On the contrary, it is also plausible that some of the affected methylated sites function as methyl sinks in order to maintain SAM homeostasis without altering transcription at specific genomic loci (Ye and Tu 2018).

Beyond the epigenetic regulation of metabolism, NAA40 could also have a more direct effect on the metabolome of cancer cells. Given the fact that Nt-ac decorates 85-99% of histones H4/H2A (19,20) a challenging question arises: Could a significant increase or decrease in the levels of Nt-acetylation have a prominent effect on the acetyl-CoA pool of cells? It is estimated that the approximately six billion nucleotides of the human genome are wrapped around 3x10^7 nucleosome units. The potential maximum acetylation of N-acH4/H2A (100% of H2A and H4 acetylated) would therefore require close to 100 μM of Ac-CoA units (3.2x10^7 nucleosomes X 4 H2A and H4 molecules per nucleosome), an amount that is much higher than the free intracellular pool of Ac-CoA units in mammalian cells which is estimated at about 20 μM (34). Hence, perturbations affecting the consumption of Ac-CoA by NAA40 for catalyzing Nt-ac could possibly have an impact on cellular metabolism. In support of this notion, our data reveal that drastic loss of NAA40 at longer time points of dox treatment significantly

increases the intracellular Ac-CoA pool. Intriguingly, the LC/MS analysis showed increased levels of free cholesterol, as well as enhanced DAG production suggesting that excess levels of free Ac-CoA might be utilized in fatty acid and cholesterol metabolic pathways rather than histone acetylation. Nevertheless, further experimental evidence of how this possible link between Nt-ac and metabolic pool operates in cancer cells and whether it also affects global or local histone lysine acetylation is needed.

5.3 NAA40 serves as a promising target for cancer therapy

Given the large body of evidence strongly supporting the implication of epigenetic regulation in different tumour types, targeting histone modifiers is considered a promising approach in cancer therapy and has come under heavy investigation (Dawson 2017; Demetriadou and Kirmizis 2017). Although our understanding of the regulation and biological significance of histone N-terminal acetylation is far from complete, recent advances in the field advocate the potential of NAA40 histone acetyltransferase as an attractive therapeutic strategy. In particular, targeting NAA40 potentially could have few side effects because in contrast to the majority of chromatin modifiers, it is highly selective known to target only two substrates (histones H2A and H4) and functions as a monomer (Hole et al. 2011). Therefore, it is expected that manipulating NAA40 activity will have less off-target effects compared to other epigenetic enzymes, which act on a large number of substrates. Additionally, no detrimental effects of targeting NAA40 were observed in non-maligant mouse embryonic fibroblasts (Pavlou and Kirmizis 2016) and immortalized HEK293 cells, thus it is possible that inhibiting this histone modifier will not affect adversely normal highly-proliferative cells. However, the effects of

NAA40 inhibition on the metabolite pools should also be examined in normal tissues, including hepatic cells which are highly responsive to metabolic alterations. Furthermore, the recent elucidation of the protein structure of NAA40 revealed unique features compared to other related NAT proteins, which could allow its selected targeting without affecting other members of its family (Magin et al. 2015b).

The potential of NAA40 to serve as a target in anticancer therapy is also reinforced by the current study which shows that high levels of NAA40 are tightly associated with lower sensitivity of CRC cells to 5-FU antimetabolite drug in cell-based assays, xenograft tumours and human primary cancer tissues. At the molecular level, we show that NAA40-mediated resistance of CRC cells to 5-FU is dependent on the transcriptional regulation of the one-carbon metabolic gene TYMS whose encoded enzyme is directly targeted by 5-FU (Figure 5.2). As mentioned in the introduction, a recent study has shown that modulating one-carbon metabolism by methionine restriction can synergize with 5-FU to inhibit CRC cell growth (Gao et al. 2019). This synergistic effect possibly lies in the fact that during methionine deprivation there is an increased flux of carbon units into the methionine cycle leading to histone methylation reprogramming which antagonizes dTMP synthesis by TYMS thus rendering cells more responsive to 5-FU (Dai et al. 2018; Gao et al. 2019). It would be interesting to determine in the future if NAA40 can act as a molecular sensor coupling nutrient availability to one-carbon metabolism. Nonetheless, our data argue that targeting NAA40 could be part of such combinatorial therapies and this prospect is further supported by the fact that this enzyme can be specifically inactivated by potent small-molecule inhibitors that have been recently discovered (Deng et al. 2021). However, prior to the usage of NAA40 specific pharmacological inhibitors for colon cancer treatment,

further studies are required to more precisely characterize the phenotypic consequences of NAA40 depletion in CRC cells and also determine NAA40 functional effects in a healthy background using normal primary colonic cells.

5.4 The sub-nuclear localization of NAA40 antagonizing mark, H2A/H4S1ph, is a possible mechanism for gene regulation and drug resistance

Our findings unveil the mechanism through which NAA40 regulates TYMS expression to confer drug resistance. Specifically, we provide evidence that TYMS silencing in NAA40-deficient cells is controlled by CK2α-mediated H2A/H4S1ph which has been previously reported to negatively crosstalk with NAA40-mediated histone N-terminal acetylation and inhibit transcription (Zhang et al. 2004; Ju et al. 2017a). Nonetheless, we show for the first time to our knowledge that the NAA40 antagonizing mark H2A/H4S1ph is strikingly redistributed from the interior of the nucleus to the inner wall of the nuclear envelope where it interacts with Lamin A/C. Co-enrichment of H2A/H4S1ph and Lamin A/C on the genomic locus of TYMS upon NAA40 depletion suggests a possible mechanism of TYMS repression to confer resistance against 5-FU. In addition to ChIP analysis, fluorescence in situ hybridization (FISH) experiments would be also critical to assess localization of TYMS DNA region at the nuclear lamina upon NAA40 knockdown. Since anchoring of chromatin to the nuclear lamina associates with heterochromatin compartments and transcriptional silencing (Finlan et al. 2008; Reddy et al. 2008), our findings provide new insight on the repressive nature of H2A/H4S1ph which could serve as a critical factor for heterochromatin organization and stabilization at the nuclear periphery driving gene inactivation and halting cancer-associated

phenotypes. However, subsequent studies are needed to explore whether re-localization of H2A/H4S1ph at the nuclear periphery in the absence of NAA40 influences the expression of other genes, such as PRMT5 since the nuclear lamina serves as a docking site for several genes (Lund et al. 2013; Karoutas and Akhtar 2021). Previous work reported that histone deacetylase HDAC3 of the NCoR complex binds lamina-associating sequences (LASs) and directly interacts with components of the nuclear lamina promoting histone H4 deacetylation and tethering of compacted heterochromatin at the nuclear envelope (Demmerle et al. 2012; Finlan et al. 2008; Zullo et al. 2012; Reddy et al. 2008). Moreover, Zhang *et al*. reported that protein kinase CK2 binds and phosphorylates HDAC3 at Ser 424 to activate its enzymatic activity (Zhang et al. 2005). In support of this, another study depicted that treatment of colorectal cancer cells with the HDAC inhibitor (HDACi) sodium butyrate inhibits the activity of CK2 suggesting a potential mechanism of blocking HDAC3 activity, although this has yet to be demonstrated experimentally (Russo et al. 1997). Based on this evidence and the fact that CK2 mediates H2A/H4S1ph an appealing hypothesis could be that HDAC3 is involved in the recruitment of H2A/H4S1ph enriched chromatin at the nuclear periphery upon NAA40 depletion. In line with this, an interesting question to explore is whether HDAC3 could be also involved in the active removal of N-terminal acetylation from chromatin.

This implication of H2A/H4S1 modifications could be of particular importance in the future since it was recently shown that in tumour tissues substitution of serine (S) to cysteine (C) at position 1 is the most frequently occurring mutation on histone H2A and the second most frequent mutation on histone H4, further signifying the value of S1 modifications in carcinogenesis (Nacev et al. 2019). In addition to S1, mutation of arginine 3 to cysteine (R3C) is

the most common mutation occurring on histone H4 in a diverse range of tumours. Given the existing relationship of S1 acetylation with both R3 methylation and S1 phosphorylation, additional studies are needed to examine whether and how this combinatorial crosstalk is harnessed by cancer cells to drive transcriptional programs (Nacev et al. 2019).

5.5 Future directions

Although published work and ongoing research carried out by our group implicate NAA40 in the regulation of gene expression and oncogenesis, several fundamental questions remain to be resolved. For instance, the lamina-proximal positioning of the NAA40 antagonizing mark H2A/H4S1ph was also accompanied by significant changes in DNA compaction (Figure 4.12F), implying that NAA40 depletion might impacts chromatin architecture. It would be therefore critical to assess the effects of NAA40 knockdown on 3D chromatin organization by conducting ATAC-seq and Hi-C analysis to determine global chromatin accessibility and higher-order chromatin structure, respectively. In depth mechanistic work is also needed to uncover the precise molecular mechanism through which NAA40-dependent localization of H2A/H4S1ph operates in heterochromatin-associated compartments for the regulation of transcription. In line with this, it would be interesting to investigate the effects of CRC cells overexpressing EGFP-tagged histones H4 and H2A where serine 1 is mutated to cysteine (S1C) or aspartic acid (S1D), and whether these substitutions can phenocopy the loss of NAA40 activity. Additionally, DamID experiments using Lamin B1 or Lamin A fused to E.coli DNA adenine methyltransferase (Dam) followed by sequencing could reveal all the genomic loci that are recruited to the nuclear lamina in the absence of NAA40 (Borsos et al. 2019). Alternatively,

DamID can be combined with single cell live imaging by using Dpn1-GFP fusion protein to track the fate of H2A/H4S1ph enriched LADs across mitotic divisions (Kind et al. 2013).

The human acetyltransferase NAA40 is thus far considered to target histones H4 and H2A only (Hole et al. 2011; Poledova et al. 1999). However, a recent study proposed histone variant H2A.Z and the transcriptional regulatory protein Lge1 as possible NAA40 yeast targets but further experiments are required for the validation of those findings (Jonckheere and Van Damme 2021). Despite the lack of experimental data, histone variant H2A.X, which is rapidly exchanged and subjected to phosphorylation on serine 139 (γH2AX) during double strand break (DSB) formation, also bears the SGRG recognition sequence and could be potentially subjected to N-terminal acetylation by NAA40. Hence, it is important to determine the existence and potential of H2A.X N-terminal acetylation (N-acH2A.X) and/or phosphorylation (H2A.XS1ph) on serine 1 as novel regulators of DNA damage response and repair. Beyond H2A.X, the ability of NAA40 to recognize and acetylate the primary amine group of histone variants MacroH2A1 and MacroH2A2 which share an N-terminal SSRG and SGRS sequence, respectively should be examined.

NAA40 functions as a monomer and is known to primarily associate with ribosomal proteins targeting nascent polypeptides. Nevertheless, our immunofluorescence and biochemical fractionation analysis in support of previous evidence pinpoints an interaction of NAA40 with chromatin within the nucleus (Hole et al. 2011; Jonckheere and Van Damme 2021). This observation raises numerous questions: 1) How is NAA40 recruited in the nucleus? 2) Is NAA40 targeted to specific genomic loci by interacting with other nuclear proteins? 3) Does NAA40 acetylate histones post-translationally? To answer those questions,

mass-spectrometry analysis of NAA40 and V5-tag in the nuclear fraction of cells overexpressing the wild-type or catalytically dead NAA40 protein will identify potential interactors that might recruit NAA40 to DNA-specific regions. A high-throughput protein-protein interaction analysis previously conducted in HCT116 and HEK293 cells identified Xeroderma Pigmentosum Complementation Group C (XPC) and FACT complex subunits (SSRP1 and SUPT16H) as possible interactor candidates (Huttlin et al. 2017; Huttlin et al. 2015). Interestingly, XPC protein is a key sensor of DSB formation while FACT complex mediates the exchange of histone H2A with H2A.X further supporting a nuclear role of NAA40 in DNA damage. More recently, proximity-dependent biotin identification (BioID) experiments unveiled a possible interactome network of NAA40. In the same study they reported that Nt-myristoylation of NAA40 through interaction with N-myristoyltransferase 1 (NMT1) might act as a nuclear localization signal (Jonckheere and Van Damme 2021). Moreover, to investigate the mechanistic insights underlying the nuclear localization of NAA40 and its possible post-translational activity, ChIP-seq experiments should be performed in cells expressing the endogenous or exogenous NAA40 protein.

Given that malignant cells and embryonic stem cells share the same metabolic requirements for rapid proliferation, it is perhaps expected that similar molecular mechanisms could be applied in both tumourigenesis and normal development. Intriguingly, a CRISPR-Cas9 knockout screening of 18000 genes in HUES62 human embryonic stem cell line identified NAA40 among the top 1000 genes whose sgRNA guided deletion reduces cell viability (Shalem et al. 2014). Gene ontology (GO) analysis of the essential genes revealed N-acetyltransferase activity among the most significantly enriched GO terms (Shalem et al. 2014). Hence, it would be interesting in the future to examine the role of NAA40 in the

context of ESC self-renewal and differentiation.

5.6 Conclusion

Epigenetic writers and their corresponding histone marks are often implicated in the expression of multiple genes with distinct biological roles in a cell type and context dependent manner. Overall, the current work identifies a regulatory function of NAA40 enzyme towards different target genes encoding both metabolic (e.g MTHFR, TYMS) and epigenetic factors (e.g. PRMT5). One possible scenario is that regulation of those different pathways might work in parallel to govern CRC cell survival. In that case someone would expect that restoration of those pathways would be adequate to fully recover CRC cell proliferation and viability in the absence of NAA40. However, whether the transcription of all deregulated genes is influenced by H2A/H4S1ph antagonistic crosstalk or if NAA40 could respond to environmental stress including nutrient deprivation, serum starvation or low oxygen availability to differentially control those target genes still remains elusive. Another reasonable explanation of how NAA40-mediated N-terminal acetylation could differentially drive the expression of certain genes to sustain CRC malignant properties might be the existence of distinct sets of reader proteins which may be recruited or occluded depending on specific chromatin environments and combinatorial patterns of N-terminal acetylation with other histone marks. Nevertheless, further studies are needed for the discovery of such reader proteins. Future work will also expand our understanding on whether ribosome- and chromatin-bound NAA40 activity exhibit differential effects on gene expression.

Taken together, our data strengthen the importance of NAA40 to maintain

colorectal cancer cell growth and drug resistance. In this study, we show that NAA40 is significantly upregulated in primary colorectal cancer tissues and promotes CRC cell growth both *in vitro* and in xenograft tumor models. The results also depict that NAA40 induces H4R3me2s levels through transcriptional activation of PRMT5. Upregulation of the latter subsequently alters the expression of its cancer-associated target genes promoting CRC cell growth (Figure 5.1). Different omic approaches also revealed that NAA40 regulates the expression of genes (e.g. MTHFR, MAT1A and TYMS) encoding vital enzymes involved in one-carbon (1C) metabolic network thereby influencing the intracellular concentration of intermediary metabolites of this pathway (e.g. SAM and UMP). Rewiring of one-carbon metabolism by NAA40 interferes with global histone methylation levels and colorectal cancer cell survival (Figure 5.2). Importantly, NAA40 stimulates transcription of the metabolic gene TYMS, whose product is targeted by 5-FU, by controlling the spatial distribution of its antagonistic histone mark H2A/H4S1ph within the nucleus. Accordingly, NAA40-mediated TYMS activation confers resistance to 5-FU *in vitro* and *in vivo* (Figure 5.2). Moreover, NAA40 expression in human CRC tumours positively correlates with TYMS levels and worse response of CRC patients to 5-FU-based chemotherapy. To conclude, these findings define NAA40 as a critical mediator at the interface between epigenetics and metabolism and signify its potential as a novel predictive factor and therapeutic target in colorectal cancer.

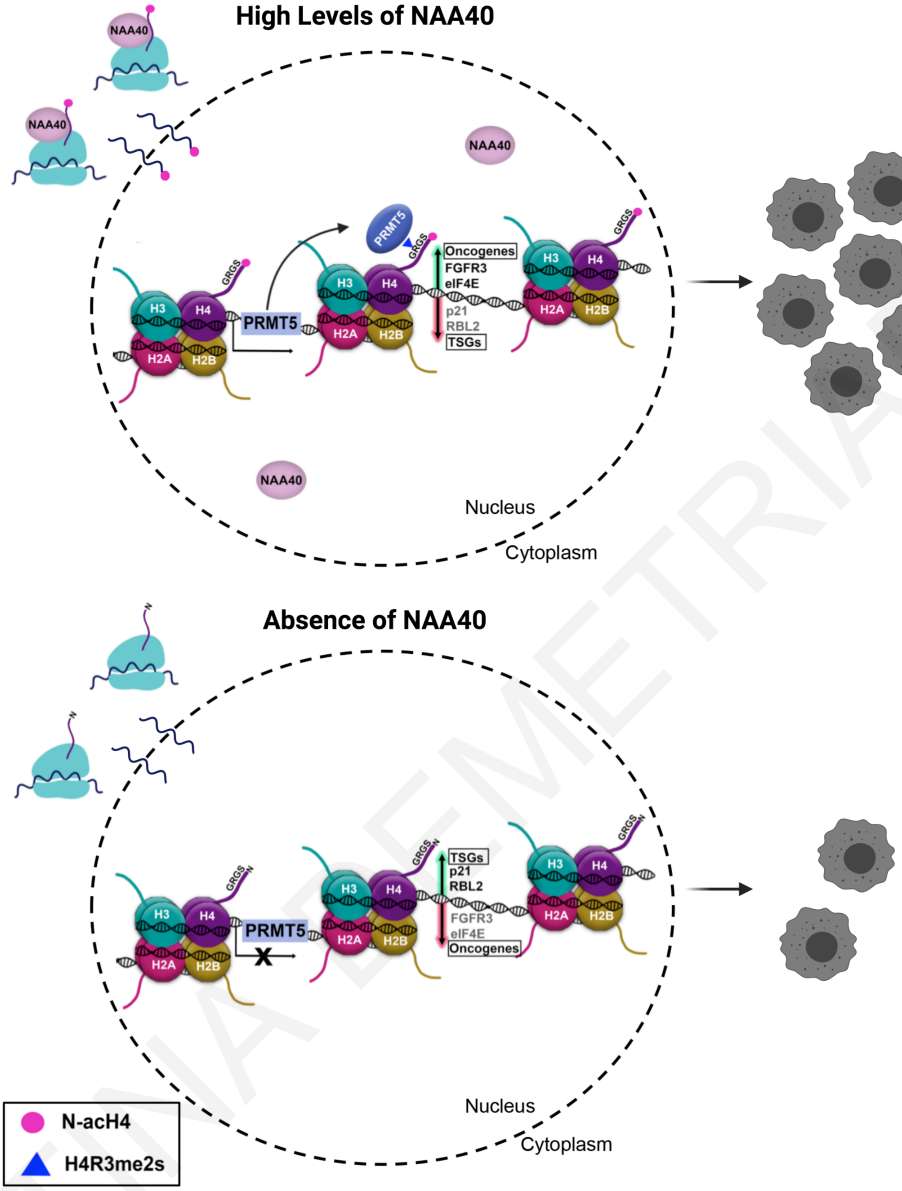

Figure 5.1. Proposed model of NAA40-mediated regulation of PRMT5. In the presence of high levels of NAA40, N-alpha terminal acetylation on histone H4 (N-acH4) catalyzed by NAA40 promotes the expression of PRMT5 enzyme which then catalyzes the addition of symmetric dimethylation on the adjacent arginine 3 residue (H4R3me2s). This activates the expression of oncogenes (e.g., FGFR3 and eIF4e) while it prevents the expression of tumour suppressor genes (TSGs) (e.g., p21 and RBL2) leading to increased CRC cell growth. Lack of NAA40 also suppresses PRMT5 expression and thus attenuates H4R3me2s resulting in silencing of oncogenes and reactivation of TSGs delaying CRC cell growth. Adapted from Demetriadou et al., 2020.

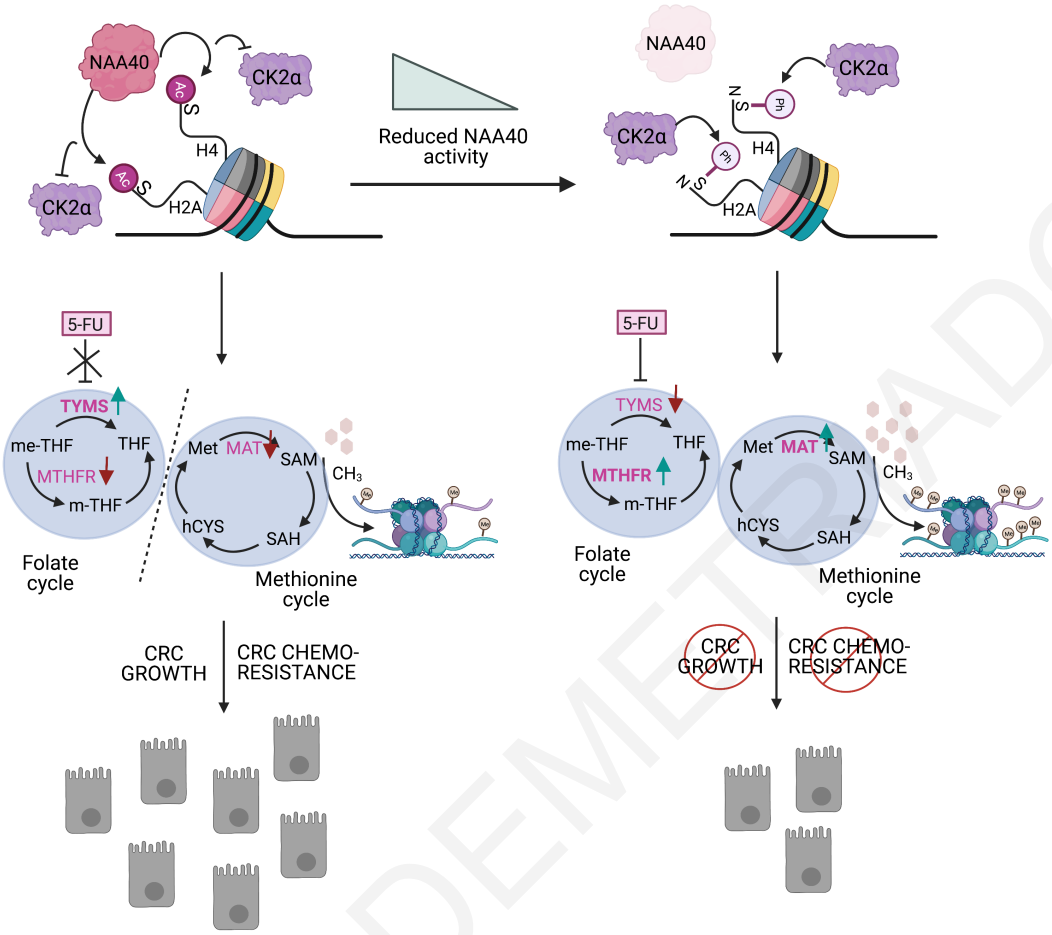

Figure 5.2. Model for the NAA40-mediated effects on cancer cell growth and chemoresistance through regulation of one-carbon metabolism. High NAA40 activity towards histones H2A and H4 in colorectal cancer (CRC) cells antagonizes CK2α-mediated H2A/H4S1ph inducing TYMS expression and promoting resistance to 5-FU anti-metabolite agent. At the same time, NAA40 upregulation decreases MTHFR and MAT1A levels resulting in low SAM concentrations, reduced global histone methylation and contributing to CRC cell growth. Conversely, loss of NAA40 activity results in the deposition of H2A/H4S1ph at the nuclear periphery, downregulation of TYMS and increased sensitivity to 5-FU, whereas concomitant upregulation of MTHFR and MAT1A lead to high SAM abundance, increased bulk histone methylation levels and reduced CRC cell growth.

CHAPTER 6

REFERENCES

Aksnes, H., Drazic, A., Marie, M. & Arnesen, T. 2016. First Things First: Vital Protein Marks by N-Terminal Acetyltransferases. *Trends Biochem Sci,* 41**,** 746-760. 10.1016/j.tibs.2016.07.005

Aksnes, H., Ree, R. & Arnesen, T. 2019. Co-translational, Post-translational, and Non-catalytic Roles of N-Terminal Acetyltransferases. *Molecular Cell,* 73**,** 1097-1114. 10.1016/j.molcel.2019.02.007

Bannister, A. J. & Kouzarides, T. 2011. Regulation of chromatin by histone modifications. *Cell Res,* 21**,** 381-95. 10.1038/cr.2011.22

Benson, A. B., Venook, A. P., Al-Hawary, M. M., Cederquist, L., Chen, Y.-J., Ciombor, K. K., Cohen, S., Cooper, H. S., Deming, D., Engstrom, P. F., et al. 2018. Rectal Cancer, Version 2.2018, NCCN Clinical Practice Guidelines in Oncology. *Journal of the National Comprehensive Cancer Network,* 16**,** 874-901. 10.6004/jnccn.2018.0061

Bergman, Y. & Cedar, H. 2013. DNA methylation dynamics in health and disease. *Nature Structural & Molecular Biology,* 20**,** 274-281. 10.1038/nsmb.2518

Black, Joshua c., Van rechem, C. & Whetstine, Johnathan r. 2012. Histone Lysine Methylation Dynamics: Establishment, Regulation, and Biological Impact. *Molecular Cell,* 48**,** 491-507. 10.1016/j.molcel.2012.11.006

Blanc, R. S. & Richard, S. 2017. Arginine Methylation: The Coming of Age. *Mol Cell,* 65**,** 8-24. 10.1016/j.molcel.2016.11.003

Borsos, M., Perricone, S. M., Schauer, T., Pontabry, J., De Luca, K. L., De Vries, S. S., Ruiz-Morales, E. R., Torres-Padilla, M.-E. & Kind, J. 2019. Genome–lamina interactions are established de novo in the early mouse embryo. *Nature,* 569**,** 729-733. 10.1038/s41586-019-1233-0

Buchwalter, A., Kaneshiro, J. M. & Hetzer, M. W. 2018. Coaching from the sidelines: the nuclear periphery in genome regulation. *Nature Reviews Genetics,* 20**,** 39-50. 10.1038/s41576-018-0063-5

Cai, L., Sutter, Benjamin m., Li, B. & Tu, Benjamin p. 2011. Acetyl-CoA Induces Cell Growth and Proliferation by Promoting the Acetylation of Histones at Growth Genes. *Molecular Cell,* 42**,** 426-437. 10.1016/j.molcel.2011.05.004

Calvert, A. E., Chalastanis, A., Wu, Y., Hurley, L. A., Kouri, F. M., Bi, Y., Kachman, M., May, J. L., Bartom, E., Hua, Y., et al. 2017. Cancer-Associated IDH1 Promotes Growth and Resistance to Targeted Therapies in the Absence of Mutation. *Cell Reports,* 19**,** 1858-1873. 10.1016/j.celrep.2017.05.014

Campbell, S. L. & Wellen, K. E. 2018. Metabolic Signaling to the Nucleus in Cancer. *Molecular Cell,* 71**,** 398-408. 10.1016/j.molcel.2018.07.015

Carrer, A. & Wellen, K. E. 2015. Metabolism and epigenetics: a link cancer cells exploit. *Current Opinion in Biotechnology,* 34**,** 23-29. 10.1016/j.copbio.2014.11.012

Chalkiadaki, A. & Guarente, L. 2012. Sirtuins mediate mammalian metabolic responses to nutrient availability. *Nature Reviews Endocrinology,* 8**,** 287-296. 10.1038/nrendo.2011.225

Chung, J., Karkhanis, V., Tae, S., Yan, F., Smith, P., Ayers, L. W., Agostinelli, C., Pileri, S., Denis, G. V., Baiocchi, R. A., et al. 2013. Protein arginine methyltransferase 5 (PRMT5) inhibition induces lymphoma cell death through reactivation of the retinoblastoma tumor suppressor pathway and polycomb repressor complex 2 (PRC2) silencing. *J Biol Chem,* 288**,** 35534-47. 10.1074/jbc.M113.510669

Dai, Z., Mentch, S. J., Gao, X., Nichenametla, S. N. & Locasale, J. W. 2018. Methionine metabolism influences genomic architecture and gene expression through H3K4me3 peak width. *Nature Communications,* 9. 10.1038/s41467-018-04426-y

Dai, Z., Ramesh, V. & Locasale, J. W. 2020. The evolving metabolic landscape of chromatin biology and epigenetics. *Nature Reviews Genetics,* 21**,** 737-753. 10.1038/s41576-020-0270-8

Danieli, A. & Papantonis, A. 2020. Spatial genome architecture and the emergence of malignancy. *Human Molecular Genetics,* 29**,** R197-R204. 10.1093/hmg/ddaa128

Dann, S. G., Ryskin, M., Barsotti, A. M., Golas, J., Shi, C., Miranda, M., Hosselet, C., Lemon, L., Lucas, J., Karnoub, M., et al. 2015. Reciprocal regulation of amino acid import and epigenetic state through Lat1 and
EZH
2. *The EMBO Journal,* 34**,** 1773-1785. 10.15252/embj.201488166

Dawson, M. A. 2017. The cancer epigenome: Concepts, challenges, and therapeutic opportunities. *Science,* 355**,** 1147-1152. 10.1126/science.aam7304

Dawson, M. A. & Kouzarides, T. 2012. Cancer epigenetics: from mechanism to therapy. *Cell,* 150**,** 12-27. 10.1016/j.cell.2012.06.013

Deberardinis, R. J. & Chandel, N. S. 2016. Fundamentals of cancer metabolism. *Sci. Adv.,* 2**,** e1600200.

Demetriadou, C. & Kirmizis, A. 2017. Histone Acetyltransferases in Cancer: Guardians or Hazards? *Critical Reviews in Oncogenesis* 22**,** 195-218.

Demetriadou, C., Koufaris, C. & Kirmizis, A. 2020. Histone N-alpha terminal modifications: genome regulation at the tip of the tail. *Epigenetics & Chromatin,* 13. 10.1186/s13072-020-00352-w

Demmerle, J., Koch, A. J. & Holaska, J. M. 2012. The Nuclear Envelope Protein Emerin Binds Directly to Histone Deacetylase 3 (HDAC3) and Activates HDAC3 Activity. *Journal of Biological Chemistry,* 287**,** 22080-22088. 10.1074/jbc.M111.325308

Deng, S. & Marmorstein, R. 2021. Protein N-Terminal Acetylation: Structural Basis, Mechanism, Versatility, and Regulation. *Trends in Biochemical Sciences,* 46**,** 15-27. 10.1016/j.tibs.2020.08.005

Deng, X., Shao, G., Zhang, H. T., Li, C., Zhang, D., Cheng, L., Elzey, B. D., Pili, R., Ratliff, T. L., Huang, J., et al. 2017. Protein arginine methyltransferase 5 functions as an epigenetic activator of the androgen receptor to promote prostate cancer cell growth. *Oncogene,* 36**,** 1223-1231. 10.1038/onc.2016.287

Deng, Y., Deng, S., Ho, Y.-H., Gardner, S. M., Huang, Z., Marmorstein, R. & Huang, R. 2021. Title. Journal, Volume. 10.1101/2021.01.24.427995

Diehl, K. L. & Muir, T. W. 2020. Chromatin as a key consumer in the metabolite economy. *Nature Chemical Biology,* 16**,** 620-629. 10.1038/s41589-020-0517-x

Ding, J., Li, T., Wang, X., Zhao, E., Choi, J.-H., Yang, L., Zha, Y., Dong, Z., Huang, S., Asara, John m., et al. 2013. The Histone H3 Methyltransferase G9A Epigenetically Activates the Serine-Glycine Synthesis Pathway to Sustain Cancer Cell Survival and Proliferation. *Cell Metabolism,* 18**,** 896-907. 10.1016/j.cmet.2013.11.004

Dinh, T. V., Bienvenut, W. V., Linster, E., Feldman-Salit, A., Jung, V. A., Meinnel, T., Hell, R., Giglione, C. & Wirtz, M. 2015. Molecular identification and functional characterization of the first Nalpha-acetyltransferase in plastids by global acetylome profiling. *Proteomics,* 15**,** 2426-35. 10.1002/pmic.201500025

Dobin, A., Davis, C. A., Schlesinger, F., Drenkow, J., Zaleski, C., Jha, S., Batut, P., Chaisson, M. & Gingeras, T. R. 2013. STAR: ultrafast universal RNA-seq aligner. *Bioinformatics,* 29**,** 15-21. 10.1093/bioinformatics/bts635

Drazic, A., Aksnes, H., Marie, M., Boczkowska, M., Varland, S., Timmerman, E., Foyn, H., Glomnes, N., Rebowski, G., Impens, F., et al. 2018. NAA80 is actin's N-terminal acetyltransferase and regulates cytoskeleton assembly and cell motility. *Proc Natl Acad Sci U S A,* 115**,** 4399-4404. 10.1073/pnas.1718336115

Drazic, A., Myklebust, L. M., Ree, R. & Arnesen, T. 2016. The world of protein acetylation. *Biochim Biophys Acta,* 1864**,** 1372-401. 10.1016/j.bbapap.2016.06.007

Ducker, G. S. & Rabinowitz, J. D. 2017. One-Carbon Metabolism in Health and Disease. *Cell Metabolism,* 25**,** 27-42. 10.1016/j.cmet.2016.08.009

Easwaran, H., Johnstone, S. E., Van Neste, L., Ohm, J., Mosbruger, T., Wang, Q., Aryee, M. J., Joyce, P., Ahuja, N., Weisenberger, D., et al. 2012. A DNA hypermethylation module for the stem/progenitor cell signature of cancer. *Genome Research,* 22**,** 837-849. 10.1101/gr.131169.111

Etchegaray, J.-P. & Mostoslavsky, R. 2016. Interplay between Metabolism and Epigenetics: A Nuclear Adaptation to Environmental Changes. *Molecular Cell,* 62**,** 695-711. 10.1016/j.molcel.2016.05.029

Finlan, L. E., Sproul, D., Thomson, I., Boyle, S., Kerr, E., Perry, P., Ylstra, B., Chubb, J. R. & Bickmore, W. A. 2008. Recruitment to the Nuclear Periphery Can Alter Expression of Genes in Human Cells. *PLoS Genetics,* 4**,** e1000039. 10.1371/journal.pgen.1000039

Flavahan, W. A., Drier, Y., Liau, B. B., Gillespie, S. M., Venteicher, A. S., Stemmer-Rachamimov, A. O., Suvà, M. L. & Bernstein, B. E. 2015. Insulator dysfunction and oncogene activation in IDH mutant gliomas. *Nature,* 529**,** 110-114. 10.1038/nature16490

Flavahan, W. A., Gaskell, E. & Bernstein, B. E. 2017. Epigenetic plasticity and the hallmarks of cancer. *Science,* 357**,** eaal2380. 10.1126/science.aal2380

Folch, J., Lees, M. & Stanley, G. H. S. 1957. A Simple Method for the Isolation and Purification of Total Lipides from Animal Tissues. *Journal of Biological Chemistry,* 226**,** 497-509. 10.1016/s0021-9258(18)64849-5

Fulton, M. D., Zhang, J., He, M., Ho, M. C. & Zheng, Y. G. 2017. Intricate Effects of alpha-Amino and Lysine Modifications on Arginine Methylation of the N-Terminal Tail of Histone H4. *Biochemistry,* 56**,** 3539-3548. 10.1021/acs.biochem.7b00450

Gao, X., Lin, S.-H., Ren, F., Li, J.-T., Chen, J.-J., Yao, C.-B., Yang, H.-B., Jiang, S.-X., Yan, G.-Q., Wang, D., et al. 2016. Acetate functions as an epigenetic metabolite to promote lipid synthesis under hypoxia. *Nature Communications,* 7. 10.1038/ncomms11960

Gao, X., Sanderson, S. M., Dai, Z., Reid, M. A., Cooper, D. E., Lu, M., Richie, J. P., Ciccarella, A., Calcagnotto, A., Mikhael, P. G., et al. 2019. Dietary methionine influences therapy in mouse cancer models and alters human metabolism. *Nature,* 572**,** 397-401. 10.1038/s41586-019-1437-3

Gautschi, M., Just, S. R., Mun, A., Ross, S., RüCknagel, P., Dubaquié, Y., Ehrenhofer-Murray, A. & Rospert, S. 2003. The Yeast Nα-Acetyltransferase NatA Is Quantitatively Anchored to the Ribosome and Interacts with Nascent Polypeptides. *Molecular and Cellular Biology,* 23**,** 7403-7414. 10.1128/mcb.23.20.7403-7414.2003

Ghandi, M., Huang, F. W., Jané-Valbuena, J., Kryukov, G. V., Lo, C. C., Mcdonald, E. R., Barretina, J., Gelfand, E. T., Bielski, C. M., Li, H., et al. 2019. Next-generation characterization of the Cancer Cell Line Encyclopedia. *Nature,* 569**,** 503-508. 10.1038/s41586-019-1186-3

Girelli, G., Custodio, J., Kallas, T., Agostini, F., Wernersson, E., Spanjaard, B., Mota, A., Kolbeinsdottir, S., Gelali, E., Crosetto, N., et al. 2020. GPSeq reveals the radial organization of chromatin in the cell nucleus. *Nature Biotechnology,* 38**,** 1184-1193. 10.1038/s41587-020-0519-y

Goldberg, A. D., Allis, D. C. & Bernstein, E. 2007. Epigenetics: A Landscape Takes Shape. *Cell,* 128**,** 635-638. 10.1016/j.cell.2007.02.006

Goldman, M., Craft, B., Hastie, M., Repečka, K., Kamath, A., Mcdade, F., Rogers, D., Brooks, A. N., Zhu, J. & Haussler, D. 2019. Title. Journal, Volume. 10.1101/326470

Greenberg, M. V. C. 2021. Get Out and Stay Out: New Insights Into DNA Methylation Reprogramming in Mammals. *Frontiers in Cell and Developmental Biology,* 8. 10.3389/fcell.2020.629068

Greenberg, M. V. C. & Bourc'his, D. 2019. The diverse roles of DNA methylation in mammalian development and disease. *Nature Reviews Molecular Cell Biology,* 20**,** 590-607. 10.1038/s41580-019-0159-6

Hammond, W. A., Swaika, A. & Mody, K. 2016. Pharmacologic resistance in colorectal cancer: a review. *Therapeutic Advances in Medical Oncology* 8**,** 57-84. 10.1177/

Hatzivassiliou, G., Zhao, F., Bauer, D. E., Andreadis, C., Shaw, A. N., Dhanak, D., Hingorani, S. R., Tuveson, D. A. & Thompson, C. B. 2005. ATP citrate lyase inhibition can suppress tumor cell growth. *Cancer Cell,* 8**,** 311-321. 10.1016/j.ccr.2005.09.008

Haws, S. A., Leech, C. M. & Denu, J. M. 2020. Metabolism and the Epigenome: A Dynamic Relationship. *Trends in Biochemical Sciences,* 45**,** 731-747. 10.1016/j.tibs.2020.04.002

Herbig, K., Chiang, E.-P., Lee, L.-R., Hills, J., Shane, B. & Stover, P. J. 2002. Cytoplasmic Serine Hydroxymethyltransferase Mediates Competition between Folate-dependent Deoxyribonucleotide andS-Adenosylmethionine Biosyntheses. *Journal of Biological Chemistry,* 277**,** 38381-38389. 10.1074/jbc.M205000200

Hershko, A. H., H.; Eytan, E.; Kaklij, G.; and Rose, I.A. 1984. Role of the a-amino group of protein in ubiquitin-mediated protein breakdown. *PNAS,* 81**,** 7021-7025.

Hino, S., Sakamoto, A., Nagaoka, K., Anan, K., Wang, Y., Mimasu, S., Umehara, T., Yokoyama, S., Kosai, K.-I. & Nakao, M. 2012. FAD-dependent lysine-specific demethylase-1 regulates cellular energy expenditure. *Nature Communications,* 3. 10.1038/ncomms1755

Hole, K., Van Damme, P., Dalva, M., Aksnes, H., Glomnes, N., Varhaug, J. E., Lillehaug, J. R., Gevaert, K. & Arnesen, T. 2011. The Human N-Alpha-Acetyltransferase 40 (hNaa40p/hNatD) Is Conserved from Yeast and N-Terminally Acetylates Histones H2A and H4. *PLoS ONE,* 6**,** e24713. 10.1371/journal.pone.0024713

Huttlin, E. L., Bruckner, R. J., Paulo, J. A., Cannon, J. R., Ting, L., Baltier, K., Colby, G., Gebreab, F., Gygi, M. P., Parzen, H., et al. 2017. Architecture of the human interactome defines protein communities and disease networks. *Nature,* 545**,** 505-509. 10.1038/nature22366

Huttlin, E. L., Ting, L., Bruckner, R. J., Gebreab, F., Gygi, M. P., Szpyt, J., Tam, S., Zarraga, G., Colby, G., Baltier, K., et al. 2015. The BioPlex Network: A

Systematic Exploration of the Human Interactome. *Cell,* 162**,** 425-440. 10.1016/j.cell.2015.06.043

Hwang, C. S., Shemorry, A. & Varshavsky, A. 2010. N-Terminal Acetylation of Cellular Proteins Creates Specific Degradation Signals. *Sciene,* 327**,** 973-977.

Hyun, K., Jeon, J., Park, K. & Kim, J. 2017. Writing, erasing and reading histone lysine methylations. *Experimental & Molecular Medicine,* 49**,** e324-e324. 10.1038/emm.2017.11

Jonckheere, V. & Van Damme, P. 2021. Title. Journal, Volume. 10.1101/2021.02.26.433048

Ju, J., Chen, A., Deng, Y., Liu, M., Wang, Y., Wang, Y., Nie, M., Wang, C., Ding, H., Yao, B., et al. 2017a. NatD promotes lung cancer progression by preventing histone H4 serine phosphorylation to activate Slug expression. *Nature Communications,* 8. 10.1038/s41467-017-00988-5

Ju, J., Chen, A., Deng, Y., Liu, M., Wang, Y., Wang, Y., Nie, M., Wang, C., Ding, H., Yao, B., et al. 2017b. NatD promotes lung cancer progression by preventing histone H4 serine phosphorylation to activate Slug expression. *Nat Commun,* 8**,** 928. 10.1038/s41467-017-00988-5

Karoutas, A. & Akhtar, A. 2021. Functional mechanisms and abnormalities of the nuclear lamina. *Nature Cell Biology,* 23**,** 116-126. 10.1038/s41556-020-00630-5

Kasinath, V., Beck, C., Sauer, P., Poepsel, S., Kosmatka, J., Faini, M., Toso, D., Aebersold, R. & Nogales, E. 2021. JARID2 and AEBP2 regulate PRC2 in the presence of H2AK119ub1 and other histone modifications. *Science,* 371**,** eabc3393. 10.1126/science.abc3393

Kaushik, S., Liu, F., Veazey, K. J., Gao, G., Das, P., Neves, L. F., Lin, K., Zhong, Y., Lu, Y., Giuliani, V., et al. 2018. Genetic deletion or small-molecule inhibition of the arginine methyltransferase PRMT5 exhibit anti-tumoral activity in mouse models of MLL-rearranged AML. *Leukemia,* 32**,** 499-509. 10.1038/leu.2017.206

Kebede, A. F., Schneider, R. & Daujat, S. 2015. Novel types and sites of histone modifications emerge as players in the transcriptional regulation contest. *FEBS J,* 282**,** 1658-74. 10.1111/febs.13047

Kind, J., Pagie, L., Ortabozkoyun, H., Boyle, S., De vries, Sandra s., Janssen, H., Amendola, M., Nolen, Leisha d., Bickmore, Wendy a. & Van steensel, B. 2013. Single-Cell Dynamics of Genome-Nuclear Lamina Interactions. *Cell,* 153**,** 178-192. 10.1016/j.cell.2013.02.028

Kinnaird, A., Zhao, S., Wellen, K. E. & Michelakis, E. D. 2016. Metabolic control of epigenetics in cancer. *Nature Reviews Cancer,* 16**,** 694-707. 10.1038/nrc.2016.82

Kottakis, F., Nicolay, B. N., Roumane, A., Karnik, R., Gu, H., Nagle, J. M., Boukhali, M., Hayward, M. C., Li, Y. Y., Chen, T., et al. 2016. LKB1 loss links serine metabolism to DNA methylation and tumorigenesis. *Nature,* 539**,** 390-395. 10.1038/nature20132

Koufaris, C. & Kirmizis, A. 2020. N-Terminal Acetyltransferases Are Cancer-Essential Genes Prevalently Upregulated in Tumours. *Cancers,* 12**,** 2631. 10.3390/cancers12092631

Kouzarides, T. 2007. Chromatin modifications and their function. *Cell,* 128**,** 693-705. 10.1016/j.cell.2007.02.005

Langmead, B. & Salzberg, S. L. 2012. Fast gapped-read alignment with Bowtie 2. *Nature Methods,* 9**,** 357-359. 10.1038/nmeth.1923

Lee, J.-S., Smith, E. & Shilatifard, A. 2010. The Language of Histone Crosstalk. *Cell,* 142**,** 682-685. 10.1016/j.cell.2010.08.011

Lee, K. E., Heo, J. E., Kim, J. M. & Hwang, C. S. 2016. N-Terminal Acetylation-Targeted N-End Rule Proteolytic System: The Ac/N-End Rule Pathway. *Mol Cells,* 39**,** 169-78. 10.14348/molcells.2016.2329

Li, G., Tian, Y. & Zhu, W.-G. 2020. The Roles of Histone Deacetylases and Their Inhibitors in Cancer Therapy. *Frontiers in Cell and Developmental Biology,* 8. 10.3389/fcell.2020.576946

Li, X., Egervari, G., Wang, Y., Berger, S. L. & Lu, Z. 2018. Regulation of chromatin and gene expression by metabolic enzymes and metabolites. *Nature Reviews Molecular Cell Biology,* 19**,** 563-578. 10.1038/s41580-018-0029-7

Liu, Y., Zhou, D., Zhang, F., Tu, Y., Xia, Y., Wang, H., Zhou, B., Zhang, Y., Wu, J., Gao, X., et al. 2012. Liver Patt1 deficiency protects male mice from age-associated but not high-fat diet-induced hepatic steatosis. *Journal of Lipid Research,* 53**,** 358-367. 10.1194/jlr.M019257

Liu, Z., Liu, Y., Wang, H., Ge, X., Jin, Q., Ding, G., Hu, Y., Zhou, B., Chen, Z., Ge, X., et al. 2009a. Patt1, a novel protein acetyltransferase that is highly expressed in liver and downregulated in hepatocellular carcinoma, enhances apoptosis of hepatoma cells. *The International Journal of Biochemistry & Cell Biology,* 41**,** 2528-2537. 10.1016/j.biocel.2009.08.009

Liu, Z., Liu, Y., Wang, H., Ge, X., Jin, Q., Ding, G., Hu, Y., Zhou, B., Chen, Z., Ge, X., et al. 2009b. Patt1, a novel protein acetyltransferase that is highly expressed in liver and downregulated in hepatocellular carcinoma, enhances apoptosis of hepatoma cells. *Int J Biochem Cell Biol,* 41**,** 2528-37. 10.1016/j.biocel.2009.08.009

Lo, W. S., Trievel, R. C., Rojas, J. R., Duggan, L., Hsu, J. Y., Allis, C. D., Marmorstein, R. & Berger, S. L. 2000. Phosphorylation of serine 10 in histone H3 is functionally linked in vitro and in vivo to Gcn5-mediated acetylation at lysine 14. *Mol Cell,* 5**,** 917-26.

Locasale, J. W. 2013. Serine, glycine and one-carbon units: cancer metabolism in full circle. *Nature Reviews Cancer,* 13**,** 572-583. 10.1038/nrc3557

Low, J. K. & Wilkins, M. R. 2012. Protein arginine methylation in Saccharomyces cerevisiae. *FEBS J,* 279**,** 4423-43. 10.1111/febs.12039

Luger, K., Mader, A. W., Richmond, R. K., Sargent, D. F. & Richmond, T. J. 1997. Crystal structure of the nucleosome core particle at 2.8 A˚ resolution. *Nature,* 389**,** 251-260.

Lund, E., Oldenburg, A. R., Delbarre, E., Freberg, C. T., Duband-Goulet, I., Eskeland, R., Buendia, B. & Collas, P. 2013. Lamin A/C-promoter interactions specify chromatin state-dependent transcription outcomes. *Genome Research,* 23**,** 1580-1589. 10.1101/gr.159400.113

Lyko, F. 2017. The DNA methyltransferase family: a versatile toolkit for epigenetic regulation. *Nature Reviews Genetics,* 19**,** 81-92. 10.1038/nrg.2017.80

Macfarlane, A. J., Perry, C. A., Girnary, H. H., Gao, D., Allen, R. H., Stabler, S. P., Shane, B. & Stover, P. J. 2009. Mthfd1 Is an Essential Gene in Mice and Alters Biomarkers of Impaired One-carbon Metabolism. *Journal of Biological Chemistry,* 284**,** 1533-1539. 10.1074/jbc.M808281200

Maddocks, Oliver d. K., Labuschagne, Christiaan f., Adams, Peter d. & Vousden, Karen h. 2016. Serine Metabolism Supports the Methionine Cycle and DNA/RNA Methylation through De Novo ATP Synthesis in Cancer Cells. *Molecular Cell,* 61**,** 210-221. 10.1016/j.molcel.2015.12.014

Madeo, F., Pietrocola, F., Eisenberg, T. & Kroemer, G. 2014. Caloric restriction mimetics: towards a molecular definition. *Nature,* 13**,** 727-740. 10.1038/nrd4391

Magin, R. S., Liszczak, G. P. & Marmorstein, R. 2015a. The molecular basis for histone H4- and H2A-specific amino-terminal acetylation by NatD. *Structure,* 23**,** 332-41. 10.1016/j.str.2014.10.025

Magin, Robert s., Liszczak, Glen p. & Marmorstein, R. 2015b. The Molecular Basis for Histone H4- and H2A-Specific Amino-Terminal Acetylation by NatD. *Structure,* 23**,** 332-341. 10.1016/j.str.2014.10.025

Marine, J.-C., Dawson, S.-J. & Dawson, M. A. 2020. Non-genetic mechanisms of therapeutic resistance in cancer. *Nature Reviews Cancer,* 20**,** 743-756. 10.1038/s41568-020-00302-4

Martinez-Pastor, B., Cosentino, C. & Mostoslavsky, R. 2013. A Tale of Metabolites: The Cross-Talk between Chromatin and Energy Metabolism. *Cancer Discovery,* 3**,** 497-501. 10.1158/2159-8290.cd-13-0059

May, J. L., Kouri, F. M., Hurley, L. A., Liu, J., Tommasini-Ghelfi, S., Ji, Y., Gao, P., Calvert, A. E., Lee, A., Chandel, N. S., et al. 2019. IDH3a regulates one-carbon metabolism in glioblastoma. *Sci. Adv.,* 5**,** eaat0456.

Mentch, S. J. & Locasale, J. W. 2016. One-carbon metabolism and epigenetics: understanding the specificity. *Annals of the New York Academy of Sciences,* 1363**,** 91-98. 10.1111/nyas.12956

Mentch, Samantha j., Mehrmohamadi, M., Huang, L., Liu, X., Gupta, D., Mattocks, D., Gómez padilla, P., Ables, G., Bamman, Marcas m., Thalacker-Mercer, Anna e., et al. 2015. Histone Methylation Dynamics and Gene Regulation Occur through

the Sensing of One-Carbon Metabolism. *Cell Metabolism,* 22**,** 861-873. 10.1016/j.cmet.2015.08.024

Mizi, A., Zhang, S. & Papantonis, A. 2020. Genome folding and refolding in differentiation and cellular senescence. *Current Opinion in Cell Biology,* 67**,** 56-63. 10.1016/j.ceb.2020.08.002

Molina-Serrano, D., Schiza, V., Demosthenous, C., Stavrou, E., Oppelt, J., Kyriakou, D., Liu, W., Zisser, G., Bergler, H., Dang, W., et al. 2016. Loss of Nat4 and its associated histone H4 N-terminal acetylation mediates calorie restriction-induced longevity. *EMBO Rep,* 17**,** 1829-1843. 10.15252/embr.201642540

Molina-Serrano, D., Schiza, V. & Kirmizis, A. 2013. Cross-talk among epigenetic modifications: lessons from histone arginine methylation. *Biochem Soc Trans,* 41**,** 751-9. 10.1042/BST20130003

Moran, S., Arribas, C. & Esteller, M. 2016. Validation of a DNA methylation microarray for 850,000 CpG sites of the human genome enriched in enhancer sequences. *Epigenomics,* 8**,** 389-399.

Mylonas, C. & Tessarz, P. 2018. Transcriptional repression by FACT is linked to regulation of chromatin accessibility at the promoter of ES cells. *Life Science Alliance,* 1**,** e201800085. 10.26508/lsa.201800085

Nacev, B. A., Feng, L., Bagert, J. D., Lemiesz, A. E., Gao, J., Soshnev, A. A., Kundra, R., Schultz, N., Muir, T. W. & Allis, C. D. 2019. The expanding landscape of 'oncohistone' mutations in human cancers. *Nature,* 567**,** 473-478. 10.1038/s41586-019-1038-1

Papageorgis, P., Ozturk, S., Lambert, A. W., Neophytou, C. M., Tzatsos, A., Wong, C. K., Thiagalingam, S. & Constantinou, A. I. 2015. Targeting IL13Ralpha2 activates STAT6-TP63 pathway to suppress breast cancer lung metastasis. *Breast Cancer Res,* 17**,** 98. 10.1186/s13058-015-0607-y

Park, S. E., Kim, J. M., Seok, O. H., Cho, H., Wadas, B., Kim, S. Y., Varshavsky, A. & Hwang, C. S. 2015. Control of mammalian G protein signaling by N-terminal acetylation and the N-end rule pathway. *Science,* 347**,** 1249-1252. 10.1126/science.aaa3844

Pavlou, D. & Kirmizis, A. 2016. Depletion of histone N-terminal-acetyltransferase Naa40 induces p53-independent apoptosis in colorectal cancer cells via the mitochondrial pathway. *Apoptosis,* 21**,** 298-311. 10.1007/s10495-015-1207-0

Poledova, B., Norbeck, J., Takakura, H., Blomberg, A. & Sherman, F. 1999. Identification and specificities of N-terminal acetyltransferases from Saccharomyces cerevisiae. *The EMBO journal* 18**,** 6155-6168.

Posavec Marjanović, M., Hurtado-Bagès, S., Lassi, M., Valero, V., Malinverni, R., Delage, H., Navarro, M., Corujo, D., Guberovic, I., Douet, J., et al. 2017. MacroH2A1.1 regulates mitochondrial respiration by limiting nuclear NAD+ consumption. *Nature Structural & Molecular Biology,* 24**,** 902-910. 10.1038/nsmb.3481

Rada‐Iglesias, A., Grosveld, F. G. & Papantonis, A. 2018. Forces driving the three‐dimensional folding of eukaryotic genomes. *Molecular Systems Biology,* 14. 10.15252/msb.20188214

Rahman, L., Voeller, D., Rahman, M., Lipkowitz, S., Allegra, C., Barrett, J. C., Kaye, F. J. & Zajac-Kaye, M. 2004. Thymidylate synthase as an oncogene: A novel role for an essential DNA synthesis enzyme. *Cancer Cell,* 5**,** 341-351.

Reddy, K. L., Zullo, J. M., Bertolino, E. & Singh, H. 2008. Transcriptional repression mediated by repositioning of genes to the nuclear lamina. *Nature,* 452**,** 243-247. 10.1038/nature06727

Ree, R., Varland, S. & Arnesen, T. 2018. Spotlight on protein N-terminal acetylation. *Experimental & Molecular Medicine,* 50**,** 1-13. 10.1038/s12276-018-0116-z

Reynolds, N., Salmon-Divon, M., Dvinge, H., Hynes-Allen, A., Balasooriya, G., Leaford, D., Behrens, A., Bertone, P. & Hendrich, B. 2012. NuRD-mediated deacetylation of H3K27 facilitates recruitment of Polycomb Repressive Complex 2 to direct gene repression. *EMBO J,* 31**,** 593-605. 10.1038/emboj.2011.431

Ritchie, M. E., Phipson, B., Wu, D., Hu, Y., Law, C. W., Shi, W. & Smyth, G. K. 2015. limma powers differential expression analyses for RNA-sequencing and microarray studies. *Nucleic Acids Research,* 43**,** e47-e47. 10.1093/nar/gkv007

Robinson, M. D. & Oshlack, A. 2010. A scaling normalization method for differential expression analysis of RNA-seq data. *Genome Biol.,* 11**,** R25.

Rohle, D., Popovici-Muller, J., Palaskas, N., Turcan, S., Grommes, C., Campos, C., Tsoi, J., Clark, O., Oldrini, B., Komisopoulou, E., et al. 2013. An Inhibitor of Mutant IDH1 Delays Growth and Promotes Differentiation of Glioma Cells. *Science,* 340**,** 626-630.

Roy, D. G., Chen, J., Mamane, V., Ma, E. H., Muhire, B. M., Sheldon, R. D., Shorstova, T., Koning, R., Johnson, R. M., Esaulova, E., et al. 2020. Methionine Metabolism Shapes T Helper Cell Responses through Regulation of Epigenetic Reprogramming. *Cell Metabolism,* 31**,** 250-266.e9. 10.1016/j.cmet.2020.01.006

Russo, G. L., Pietra, D. E., Mercurio, C., Ragione, F. D., Marshak, D. R., Oliva, A. & Zappia, V. 1997. Down-Regulation of Protein Kinase CKII Activity by Sodium Butyrate. *Biochemical and Biophysical Research Communications,* 233**,** 673-677.

Salvarani, N., Crasto, S., Miragoli, M., Bertero, A., Paulis, M., Kunderfranco, P., Serio, S., Forni, A., Lucarelli, C., Dal Ferro, M., et al. 2019. The K219T-Lamin mutation induces conduction defects through epigenetic inhibition of SCN5A in human cardiac laminopathy. *Nature Communications,* 10. 10.1038/s41467-019-09929-w

Schiza, V., Molina-Serrano, D., Kyriakou, D., Hadjiantoniou, A. & Kirmizis, A. 2013. N-alpha-terminal acetylation of histone H4 regulates arginine methylation and ribosomal DNA silencing. *PLoS Genet,* 9**,** e1003805. 10.1371/journal.pgen.1003805

Schmoll, H. J., Van Cutsem, E., Stein, A., Valentini, V., Glimelius, B., Haustermans, K., Nordlinger, B., Van De Velde, C. J., Balmana, J., Regula, J., et al. 2012. ESMO Consensus Guidelines for management of patients with colon and rectal cancer. A personalized approach to clinical decision making. *Annals of Oncology,* 23**,** 2479-2516. 10.1093/annonc/mds236

Schvartzman, J. M., Thompson, C. B. & Finley, L. W. S. 2018. Metabolic regulation of chromatin modifications and gene expression. *Journal of Cell Biology,* 217**,** 2247-2259. 10.1083/jcb.201803061

Sebastián, C., Zwaans, Bernadette m. M., Silberman, Dafne m., Gymrek, M., Goren, A., Zhong, L., Ram, O., Truelove, J., Guimaraes, Alexander r., Toiber, D., et al. 2012. The Histone Deacetylase SIRT6 Is a Tumor Suppressor that Controls Cancer Metabolism. *Cell,* 151**,** 1185-1199. 10.1016/j.cell.2012.10.047

Serefidou, M., Venkatasubramani, A. V. & Imhof, A. 2019. The Impact of One Carbon Metabolism on Histone Methylation. *Frontiers in Genetics,* 10. 10.3389/fgene.2019.00764

Shalem, O., Sanjana, N. E., Hartenian, E., Shi, X., Scott, D. A., Mikkelsen, T. S., Heckl, D., Ebert, B. L., Root, D. E., Doench, J. G., et al. 2014. Genome-Scale CRISPR-Cas9 Knockout Screening in Human Cells. *Science,* 343**,** 84-87.

Shemorry, A., Hwang, C.-S. & Varshavsky, A. 2013. Control of Protein Quality and Stoichiometries by N-Terminal Acetylation and the N-End Rule Pathway. *Molecular Cell,* 50**,** 540-551. 10.1016/j.molcel.2013.03.018

Shi, Y., Lan, F., Matson, C., Mulligan, P., Whetstine, J. R., Cole, P. A., Casero, R. A. & Shi, Y. 2004. Histone Demethylation Mediated by the Nuclear Amine Oxidase Homolog LSD1. *Cell,* 119**,** 941-953. 10.1016/j.cell.2004.12.012

Shiraki, N., Shiraki, Y., Tsuyama, T., Obata, F., Miura, M., Nagae, G., Aburatani, H., Kume, K., Endo, F. & Kume, S. 2014. Methionine Metabolism Regulates Maintenance and Differentiation of Human Pluripotent Stem Cells. *Cell Metabolism,* 19**,** 780-794. 10.1016/j.cmet.2014.03.017

Shuvalov, O., Petukhov, A., Daks, A., Fedorova, O., Vasileva, E. & Barlev, N. A. 2017. One-carbon metabolism and nucleotide biosynthesis as attractive targets for anticancer therapy. *Oncotarget,* 8**,** 23955-23977.

Shyh-Chang, N., Locasale, Jason w., A., L. C., Zheng, Y., Teo, R. Y., Ratanasirintrawoot, S., Zhang, J., Onder, T., Unternaehrer, J. J., Zhu, H., et al. 2012. Influence of Threonine Metabolism on S-Adenosylmethionine and Histone Methylation. *Science,* 339**,** 222-226.

Sivanand, S., Viney, I. & Wellen, K. E. 2018. Spatiotemporal Control of Acetyl-CoA Metabolism in Chromatin Regulation. *Trends in Biochemical Sciences,* 43**,** 61-74. 10.1016/j.tibs.2017.11.004

Song, O. K., Wang, X., Waterborg, J. H. & Sternglanz, R. 2003. An Nalpha-acetyltransferase responsible for acetylation of the N-terminal residues of histones H4 and H2A. *J Biol Chem,* 278**,** 38109-12. 10.1074/jbc.C300355200

Sperber, H., Mathieu, J., Wang, Y., Ferreccio, A., Hesson, J., Xu, Z., Fischer, K. A., Devi, A., Detraux, D., Gu, H., et al. 2015. The metabolome regulates the epigenetic landscape during naive-to-primed human embryonic stem cell transition. *Nature Cell Biology,* 17**,** 1523-1535. 10.1038/ncb3264

Starheim, K. K., Gevaert, K. & Arnesen, T. 2012. Protein N-terminal acetyltransferases: when the start matters. *Trends in Biochemical Sciences,* 37**,** 152-161. 10.1016/j.tibs.2012.02.003

Suganuma, T. & Workman, J. L. 2008. Crosstalk among Histone Modifications. *Cell,* 135**,** 604-7. 10.1016/j.cell.2008.10.036

Tae, S., Karkhanis, V., Velasco, K., Yaneva, M., Erdjument-Bromage, H., Tempst, P. & Sif, S. 2011. Bromodomain protein 7 interacts with PRMT5 and PRC2, and is involved in transcriptional repression of their target genes. *Nucleic Acids Res,* 39**,** 5424-38. 10.1093/nar/gkr170

Tsukada, Y.-I., Fang, J., Erdjument-Bromage, H., Warren, M. E., Borchers, C. H., Tempst, P. & Zhang, Y. 2005. Histone demethylation by a family of JmjC domain-containing proteins. *Nature,* 439**,** 811-816. 10.1038/nature04433

Tweedie-Cullen, R. Y., Brunner, A. M., Grossmann, J., Mohanna, S., Sichau, D., Nanni, P., Panse, C. & Mansuy, I. M. 2012. Identification of combinatorial patterns of post-translational modifications on individual histones in the mouse brain. *PLoS One,* 7**,** e36980. 10.1371/journal.pone.0036980

Ulanovskaya, O. A., Zuhl, A. M. & Cravatt, B. F. 2013. NNMT promotes epigenetic remodeling in cancer by creating a metabolic methylation sink. *Nature Chemical Biology,* 9**,** 300-306. 10.1038/nchembio.1204

Valencia-Sánchez, M. I., De Ioannes, P., Wang, M., Truong, D. M., Lee, R., Armache, J.-P., Boeke, J. D. & Armache, K.-J. 2021. Regulation of the Dot1 histone H3K79 methyltransferase by histone H4K16 acetylation. *Science,* 371**,** eabc6663. 10.1126/science.abc6663

Van Damme, P., Hole, K., Pimenta-Marques, A., Helsens, K., Vandekerckhove, J., Martinho, R. G., Gevaert, K. & Arnesen, T. 2011. NatF contributes to an evolutionary shift in protein N-terminal acetylation and is important for normal chromosome segregation. *PLoS Genet,* 7**,** e1002169. 10.1371/journal.pgen.1002169

Varghese, V., Magnani, L., Harada-Shoji, N., Mauri, F., Szydlo, R. M., Yao, S., Lam, E. W. F. & Kenny, L. M. 2019. FOXM1 modulates 5-FU resistance in colorectal cancer through regulating TYMS expression. *Scientific Reports,* 9. 10.1038/s41598-018-38017-0

Varland, S., Osberg, C. & Arnesen, T. 2015. N‐terminal modifications of cellular proteins: The enzymes involved, their substrate specificities and biological effects. *Proteomics,* 15**,** 2385-2401. 10.1002/pmic.201400619

Wakasa, K., Kawabata, R., Nakao, S., Hattori, H., Taguchi, K., Uchida, J., Yamanaka, T., Maehara, Y., Fukushima, M. & Oda, S. 2015. Dynamic Modulation

of Thymidylate Synthase Gene Expression and Fluorouracil Sensitivity in Human Colorectal Cancer Cells. *Plos One,* 10**,** e0123076. 10.1371/journal.pone.0123076

Wang, H., Huang, Z., Xia, L., Feng, Q., Erdjument-Bromage, H., Strahl, D. B., Briggs, D. S., Allis, C. D., Wong, J., Tempst, P., et al. 2001. Methylation of Histone H4 at Arginine 3 Facilitating Transcriptional Activation by Nuclear Hormone Receptor. *Science* 293.

Wang, L., Pal, S. & Sif, S. 2008. Protein arginine methyltransferase 5 suppresses the transcription of the RB family of tumor suppressors in leukemia and lymphoma cells. *Mol Cell Biol,* 28**,** 6262-77. 10.1128/MCB.00923-08

Wang, T., Holt, M. V. & Young, N. L. 2018a. Early butyrate induced acetylation of histone H4 is proteoform specific and linked to methylation state. *Epigenetics,* 13**,** 519-535. 10.1080/15592294.2018.1475979

Wang, T., Holt, M. V. & Young, N. L. 2018b. The histone H4 proteoform dynamics in response to SUV4-20 inhibition reveals single molecule mechanisms of inhibitor resistance. *Epigenetics & Chromatin,* 11. 10.1186/s13072-018-0198-9

Wang, Y.-C., Tang, F.-Y., Chen, S.-Y., Chen, Y.-M. & Chiang, E.-P. I. 2011. Glycine-N Methyltransferase Expression in HepG2 Cells Is Involved in Methyl Group Homeostasis by Regulating Transmethylation Kinetics and DNA Methylation. *The Journal of Nutrition,* 141**,** 777-782. 10.3945/jn.110.135954

Wellen, K. E., Hadjiantoniou, G., Sachdeva, U., Bui, T. V., Cross, J. R. & Thompson, C. B. 2009. ATP-Citrate Lyase Links Cellular Metabolism to Histone Acetylation. *Science,* 324**,** 1076-1080.

Wong, C. C., Qian, Y. & Yu, J. 2017. Interplay between epigenetics and metabolism in oncogenesis: mechanisms and therapeutic approaches. *Oncogene,* 36**,** 3359-3374. 10.1038/onc.2016.485

Wu, H., Coskun, V., Tao, J., Xie, W., Ge, W., Yoshikawa, K., Li, E., Zhang, Y. & Sun, Y. E. 2010. Dnmt3a-Dependent Nonpromoter DNA Methylation Facilitates Transcription of Neurogenic Genes. *Science,* 329**,** 444-448.

Wu, X. & Zhang, Y. 2017. TET-mediated active DNA demethylation: mechanism, function and beyond. *Nature Reviews Genetics,* 18**,** 517-534. 10.1038/nrg.2017.33

Xiao, M., Yang, H., Xu, W., Ma, S., Lin, H., Zhu, H., Liu, L., Liu, Y., Yang, C., Xu, Y., et al. 2012. Inhibition of -KG-dependent histone and DNA demethylases by fumarate and succinate that are accumulated in mutations of FH and SDH tumor suppressors. *Genes & Development,* 26**,** 1326-1338. 10.1101/gad.191056.112

Xie, Z., Dai, J., Dai, L., Tan, N., Cheng, Z., Wu, Y., Boeke, J. D. & Zhao, Y. 2012. Lysine Succinylation and Lysine Malonylation in Histones. *Molecular & Cellular Proteomics,* 11**,** 100-107. 10.1074/

Xu, W., Yang, H., Liu, Y., Yang, Y., Wang, P., Kim, S.-H., Ito, S., Yang, C., Wang, P., Xiao, M.-T., et al. 2011. Oncometabolite 2-Hydroxyglutarate Is a Competitive

Inhibitor of α-Ketoglutarate-Dependent Dioxygenases. *Cancer Cell,* 19**,** 17-30. 10.1016/j.ccr.2010.12.014

Ye, C., Sutter, B. M., Wang, Y., Kuang, Z. & Tu, B. P. 2017. A Metabolic Function for Phospholipid and Histone Methylation. *Molecular Cell,* 66**,** 180-193.e8. 10.1016/j.molcel.2017.02.026

Ye, C. & Tu, B. P. 2018. Sink into the Epigenome: Histones as Repositories That Influence Cellular Metabolism. *Trends in Endocrinology & Metabolism,* 29**,** 626-637. 10.1016/j.tem.2018.06.002

Yen, K., Travins, J., Wang, F., David, M. D., Artin, E., Straley, K., Padyana, A., Gross, S., Delabarre, B., Tobin, E., et al. 2017. AG-221, a First-in-Class Therapy Targeting Acute Myeloid Leukemia Harboring Oncogenic IDH2 Mutations. *Cancer Discovery,* 7**,** 478-493. 10.1158/2159-8290.cd-16-1034

Yu, W., Wang, Z., Zhang, K., Chi, Z., Xu, T., Jiang, D., Chen, S., Li, W., Yang, X., Zhang, X., et al. 2019. One-Carbon Metabolism Supports S-Adenosylmethionine and Histone Methylation to Drive Inflammatory Macrophages. *Molecular Cell,* 75**,** 1147-1160.e5. 10.1016/j.molcel.2019.06.039

Zhang, B., Dong, S., Zhu, R., Hu, C., Hou, J., Li, Y., Zhao, Q., Shao, X., Bu, Q., Li, H., et al. 2015. Targeting protein arginine methyltransferase 5 inhibits colorectal cancer growth by decreasing arginine methylation of eIF4E and FGFR3. *Oncotarget,* 6**,** 22799-22811.

Zhang, X., Ozawa, Y., Lee, H., Wen, Y., Tan, T., Wadzinski, B. E. & Seto, E. 2005. Histone deacetylase 3 (HDAC3) activity is regulated by interaction with protein serine/threonine phosphatase 4. *Genes & Development,* 19**,** 827-839. 10.1101/

Zhang, Y., Griffin, K., Mondal, N. & Parvin, J. D. 2004. Phosphorylation of Histone H2A Inhibits Transcription on Chromatin Templates. *Journal of Biological Chemistry,* 279**,** 21866-21872. 10.1074/jbc.M400099200

Zhang, Y., Jurkowska, R., Soeroes, S., Rajavelu, A., Dhayalan, A., Bock, I., Rathert, P., Brandt, O., Reinhardt, R., Fischle, W., et al. 2010. Chromatin methylation activity of Dnmt3a and Dnmt3a/3L is guided by interaction of the ADD domain with the histone H3 tail. *Nucleic Acids Research,* 38**,** 4246-4253. 10.1093/nar/gkq147

Zhao, E., Ding, J., Xia, Y., Liu, M., Ye, B., Choi, J.-H., Yan, C., Dong, Z., Huang, S., Zha, Y., et al. 2016. KDM4C and ATF4 Cooperate in Transcriptional Control of Amino Acid Metabolism. *Cell Reports,* 14**,** 506-519. 10.1016/j.celrep.2015.12.053

Zhao, Q., Rank, G., Tan, Y. T., Li, H., Moritz, R. L., Simpson, R. J., Cerruti, L., Curtis, D. J., Patel, D. J., Allis, C. D., et al. 2009. PRMT5-mediated methylation of histone H4R3 recruits DNMT3A, coupling histone and DNA methylation in gene silencing. *Nat Struct Mol Biol,* 16**,** 304-311. 10.1038/nsmb.1568

Zhong, L., D'urso, A., Toiber, D., Sebastian, C., Henry, R. E., Vadysirisack, D. D., Guimaraes, A., Marinelli, B., Wikstrom, J. D., Nir, T., et al. 2010. The Histone

Deacetylase Sirt6 Regulates Glucose Homeostasis via Hif1α. *Cell,* 140**,** 280-293. 10.1016/j.cell.2009.12.041

Zippo, A., Serafini, R., Rocchigiani, M., Pennacchini, S., Krepelova, A. & Oliviero, S. 2009. Histone crosstalk between H3S10ph and H4K16ac generates a histone code that mediates transcription elongation. *Cell,* 138**,** 1122-36. 10.1016/j.cell.2009.07.031

Zullo, Joseph m., Demarco, Ignacio a., Piqué-Regi, R., Gaffney, Daniel j., Epstein, Charles b., Spooner, Chauncey j., Luperchio, Teresa r., Bernstein, Bradley e., Pritchard, Jonathan k., Reddy, Karen l., et al. 2012. DNA Sequence-Dependent Compartmentalization and Silencing of Chromatin at the Nuclear Lamina. *Cell,* 149**,** 1474-1487. 10.1016/j.cell.2012.04.035